2005

A numerical model for biomass pyrolysis

Mathew John Hagge
Iowa State University

A numerical model for biomass pyrolysis

by

Mathew John Hagge

A dissertation submitted to the graduate faculty

in partial fulfillment of the requirements for the degree of

DOCTOR OF PHILOSOPHY

Major: Mechanical Engineering

Program of Study Committee:
K.M. Bryden, Major Professor
Francine Battaglia
Robert Brown
Richard Hindman
Dennis Vigil

Iowa State University

Ames, Iowa

2005

Graduate College

Iowa State University

This is to certify that the doctoral dissertation of

Mathew John Hagge

has met the dissertation requirements of Iowa State University

Signature was redacted for privacy.

Major Professor

Signature was redacted for privacy.

For the Major Program

TABLE OF CONTENTS

Chapter 1

Introduction

Biomass materials are used in society to furnish homes, as structural components of buildings, as a source of bio-derived products, and as a source of energy. The extent and type of biomass usage varies depending on the type of biomass materials that are available, the availability and price of competing resources, and the level of available technology. The thermal/combustion performance of biomass materials is important because of the many uses of biomass materials.

Biomass pyrolysis is the thermal degradation of biomass materials at elevated temperatures. This thermal degradation converts solid biomass materials into a chemically altered solid structure and releases gases, liquids, and tarry materials from the solid particle. Pyrolysis is typically an important process when studying the failure of wood structural components at high temperatures, determining the rate of release of pyrolysis gases, or determining the combustion performance of biomass fuel.

In this work, the focus will be on the pyrolysis of a single particle of wood. The thermal degradation of a single particle of wood is important for gasification systems and for biomass combustion systems. In gasification systems, the amount and type of pyrolysis gases that are produced, as well as the rate of gas production depend on the performance of the solid particle. In biomass combustion systems, the pyrolysis of the solid particle and the gas phase combustion reactions are tightly coupled. Radiant energy is produced by exothermic gas phase combustion reactions. Much of this radiant energy is transported to the surface of the solid biomass particle. The radiant energy causes temperatures to rise within the particle,

and at temperatures above 225°C pyrolysis gases are produced. These pyrolysis gases are forced out of the particle by the pressure gradient within the particle and provide the fuel for the combustion reactions. During combustion, the rate of fuel consumption and the rate of pyrolysis gas production quickly reach a quasi-equilibrium state, in that the size of the flame (and rate of gas phase combustion) adjusts quickly to the rate of unburned fuel provided by the pyrolysis reactions.

The motivation of this research is to produce a computational model for pyrolysis that can predict the performance of solid biomass under many different situations. The complexity of the physical system has encouraged simplifying assumptions which have limited the ability of existing models to predict pyrolysis performance for a useful range of pyrolysis situations. The importance of physical processes, such as changes in chemical composition and physical properties, moisture movement within the particle, shrinkage of the solid structure, and plastic deformation and cracking of the solid surface must be understood to provide useful pyrolysis models.

The development of pyrolysis models is also motivated by the need to produce methods which are less time consuming and cheaper than detailed experiments. For biomass pyrolysis, it is difficult to obtain information on the conditions within a biomass particle without altering the biomass particle. Temperature, wood, char, moisture content, and gas compositions change continuously within the particle. Steep temperature gradients within the active pyrolysis region cause pressurization of the particle and induce gas flow through the particle. The particle temperature, pressure, and composition will vary with time depending on the transient pyrolysis and combustion conditions. Particles will respond differently depending on the size of the particle, the shape of the particle, the conditions within the

particle, and the rate of external heat flux. Material properties vary within the particle and the biomass particle shrinks during pyrolysis because of chemical restructuring that occurs as virgin wood is converted into char. Stresses within the particle are induced by the shrinkage of the char layer and the pressure within the wood pores. These stresses are relieved by plastic deformation of the particle. It is difficult to measure temperatures and pressures within the particle without significantly altering the conditions within the biomass particle. In addition, transient material data is hard to obtain. Because much of the information within the particle is difficult to measure or cannot be measured directly, computational methods have become an important tool for understanding the complex interactions within a biomass particle.

In this work, a detailed, transient, multi-dimensional biomass pyrolysis model has been developed. The model includes conservation of mass, momentum, and energy within the biomass particle. Heat reaches the surface of the particle through radiation and convection. The energy transferred within the particle, the chemical decomposition, the pressure gradient, and gas flow through the particle are all solved with respect to time. A competitive pyrolysis reaction scheme is used to produce pyrolysis products that are a function of the conditions within the particle. The computational model includes shrinkage of the solid particle, moisture content, and anisotropic properties. The material properties change with time and vary based on the transient composition within the particle. The computational model is used to study the effects of external heating, particle size, and particle shape on biomass performance. This is the most detailed 2-D computational model of biomass pyrolysis currently available.

The goal of this research will be to develop and validate a two-dimensional model of wood pyrolysis that includes Darcy flow, moisture content, and shrinkage of the solid domain. The model solves for the performance of a two-dimensional biomass particle with given external (boundary) conditions, such as an oven that provides a fixed external temperature. Computational methods are based on finite volume discretization of the solid particle, and volume and surface integral formulations of the conservation equations within an unstructured grid. The unstructured grid development requires significantly more computational work to solve than structured methods. It provides additional flexibility in the ability to model a changing particle shape as the particle shrinks during pyrolysis. Unstructured grids are also necessary for multi-dimensional particle-gas phase systems because additional finite volumes may need to be added to the computational domain during pyrolysis because the shrinking particle will cause finite volumes in the gas domain to become extremely distorted.

This two-dimensional formulation of a biomass system is unique in that it accounts for all major physical and transport phenomena within the particle except for the cracking and deformation of the biomass particle, and provides a basis for more complicated models in the future. The system being modeled is shown in Fig 1. As shown, the wood particle pyrolysis system consists of a solid two-dimensional solid particle subjected to known external conditions. Validation of the model is based on the experimental work of Hoerning (1999), in which different sized particles were placed within a furnace, exposed to oven temperatures of 800°C, 1100°C, and 1400°C. The particle was placed within inert environment by blowing nitrogen across the surface of the particle, and the particle

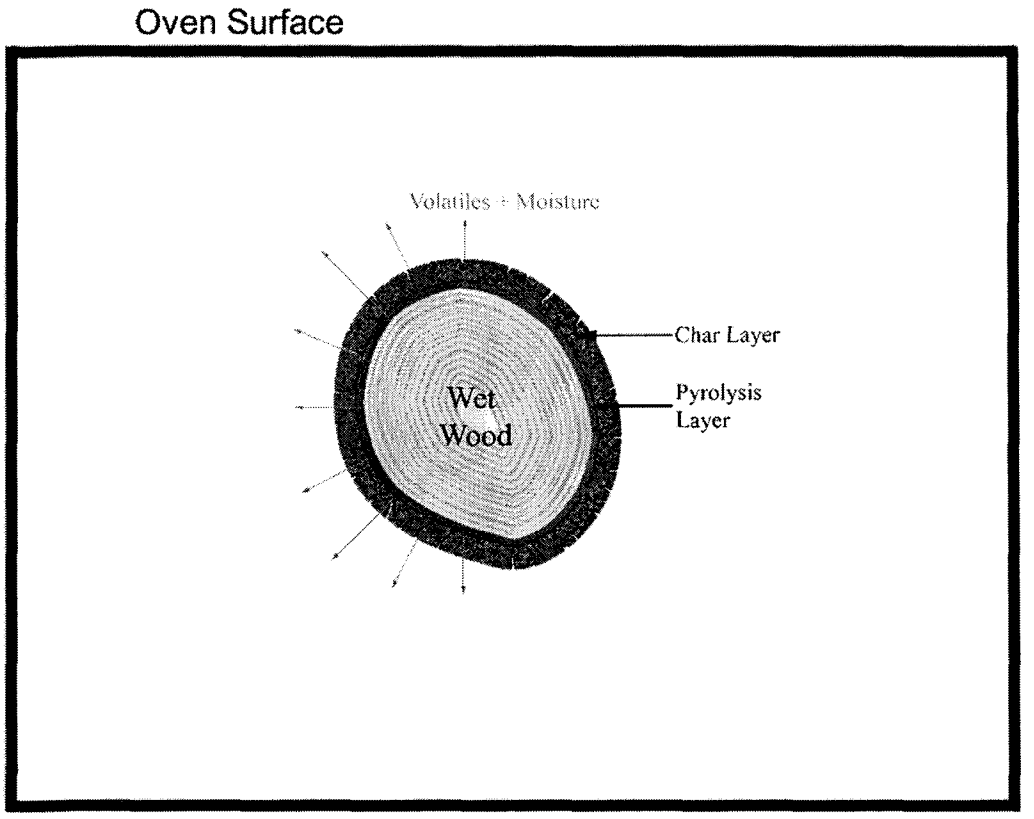

Fig 1. Two Dimensional System Model

temperature and the rate of mass loss were measured for various particle sizes, temperatures and moisture contents. Additional details are provided in Chapter 5. The computational model was validated using a known external heat source and a prescribed flow field. The computational model was then used to study the effects of particle shape, char shrinkage, and grain direction on the pyrolysis of a biomass particle. Comparisons of 1D and 2D results are given in Chapter 6 to demonstrate the effects of multi-dimensional heat and mass transfer on the predicted performance, and to identify areas in which current models may need modification to account for particle shape and size.

Chapter 2

Background

Biomass materials, primarily in the form of wood, have been used for many different applications. Wood fuels have been used as a source of energy for cooking and heating since man developed the ability to harness fire. Wood has been widely used for building machinery and in structural applications due to the relatively high strength and the availability of many species of wood. During the middle ages, iron, copper, and other metals were smelted using wood as a heat source, allowing the production of many new products and materials. For many years, wood was a plentiful source of energy due to agricultural clearing. As the demand for industrial products and sources of energy outpaced the production of raw wood, there became a need for more efficient combustion of the available resources or for the development of alternative sources of energy. When it was discovered that coal could be used to produce coke, coal rapidly replaced wood for metals production, marking the beginning of the modern industrial era. The discovery of coal was followed by the use of oil, natural gas, and nuclear energy.

Biomass fuels continue to be the primary source of energy for one half of the world's population. In less developed countries, cooking or heating are typically done using wood, grass, or dried dung as the fuel source. The cooking and heating is often done within enclosed rooms with inadequate or no ventilation. There are many detrimental health effects to enclosed heating and cooking, with respiratory illness being the leading cause of death in many third world countries. Enclosed heating increases the chance of getting pneumonia,

which is often fatal in less developed countries. Prolonged exposure to combustion radicals can cause blindness, and severe burns can result when people are in close contact with fire.

For industrialized nations, biomass fuels offer an alternative source of solid fuel that is renewable and has decreased emissions of sulfur dioxide and carbon dioxide over traditional sources of energy such as coal. The benefits of biomass are offset by the generally higher costs of biomass fuels. Wood combustion is important for purposes other than power generation. Because woody materials are used extensively in buildings, a large number of tests have been done to determine the flammability of woody materials and the strength of structural materials under load. For example, flammability tests are used to find treatments for wood that can reduce the risk of personal injury as a result of a fire, loading tests are used to determine the safety of structures during fires. Flammability issues include ignition, flame-spread rates, and the build-up and rapid explosion of large quantities of gases in enclosed rooms. Recent attention has also been focused on the combustion of forest fires. Researchers are concerned with predicting the rate of spread of forest fires. The magnitude of these fires in recent years has been partially attributed to the increased density of today's forests due to many successful years of firefighting. Combustion modeling may help identify an appropriate forest density that maintains a reasonable level of safety, while the excess trees may provide additional sources of biomass energy. Biomass fuels may also become an important renewable source for light hydrocarbon fuels as we try to find viable alternatives to fossil fuels.

Biomass fuels are composed from living organisms and include a large variety of plant materials and animal waste that can be used for combustion. Sources of biomass fuels include rapid growth poplar trees, agricultural waste, corn stover, paper waste products,

landfill gases, animal waste, and plant derived materials. Biomass fuels contain the materials that are needed for life and are primarily composed of carbon, hydrogen, oxygen, nitrogen, and sulfur.

There are many reasons why biomass fuels have not gained widespread attention in the past. Biomass fuels contain impurities in their unrefined state that reduce the specific energy content of biomass when compared to purely hydrocarbon fuels, primarily in the form of oxygen atoms. Biomass is currently more expensive than traditional sources of energy such as oil and coal. Transportation of biomass fuels is expensive relative to the energy content of the fuel, and storage of biomass fuels can become an additional problem because living materials naturally decompose.

With all these disadvantages it is not surprising that biomass fuels have not previously gained widespread use in industrialized nations. These industrialized nations have shown an ever-increasing demand for sources of power. The current push for biomass fuels is a result of the need for renewable sources of energy that can help to satisfy the increasing energy demands of industrialized nations, while reducing the release of harmful greenhouse gases.

Biomass fuel is attractive for electric power generation because it is a locally available renewable fuel. Woody products have very low sulfur content and remove carbon dioxide from the atmosphere during the life of the plant, thus providing a source of fuel that can reduce carbon dioxide and sulfur dioxide emissions over traditional sources of energy such as oil or coal. Replacing 1,000 megawatts of coal derived energy with biomass can reduce carbon dioxide emissions to the atmosphere by 5 million tons per year (Berger, 1997).

Biomass fuels can be cost competitive, particularly when using waste products, as is done in the paper industry.

In 2003, renewable energy sources accounted for 6% of the 98 quadrillion BTU's that were consumed in the U.S. Biomass accounted for 47% of renewable energy production. Biomass was closely followed by hydroelectric power (45%), with solar energy and wind energy accounting for less than 3% of renewable energy sources (Renewable Energy Annual 2003). 80% of the nation's biomass energy comes from wood. Roughly one-half of the wood products are produced as a byproduct of paper pulp manufacturing (Berger 1997). Globally, biomass accounts for 15% of the world's energy supply, with over 90% of energy from biomass in some developing countries (Biomass Energy: Data Analysis and Trends, Conference Proceedings 1998).

There are many technical challenges to using biomass energy for power for electric generation. Plant efficiency and air regulations have gradually increased in coal power plants for many years, resulting in improvements in our understanding of coal combustion mechanisms and improvements in coal power plant design. Biomass power plants typically are smaller and have a lower efficiency than coal power plants. Additionally, our understanding of biomass combustion and pyrolysis is limited. Biomass energy systems typically utilize locally available fuel, and biomass sources may range in sizes from whole trees to wood chips. The moisture content of the fuel can vary widely, from about 5% for dried wood to over 50% in very green wood. Because of this, developing detailed models of biomass pyrolysis remains an ongoing research topic.

2.1 The Combustion Process

Wood combustion is a complex process that is not completely understood. Within a wood particle, drying and pyrolysis may be occurring in different portions of the particle at the same time. Pyrolysis gases are produced at elevated temperatures from the thermal decomposition of wood. These gases are produced within a pyrolysis layer, travel through the external char layer, and then escape from the particle. At high enough temperatures, these pyrolysis gases will combust in the presence of oxygen to form an attached or unattached flame zone that feeds energy back to the surface. In the absence of a flame, free stream oxygen diffuses to the surface of the particle and reacts with the char external layer. Carbon dioxide and water vapor may also react with the char surface, forming the char surface reactions. The gas flow is shown in Fig 2 (Bryden 1998).

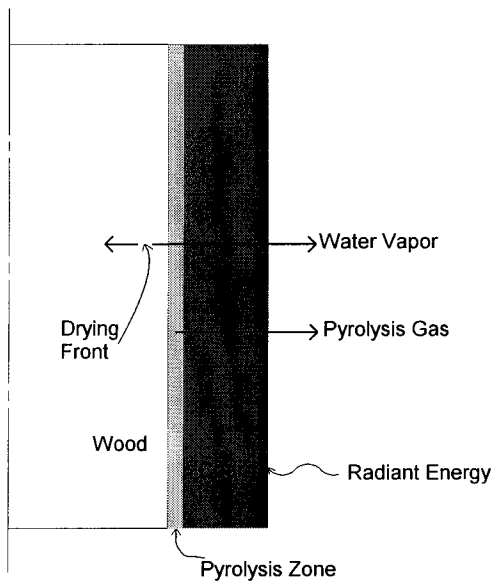

Fig 2. Gas Flow

Fig 2 shows a one-dimensional representation of the response of a wood particle. Radiant energy at the surface of the particle dries and then pyrolyzes the wood near the particle surface, forming a char layer at the surface. Underneath the char layer is a thin zone of active pyrolysis that is only a few millimeters thick. The differences in thermal properties between the wood and char layer cause a temperature gradient across the particle resulting in distinct regions of drying, pyrolysis, and an external char layer. The particle is pressurized from heating of the particle and from the vaporization of moist wood in the drying front, and from the release of pyrolysis gases in the active pyrolysis zone. These gases may travel towards the interior of the particle or be released through the external char layer, depending on the pressurization of the particle.

Wood combustion is a tightly coupled process in which the internal and external particle conditions are closely related. The energy produced by the flame and/or surface reactions heats the particle, releasing more pyrolysis gases and fueling additional external reactions. In a system of particles, the external conditions for each particle are influenced by the performance of neighboring particles. Predicting biomass performance thus requires an understanding of the internal transport mechanisms within the particle, the relevant chemical reactions, and the relation of the individual particle to the surroundings.

2.2 Pyrolysis Regimes

Biomass pyrolysis differs significantly from coal pyrolysis, which has received extensive research. Coal pyrolysis usually involves pulverized coal particles that are injected into a high temperature furnace. These particles are very fine, and a lumped capacitance

model can be used in conjunction with a particle distribution model to predict performance characteristics. In this case, the coal particles can be modeled as isothermal particles that dry, pyrolyze, and then react with external gases. Wood pyrolysis differs substantially from coal pyrolysis in that large pieces of wood generally can not be considered to be an isothermal particle, and internal kinetic and transport properties produce complex pyrolysis characteristics.

Wood pyrolysis can be divided into different thermal regimes (Fig 3, Bryden 1998), based on the relative importance of internal and external heat transfer, and the rate of the pyrolysis reactions. In region 1, pyrolysis is kinetically controlled and the rate of pyrolysis is controlled by the rate of the pyrolysis reactions. The pyrolysis number (Py') is the ratio of the time scale of the heat transfer to the time scale of the pyrolysis reactions.

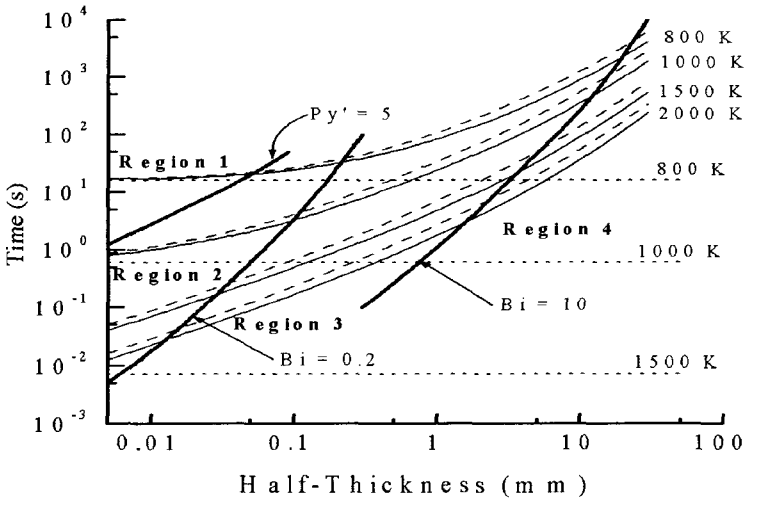

Fig 3. Thermal Regimes

Region 2 shows thermally thin particles, and can be defined by the Biot number. The Biot number is the measure of the rate of external heat transfer to the rate of internal heat transfer ($Bi = \frac{hL}{k}$). For thermally thin particles (Bi < 0.2), the particle is at a nearly constant temperature, because the rate of internal heat transfer is much faster than the rate of external heat transfer. Upon heating, the thermally thin particle will be dried uniformly. Once all of the moisture has been driven from the particle, temperatures rise and pyrolysis happens uniformly throughout the particle. Region 3 represents thermally thick particles (0.2 < Bi < 10), in which the particle can no longer be considered at a constant temperature because internal transfer properties also begin to be important. In the thermal wave regime (Bi > 10), a thermal wave develops near the surface and travels through the particle at a nearly constant velocity. This thermal wave produces a thin pyrolysis layer that is 1-3 mm in size and travels slowly inward towards the cool interior of the particle. The drying front travels ahead of the pyrolysis front, evaporating bound and unbound water within the pores of the wood and sending water vapor through the pyrolysis layer and the hot exterior char surface of the particle, cooling the exterior of the particle as the pyrolysis gases travel outward. Most biomass combustion occurs under thermally thick or thermal wave conditions, where steep temperature gradients exist within a particle. The high Bi number under these conditions indicates that the rate of external heat transfer is higher than the rate of internal heat transfer, and that the rate of internal heat transfer is the limiting mode of heat transfer. Internal transport properties become important under thermally thick and thermal wave conditions. Shrinkage of the structural matrix during pyrolysis, moisture, and internal gas flows all have an important influence on the biomass performance. Important processes in the combustion

of wood include particle drying, pyrolysis, surface and gas phase reactions, char shrinkage, cracking within the char layer, and deformation of the particle.

2.3 Drying

The amount of water within the wood can vary from over 50% on dry mass basis for green wood, to around 5% for fully dried wood. Drying occurs when the wood is heated. Water can exist within the particle as bound water, or as unbound water that can freely move within the particle. Hydrogen bonding within the wood fibers produces a strong attraction for water that holds the adsorbed water with increasing strength as the amount of moisture within the fiber decreases (Skaar 1988). At moisture contents above 30%, all of the fibers become saturated with water, and any additional water is unbound and is free to move (Forest Products Laboratory 1987). The relationship for the energy required to free the bound water was presented (Stanish, Schajer, and Kaythan 1986) by assuming that the heat of sorption decreases quadratically with moisture content and that the heat of sorption at zero moisture content is 40% of the heat of vaporization.

$$\Delta h_{sorp} = 0.4\Delta h_{vap}\left(1-\frac{M_b}{M_{fsp}}\right)^2 \qquad [1]$$

where M_b is the moisture content of the bound water and M_{fsp} is the moisture content at the fiber saturation point.

Until the fiber saturation point is reached, the wood particle swells as the moisture content increases. Additional moisture content beyond the fiber saturation point may cause an increase or decrease in the enclosed cavities of the fiber cells (lumens) depending on the

wood species. It is generally modeled that additional moisture does not cause any further swelling of the wood (Siau 1984).

The rate of evaporation of the unbound water depends on the saturation pressure of the liquid as well as the partial pressure of the water in the wood pores. The water vapor has greater volume than the liquid water, and phase change to water vapor causes an increase in the pressure within the particle. The vaporization of water produces a pressure gradient within the particle that drives liquids and gases out of the actively drying region. During the initial portion of drying, vaporization occurs near the surface of the particle. This vaporization causes a peak pressure near the particle surface. Most of the water vapor and liquids are driven towards the surface of the particle, but some gases are initially driven towards the cooler region at the center of the particle. As the pressure within the particle increases, the inward migration of water vapor from the active drying region will decrease until the pressure gradient causes all of the water vapor to be forced out of the particle. In combustion experiments with logs, Bryden and Ragland (1997) observed that the inward migration of water was significant at low moisture contents (10% to 15% as received), while the inward migration of water was limited at high moisture contents (35% to 45% as received).

2.4 Pyrolysis

The pyrolysis of wood is a chemical restructuring of the cellulose, hemicellulose, and lignin that occurs at elevated temperatures. Cellulose begins to pyrolyze at temperatures between 300°C and 350°C. Hemicellulose is pyrolyzed between 200°C and 300°C and lignin is pyrolyzed between 225°C and 475°C (Shafizadeh and Chin 1997). Volatile species from

the pyrolysis reactions include char, light hydrocarbons, tars, carbon dioxide and carbon monoxide. The volatile species produced by pyrolysis depend on the relative amounts of cellulose, hemicellulose, and lignin, as well as the rate of heating, with higher heating rates producing more volatile products.

In small particles (Bi < 0.2 ; ~ 0.1 mm), the particle will be at a nearly constant temperature. Under thermally thin conditions, the particle dries uniformly and is then pyrolyzed, with the pyrolysis zone also extending throughout particle. As heat is transferred into the particle, the temperatures in the pyrolysis zone rise, and the rate of devolatilization in the pyrolysis zone increases. The extent of the pyrolysis reactions thus becomes a function of the rate of heat transfer to the pyrolysis region, as well as the amount of volatiles remaining in the pyrolysis region. In very small particles, heat is transferred into the pyrolysis region at a much faster rate than the wood can devolatilize, and the pyrolysis reactions are controlled by the kinetic rate of the devolatilization of the wood.

In large particles (> 0.5 cm) under thermal wave conditions, the pyrolysis zone ranges from 1mm to 3mm in length, and separates the unreacted wood from the external char layer (Ragland, Boerger, and Baker 1988). For these particles, the rate of internal heat transfer through the char layer controls the rate of heat transfer to the pyrolysis region. The rate of devolatilization is thus dependent on the rate of internal heat transfer, with pyrolysis occurring at lower temperatures over a longer period of time under thermal wave conditions. The minimum pyrolysis temperature is around 225°C (Chan, Kelbon, and Krieger 1985).

The chemical pathways of the pyrolysis reactions are very complex. In computational models, global reaction rates have been used to simplify the process to reproduce the levels of char, light hydrocarbons, and tars produced in laboratory experiments. The heat of reaction

for wood pyrolysis (Roberts 1971) has been reported to be slightly endothermic (370 kJ/kg) to exothermic (-1700kJ/kg). Smaller particles tend to produce endothermic values while larger samples produce exothermic values. Chan, Kelbon and Krieger (1985) note that the exothermic values in large particles may be due to secondary reactions of the primary pyrolysis products.

2.5 Surface and Gas Phase Reactions

The production of pyrolysis gases within the solid particle are closely related to the resulting surface and gas phase combustion reactions for a solid particle in the presence of free stream oxygen. Combustion reactions are not included in this pyrolysis model, but a brief description has been included because of the importance of pyrolysis gases on the combustion reactions.

Pyrolysis gases will react with oxygen present in the external boundary layer. If the energy released from these gas phase reactions is greater than the energy losses, an attached or unattached flame will develop. The newly released pyrolysis gases shield the particle from both heat and diffusive mass transfer as the gases escape the particle. A sustained flame occurs over only a range of air-to-fuel ratios. The flame reaction can be thought of as a competition between the exothermic combustion reaction and the cooling effect of raw fuel, oxygen, and energy losses to the environment. If the oxygen level is too low, more energy will be used heating the excess fuel than is produced by the exothermic reaction, and the flame will extinguish. If oxygen levels are too high, too much energy is used to heat the excess air and the flame will extinguish. When wood is pyrolyzed, carbon atoms from the wood particle are bonded together in a nested honeycomb structure. This carbon structure

contains small quantities of hydrogen and other impurities. The oxygen atoms, many of the hydrogen atoms, and some of the carbon atoms from the virgin wood escape in the form of pyrolysis gases, which can easily pass through the honeycomb structure of the char layer. Due to the large surface area of the honeycomb structure, and a thermal mass (ρC_p) ratio for solid to gas of 650:1, the pyrolysis gases are quickly heated to the local temperature of the char layer, cooling the char layer as they pass through.

Char combustion occurs when the surface of the char is exposed at elevated temperatures to gases including oxygen, carbon dioxide, hydrogen and water (Laurendeau 1978). The principle global reactions are

$$C + 0.5O_2 \longrightarrow CO \qquad [2]$$
$$C + H_2O \longrightarrow CO + H_2$$
$$C + CO_2 \longrightarrow 2CO$$

The first reaction is the most vigorous, with a kinetic reaction rate approximately 100 times greater than the water and carbon dioxide reactions. When a flame zone is established, the oxygen reacts in the flame zone before it reaches the surface of the char, eliminating the first reaction. The carbon dioxide and water vapor formed within the particle react with the char layer, and the char and carbon dioxide reaction can become the dominant surface reaction in the absence of free-stream oxygen (Makino, Araki, and Mihara 1994).

2.6 Char Shrinkage

A biomass particle is initially composes primarily of carbon, hydrogen and oxygen atoms. Heating of the particle above 225°C causes thermal degradation of the chemical structure of the biomass. Carbon dioxide, carbon monoxide, water, light hydrocarbons and

tars are produced during the pyrolysis reactions. These volatiles leave the solid structure at elevated temperature, leaving behind carbon atoms. The char layer is composed primarily of carbon atoms, along with any impurities that did not escape during the thermal degradation of the particle. As the volatiles are released, the remaining atoms form new molecules and structures. This chemical restructuring produces a more compact structure, and causes an overall shrinkage in the dimensions of the particle. The amount of devolatilization depends on the rate of heating and the amount of time of heating at each location within the particle. Locations near the surface of the particle receive larger heat fluxes than locations within the interior of the particle. Near the surface of the particle, more volatiles will be released, and there will be more shrinkage of the char layer. The overall shrinkage of the particle depends on the transient rate of heating at every location within the particle. Shrinkage is a function of particle size, shape, external heat flux, and material properties within the particle.

2.7 Deformation and Cracking

The release of volatile gases and evaporation of liquid water causes pressurization within the particle. In moist particles with combustion level fluxes, there are high enough pressures to produce significant stresses within the solid particle. These stresses can become high enough to cause permanent deformation of the solid particle. This plastic deformation will cause the shape of the particle to change permanently. While pressurization of the particle can cause permanent deformation, or even explosion of the solid particle, most of the stresses within the solid particle are produced by the shrinkage of the char layer. Heat fluxes vary within the particle, and regions of the particle will undergo different amounts of shrinkage. This causes large stresses within the particle that can only be relieved by plastic

deformation or cracking of the particle. At the locations where these stresses are the highest, structures can be pulled apart, causing a crack to form near the surface of the particle. This initial crack formation is likely to occur at the surface in regions of high stress, and may be facilitated by the anisotropic nature of the particle and the path of water vapor escaping the particle, where transport vesicles may cause local stress concentrations. The formation of the crack relieves stress in the region near the crack. The formation of a crack causes a local stress concentration, and stresses produced by additional shrinkage are relieved by the energy used to cause additional crack growth. In this manner, cracks are formed during combustion to relieve stresses produced by the cracking and the pressurization of the particle. The size and spacing of theses cracks depend on the transient nature of pyrolysis, and will depend on the size, shape, and material properties of the biomass, as well as the external rate of heating.

2.8 Computational Modeling

Currently, the design of biomass power systems are based on experimental data with a limited amount of thermodynamic analysis. When numerical models are used, researchers typically take experimental data for a specific situation, and then produce a numerical model that adequately predicts particle devolatilization time for that situation. The problem with using this procedure is that the numerical results only apply to situations for which the experimental correlations apply, and that we already have empirical information for these conditions. These models do not account for all of the important phenomena during combustion. Many of these models are also limited because they cannot predict the products of pyrolysis. Recent models are more complex and have attempted to apply conservation equations with as few assumptions as possible to provide models that can be experimentally

validated, and can then be applied to multiple situations and used to predict the pyrolysis conditions within the particle. There is a need for more complex computational models that can adequately predict a wide range of combustion conditions. The computational models are limited by the availability of property data under combustion conditions, property variations from species to species, and the use of appropriate chemical reaction schemes. To date, the simplifying assumptions within the computational models have limited the usefulness of computational models because they cannot adequately model all of the combustion conditions, such as three-dimensional particle geometries, moisture within the particle, shrinkage of the solid matrix, cracking and deformation of the particle, and the particle's interaction with the surrounding flow field. Most computational models have been limited to generalized trends, rather than specific results that can improve combustion characteristics for a specific situation.

As the speed of computers has increased, numerical models of wood combustion have become more and more detailed, removing simplifying assumptions and more accurately depicting biomass combustion. Bamford, Crank, and Melan presented the first wood combustion model in 1946. This one-dimensional model was used to predict the rate of pyrolysis in a flat piece of wood that was exposed to a gas flame on both sides. The energy equation, shown below, consisted of conduction and a pyrolysis source term and was used to find the temperature profile as a function of time within the wood.

$$\lambda \frac{\partial^2 T}{\partial x^2} - \Delta h_{pyr} \frac{\partial(\rho - \rho_{C,\infty})}{\partial t} = c\rho_0 \frac{\partial T}{\partial t} \qquad [3]$$

Pyrolysis was modeled using a single exothermic reaction using a single Arrhenius relationship

$$-\frac{\partial(\rho-\rho_{C,\infty})}{\partial t}=(\rho-\rho_{C,\infty})A\exp(-E/RT) \qquad [4]$$

Subsequent models have built upon the Bamford model. Tinney used differing thermal properties of char and wood in 1965. In 1969, Matsumoto, Fujiwara, and Kondo used the Bamford model on plastics that included variable material properties that depend on the progression of the charring reaction. This model also assumed that volatile products were in local thermal equilibrium with the char layer. Kung applied this model to wood in 1972 and Kansa, Perlee, and Chaiken accounted for gas flow within the particle in 1977 by solving the momentum equation within the particle assuming Darcy gas flow.

More recent models are considered detailed computational models, and include work by Di Blasi (1993a,1993b,1996,1998), Melaaen and Gronli (1997), Bryden (1998), Bryden and Ragland (2001), and Hagge and Bryden (2002). These models include Darcy flow within the particle, gas and solid phase continuity, and conservation of energy within the particle. In these models, pyrolysis occurs using both primary and secondary reaction schemes. The competitive pyrolysis schemes allow for variable product compositions that depend on the conditions under which pyrolysis occurs. Di Blasi presented a one-dimensional model for wood that included char shrinkage (1996). Melaaen and Gronli (1997) presented a one-dimensional model for wet wood in which liquid water moves within the particle as a result of the pressure gradient within the wood particle. Bryden (1998) presented a model that

couples the surface and external gas phase reactions to the pyrolysis model for a one-dimensional particle subjected to a stagnation point flow field. Bryden (1998), Bryden and Ragland (2001), and Hagge and Bryden (2001) provided models that include char shrinkage and vaporization and recondensation of moisture within the particle.

There are a limited number of models that compute pyrolysis is more than one dimension and a limited number of situations that have been studied with existing two-dimensional models. Di Blasi (1994) produced a simplified two-dimensional model that neglects Darcy flow and was used for flame-spread calculations, and a two-dimensional model for cellulose pyrolysis that includes Darcy flow (1998). This thesis builds upon the equation set, shrinkage, and moisture model that can be found in Bryden (1998). These equations are applied to a two-dimensional model for pyrolysis for a range of particle sizes and temperatures.

The more detailed combustion models solve for conservation of energy, momentum, mass, and species within the reacting particle. These models generally assume one-dimensional heat and mass transfer. Although thermal conductivity can vary by a factor of 3 and permeability can vary by a factor of 10^4, one-dimensional modeling has been used almost exclusively because of the complexity of the biomass combustion system. These models also have several other similarities. Gas flow in the interior of the particle is modeled according to Darcy flow, neglecting the inertial terms of the momentum equation. Diffusive transport of species within the pores is neglected (Chan, Kelbon, and Krieger 1985). The pyrolysis gases are assumed to be in local thermal equilibrium with the solid as they travel through the particle, based on an evaluation of the Peclet number. Some of these models account for water within the solid particle (Melaaen and Gronli 1987, Bryden 1998, Bryden

and Ragland 2001, Hagge and Bryden 2002) and/or shrinkage during the pyrolysis reactions (Di Blasi 1996, Bryden 1998, Hagge and Bryden 2002). Most models do not account for recondensation of volatile species, cracking of the solid particle, or the char combustion and gasification reactions. To date, no model can account for all of these important phenomena, even on a one-dimensional basis, because of the difficulty and the amount of computational work required to solve the resulting system of equations. The cracking that occurs within the particle has not been adequately addressed by any of these models. The rapid build up of pyrolysis gases and the shrinkage of the particle cause stress within the particle. Stresses can only be relieved by the permanent deformation of the particle and the cracking of the solid matrix. Cracking creates a much larger surface area and allows internal gases to escape more easily. Cracking allows radiant external energy to go directly from the combustion reactions to the interior of the particle. Hadiwinata (2004) presented a two dimensional numerical model without gas flow for a fixed crack geometries that demonstrated that cracking can double the rate of internal heat transfer within a particle. Cracking has not been adequately modeled in any wood combustion model, because of the increased complexity of the model and the fact that these cracks are inherently a multi-dimensional process.

Some work has been done on two-dimensional and even three-dimensional models, although most of these models do not contain all of the conservation equations. These simplified models are typically limited to predicting pyrolysis times for the specific situation for which they were validated. Di Blasi (1994) presented a two-dimensional model that accounted for the conservation equations for smoldering combustion of an insulating cellulosic bed using a global reaction scheme. This two-dimensional model has been used with the Broido-Shafizadeh scheme to model two-dimensional aspects of cellulose pyrolysis

and combustion. These two-dimensional studies for cellulose have shown that the anisotropic transport properties can significantly alter particle performance.

One-dimensional models are good for predicting one-dimensional pyrolysis situations, such as radiant heat flux to a large, flat surface. Multi-dimensional models are needed whenever the geometry of the biomass or the pyrolysis system becomes important. For a single particle subjected to radiant heat flux from all sides, using the correct particle volume and surface area is important for all but the kinetically controlled pyrolysis regime, and can be considered a multi-dimensional situation. Multi-dimensional situations also include situations that might traditionally be considered one-dimensional, such as the pyrolysis of a large flat board where deformation and cracking of the slab significantly alter particle shape and external boundary conditions.

2.9 Pyrolysis Reaction Modeling

Researchers have used a variety of ways to represent the pyrolysis reactions, moisture content, and shrinkage of the char matrix in their numerical models. Reviews of the pyrolysis kinetics have been presented by Di Blasi (1993) and Antal (1995). The simplest pyrolysis reaction schemes consist of a single irreversible reaction that produces a fixed ratio of char and unspecified pyrolysis gases. Other schemes divide the pyrolysis products into char, gases and tars. The limitation of this type of model is that these schemes do not recognize the variation in pyrolysis reaction pathways that occur when different heating rates and temperatures are used. To account for variable products of pyrolysis, multiple competitive single step reactions have been used (Nunn et al. 1985, Samolada and Vasalos 1991, Hajaligol et al. 1982). These schemes typically compare well with experimental

measurements of small particles in which pyrolysis gas residence times and secondary reactions are small.

Chan, Kelbon, and Krieger presented a competitive, multi-step pyrolysis model in 1985 that did not include conservation of momentum within the particle. Experiments for wood particles vary the particle size and external temperature and measure the relative amount of tar, light hydrocarbons and char resulting from pyrolysis. These experiments for wood particles show that for small particles the tar production is several times larger than the production of light hydrocarbons. For larger particles at elevated temperatures, tar production initially dominates, but at some time the measured tar production drops to near zero, with a corresponding increase in light hydrocarbon production. This has led researchers to believe that the tars initially produced by the primary pyrolysis reactions can be broken down into light hydrocarbons, and that secondary reactions need to be included in pyrolysis reaction schemes to match these observations. The amount of tar that is broken down depends on the reaction rate as well as the amount of time the tars are within the particle. The net products of pyrolysis depend on the primary production of pyrolysis gases as well as the volatile residence times.

The most complete pyrolysis models use multiple, two-step reactions and account for volatile residence times. There are a variety of primary reactions schemes that decompose wood into char, light hydrocarbons, and intermediates. These intermediates may include a solid product, a tarry liquid, or a tar vapor. Some of these schemes divide the biomass into the respective quantities of cellulose, hemicellulose and lignin (Kuofopanos, Mashio, and Lucchesi 1989), while others consider the biomass to be a homogenous material. When wood is considered to be a homogenous material, the wood will decompose into various products

through multiple primary reactions. The most common pyrolysis primary reaction scheme (Shafizadeh and Chin 1997, Thurner and Mann 1981, Chan, Kelbon and Krieger 1985, Nunn et al. 1985, Font et al. 1990, Kuofoopanos et al. 1991) is

$$wood \xrightarrow{k1} tar \qquad [5]$$

$$wood \xrightarrow{k2} light\ gas$$

$$wood \xrightarrow{k3} char$$

In the secondary reactions, the products from the primary scheme react to form the final products of pyrolysis. These reactions may include tar decomposition to light gases (Liden, Berruti, and Scott 1988), light gases and solid residue (Kosstrin 1980), or light gases and a refractory residual (Diebold 1985). In her review, Di Blasi (1993) recommends the following secondary reactions that include tar cracking to form light gases and tar repolymerization to form char.

$$tar \xrightarrow{k4} light\ gas \qquad [6]$$

$$tar \xrightarrow{k5} char$$

2.10 Drying Modeling

The most recent models include both moisture content within the particle, and shrinkage of the solid matrix during pyrolyzation. There have been four basic ways to model the drying of wood under combustion heat fluxes. The simplest of these models is a thermal model in which the drying front is assumed to be infinitely thin and an energy sink at 100°C accounts for the heat of vaporization (Simmons 1983, Ragland, Boerger and Baker 1988,

Saastamoinen 1993). In this type of model, the movement of the drying front can be determined from a simple energy balance. A second method (Chan, Kelbon, and Krieger 1985) models the drying of wood as an additional chemical reaction using an Arrhenius expression. This method has been used in addition to an algebraic expression that is based on the gas fluxes within the particle (Bryden and Ragland, 2002) to account for recondensation. A third method (Alves and Figueiredo, 1989) uses an algebraic expression for temperature (> 100°C) as a function of moisture content to describe the equilibrium moisture content in wood in an atmosphere of superheated steam. The fourth method (Ouelhazi, Arnaud, and Fohr 1992) is based on research and numerical modeling of low temperature (< 200°C) drying of wood. In this method, the unbound water and gas movement within the wood are modeled using a modified version of Darcy's law, while the bound water movement is modeled using a diffusion expression. The evaporation of water is driven by the saturation pressure of the liquid water and the partial pressure of the water vapor. A one-dimensional wood pyrolysis model using this formulation has been presented (Melaaen and Gronli 1997).

Each of these drying models has advantages and disadvantages, and none has a clear advantage over the others. The thermal model is simple and easy to implement numerically, but it has the disadvantage that it reduces the drying front to an infinitely thin region within the biomass particle and that the recondensation of water within the cooler regions of the wood is neglected. In the thermal model, the temperature within the particle rises to 100°C, plateaus, and then resumes the temperature rise. One advantage of the kinetic scheme is that temperatures rise continuously into and out of the drying plateau, which matches experimental results. The kinetic scheme can easily be implemented in a pyrolysis scheme as an additional Arrhenius relationship in a numerical code that handles many of these.

Recondensation can also be presented as an additional algebraic relationship. The primary disadvantage of using an Arrhenius relationship for drying is that, while it can be shown that the diffusion model can be simplified to the kinetic model, many differing physical phenomena are lumped into a single expression. Additionally, only one-way coupling is maintained between the drying rate and the pressure evolution where the drying rate is set by the temperature and water density, but not by the pressure. The algebraic model does not account for drying at temperatures less than 100°C, and is only applicable to materials with moisture contents of less than 14.4%, using the thermal model above this limit. It is unlikely that equilibrium conditions exist within a moist biomass particle exposed to combustion level fluxes. The diffusion model accounts for both drying and recondensation within the wood. The recondensation is accounted for by assuming that the partial pressure of the water is equal to the equilibrium pressure. While the diffusion model accounts for much of the physical phenomena, it has been verified only for low temperature wood drying and not at combustion level fluxes. Its primary disadvantage is that the pressure wave is tightly coupled to the drying rate, and areas which are not addressed in current models such as cracking and the multi-dimensional aspects of water movement can have significant effects on the drying rate, recondensation, and temperature profile.

Results from a detailed pyrolysis model using an Arrhenius relationship (Hagge and Bryden 2002) are shown in Fig 4 to demonstrate how moisture affects particle performance. The presence of moisture within the particle affects the internal transport properties during pyrolysis. The additional energy required to evaporate the water within the particle causes increased pyrolysis times for moist particles. The evaporation of moisture in the drying front causes increased gas fluxes across the surface of the particle. These gases cool the surface.

For a fixed temperature external source, the cooler surface temperature causes increased external heat fluxes. As the moisture content is increased, the additional cooling of the surface produces higher external fluxes that offset some of the additional heat required to evaporate the moisture. This can be seen by the fact that 10% moisture causes a 20% increase in pyrolysis times, 20% moisture causes an increase of 38%, and 30% moisture will cause an increase of 54%. The cooler surface in moist particles also has a small effect on net products of pyrolysis by reducing the rate of the secondary conversion of tar. The temperature profile and gas fluxes are shown in for a 1 mm particle at 1400K in Figure 4.

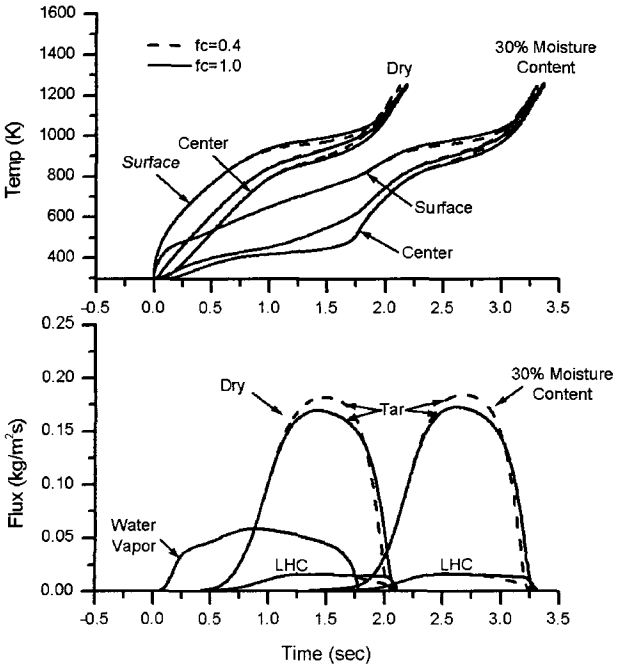

Fig 4. Effect of 30% Moisture Content on a 1mm Particle at 1400K

Moisture within the particle reduces the surface temperature of the particle and the temperature at the center of the particle. At the surface of the particle, there is a more gradual

increase in surface temperature because of the cooling effect of water vapor. The center temperature profile shows that there is a large delay before enough energy reaches the center of the particle to vaporize the water. The center temperature of the wet particle heats up more quickly than a dry particle once the thermal capacity of the water has been removed.

2.11 Shrinkage Modeling

Shrinkage can occur because of a loss of water mass or as a result of the pyrolysis reactions. Shrinkage due to a loss of water mass typically accounts for a 5 to 10 percent reduction in particle size (Forest Products Laboratory, 1987). Shrinkage occurs in the char layer during the pyrolysis reactions because of a rearrangement of chemical bonds and the coalescence of graphite nuclei within the biomass particle. The amount of char shrinkage is a function of wood species, heat flux, and temperature. Varying compositions of lignin, cellulose, hemicellulose, and other organic and inorganic materials result in different amounts of shrinkage for different species. The amount of shrinkage is also dependent on grain orientation. Char shrinkage increases as the temperature increases and also increases with the amount of time at a given temperature. Roughly one-half of the char shrinkage occurs during the rapid devolatilization of the biomass, with continued chemical rearrangement following the devolatilization process.

Four researchers have presented pyrolysis shrinkage models. Villermaux et al. (1986) presented a simplified combustion model for wood in which wood was modeled as a homogeneous particle with a constant density. The constant particle density was used in conjunction with a single first order reaction to determine a surface shrinkage rate. This simplified combustion model does not include separate char and wood species, internal flow,

or competitive pyrolysis reactions. Parker (1988) has presented a model that accounts for shrinkage by giving a prescribed change in geometry at the surface of the particle. Di Blasi (1996) presented a more complete shrinkage model that uses three parameters to account for solid shrinkage, changes in volatile fraction, and changes in wood porosity. Bryden (1998) presented a shrinkage model using a single shrinkage parameter.

Each of these models has strengths and weaknesses. Parker's model accounts for shrinkage by changing the particle geometry at the exterior of the particle. One benefit of this model is that differing amounts of shrinkage in the tangential and radial direction can be specified, but there is no experimental basis for the proposed geometry. Parker does not account for the different physical properties of char and wood (Parker, 1988). The change in geometry occurs at the location where 10% of the original mass of wood has been lost. The instantaneous change from biomass to char and the consequent instantaneous change in thickness does not allow for the continuous progression of char and biomass composition. Resistance to internal flow is not included, and the product yields cannot be determined. Di Blasi (1996) presents a more complete shrinkage model for pyrolysis that accounts for heat, momentum, and mass transport. Internal gas flow is accounted for using Darcy flow with the permeability of the medium expressed as a function of char and wood content. With internal flow and a two-step secondary reaction scheme, Di Blasi was able to predict variable product outputs. This model uses a continuous change in properties that is based on the respective amounts of char and wood at a given location using a linear progression variable. This shrinkage model does not include moisture within the particle. The primary disadvantage of this model is that three separate parameters are needed to model particle shrinkage. The model presented by Bryden (1998) uses a single shrinkage parameter that can easily be

obtained from experimental measurements. In Bryden's work, shrinkage is defined as the final dimension divided by the original dimension.

$$f_C = \frac{L_{final}}{L_o} \qquad [7]$$

Experimental data has shown that shrinkage can range from $f_C = 0.4$ to $f_C = 1.0$ (no shrinkage). The shrinkage occurs according to particle devolatilization, where the length of each edge can be calculated as

$$L = f_C L_O + (1 - f_C) \cdot \eta \; L_O \qquad [8]$$

where η is the mass of wood divided by the initial mass of wood in each finite volume. The advantage of this scheme is the ease with which shrinkage factors can be calculated. The disadvantage of all these schemes is that shrinkage parameters have to be specified for each case because shrinkage varies with heat flux and time.

Shrinkage has been shown to dramatically alter pyrolysis gas fluxes in a one-dimensional model, and can reduce pyrolysis times by over 40% in the thermal wave regime (Hagge and Bryden, 2002). In this previous study, the effect of shrinkage was shown within the thermally thin, thermally thick, and thermal wave combustion regimes for a one-dimensional particle. Results from this study are presented to show the current understanding of the effects of shrinkage.

Fig 5 and 6 shows one-dimensional particle temperature and pyrolysis gas fluxes under thermally thin conditions (Bi < 0.2) for a 0.1mm particle at 1000K. The low Bi number under thermally thin conditions indicates that the rate of external heat transfer is much smaller than the rate of internal heat transfer. The rate of external heat transfer is the limiting step, and controls the devolatilization of the biomass particle. Increasing the rate of internal

heat transfer does not change the particles performance, resulting in nearly identical temperatures and gas fluxes for the shrinking and non-shrinking particles.

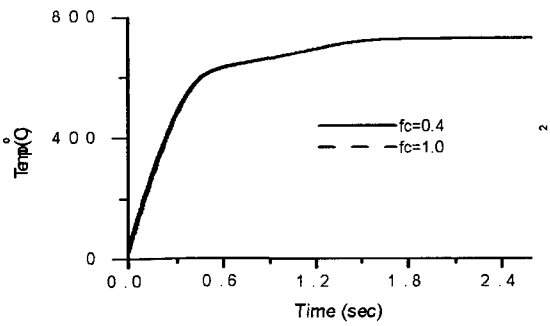

Fig 5. Effect of Shrinkage on a Thermally Thin Temperature Profile

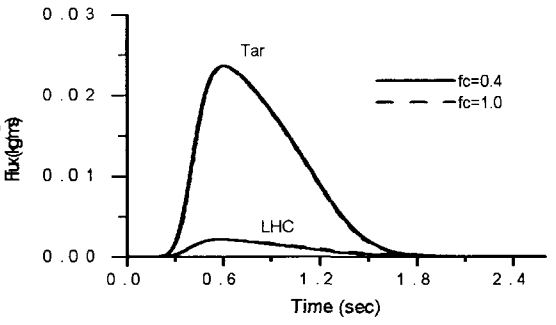

Fig 6. Effect of Shrinkage on a Thermally Thin Gas Flux Profile

In the thermally thick regime ($0.2 \leq Bi \leq 10$), the particle is no longer at a constant temperature. A 1 mm particle at 1600K is shown in Fig 7 and 8. Temperature gradients exist within the particle, but there is only a small difference between the shrinking and non-

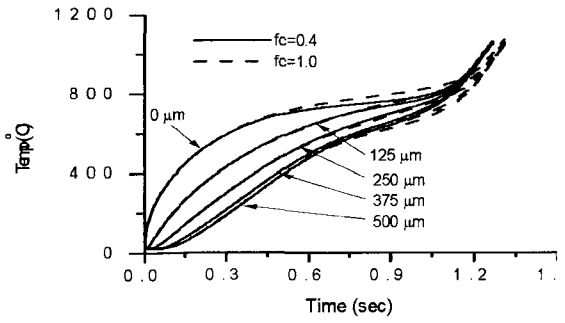

Fig 7. Effect of Shrinkage on a Thermally Thick Temperature Profile

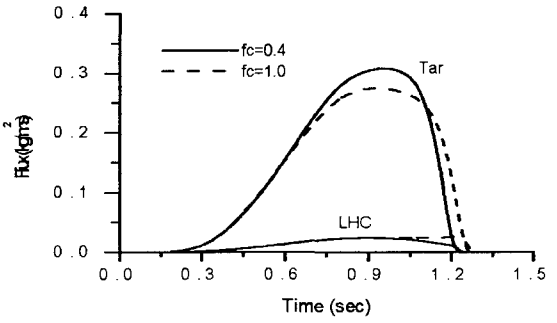

Fig 8. Effect of Shrinkage on a Thermally Thick Gas Flux Profile

shrinking case. This happens because the devolatilization and chemical conversion of the wood is happening throughout the whole particle. Shrinkage increases the rate of heat transfer at the surface of the particle only after there has been significant devolatilization at the surface. In the thermally thick case, the complete devolatilization of the surface happens relatively late in the life of the particle. There are only temperature differences during the latter part of pyrolysis, when most of the particle has already been pyrolyzed. As a result, shrinkage has a small impact on particle temperatures and gas fluxes under thermally thick combustion.

A 1 cm particle at 1600K is in the thermal wave regime, (Fig 9 and 10) a thin pyrolysis front develops that travels slowly from the surface of the particle towards the interior. An external char layer develops as the pyrolysis front moves inward. For the non-shrinking particle, a larger external char layer develops at the surface of the particle and shields the interior of the particle from the external heat source, causing increased surface temperatures.

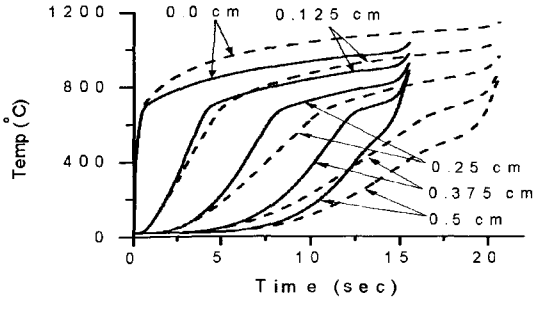

Fig 9. Effect of Shrinkage on a Thermal Wave Temperature Profile

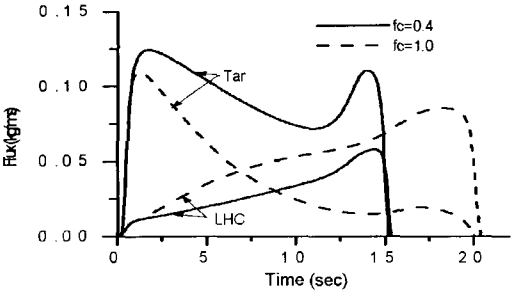

Fig 10. Effect of Shrinkage on a Thermal Wave Gas Flux Profile

The shielding of the surface causes lowered temperatures in the interior of the particle where the wood is rapidly devolatilizing. The increased surface temperatures of the non-shrinking particle reduce the rate of external heat transfer, while the decrease in temperatures within the pyrolysis front reduces the gas fluxes that would otherwise cool the surface of the particle. Shrinking particles have the opposite affect, and are characterized by lower surface temperatures and higher internal temperatures in the actively pyrolyzing region of the particle. Shrinkage thus speeds up the pyrolysis process both by raising the temperature of the pyrolysis region with the increased rate of internal heat transfer, and by increasing the external rate of heat transfer to the surface of the particle.

In the thermal wave regime, the secondary pyrolysis reactions also become important. The secondary conversion of tar to light hydrocarbons is higher in the non-shrinking particle. The lowered rate of pyrolysis gas production produces a smaller pressure gradient and reduces gas velocities within the particle. This combined with the larger external char layer and the increased surface char temperatures causes a higher rate of secondary reactions in the non-shrinking particle. The shrinking particle produces slightly more primary tar, as the tar reaction is the preferred primary reaction within the elevated temperatures of the pyrolysis region. Most of the difference in final gas composition (Fig 11 and 12) is due to the fact that the shrinking particle allows more of the primary tar to escape the particle without being converted to light hydrocarbons. Shrinking particles produce more tar and less light hydrocarbons than non-shrinking particles.

Shrinkage and moisture have additional importance that cannot be studied in one-dimensional models. Shrinkage of the solid matrix causes stresses that can only be relieved by the cracking of the solid matrix. Green wood or woods with lots of tar sometimes explode

when placed on a fire. The rapid evaporation of moisture within the particle causes much higher pressures within the particle that may also be relieved by cracking. These effects remain unstudied, but it is clear that any model that attempts to account for cracking of the solid matrix must also include char shrinkage and moisture within the particle.

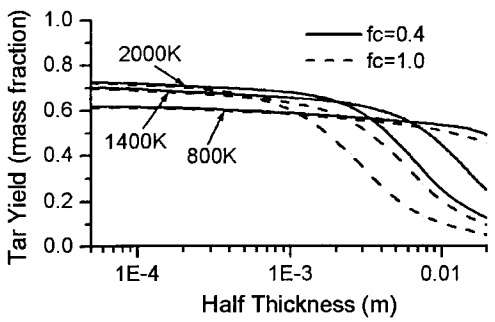

Fig 11. Effect of Shrinkage on Total Tar Production

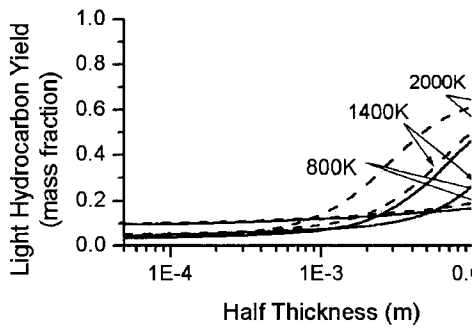

Fig 12. Effect of Shrinkage on Total Light Hydrocarbon Production

2.12 Properties of Wood

Wood is composed of cellulose, hemicellulose, and lignin as well as a small amount of extractives, and ash forming materials. The amount of each material depends on the species. Cellulose typically accounts for approximately 50% of the dry weight of the wood. The cellulose ($C_6H_{10}O_5$) is a linear polymer that forms the structural component of the cell and is composed of a condensed polymer of glucose ($C_6H_{12}O_6$). The monomers contain hydroxyl groups that give cellulose a high affinity for water. Extractives account for 5% to 10% of the dry weight of the wood, while ash content is less than 1% within the wood particle. The extractives are additional materials such as gums or oils that give the wood

additional properties. The ash consists of calcium, potassium, magnesium, manganese and several oxides and is composed from minerals that have been drawn into the tree as water and is brought in by the root system. The rest of the particle is composed of hemicellulose and lignin, with the amount varying from species to species. Hemicellulose also contains bonded polymers, but is made from sugars other than glucose. Lignin ($C_{40}H_{44}0_6$) has a three dimensional structure which preserves the structure of the wood fiber, holding the cellulose and hemicellulose in a stable structure. The structure of a wood particle has evolved to store and transport materials that are essential to the survival of a living organism. The basic building blocks of wood are long narrow fibers that can range from 1 mm to 8 mm in length, with diameters varying from 20 to 30 μm. These fibers are used to transport and store moisture, sap, and other materials in softwoods. The fibers are aligned in the longitudinal direction, with the function of transporting water and minerals up through the tree from the ground. As a result, transport properties are greater in the longitudinal direction.

Wood species are usually divided into softwoods and hardwoods. Softwoods and hardwoods have different chemical composition and structural properties. Hardwoods loose their foliage annually while softwoods are conifers. Softwood fibers range from 3 mm to 8 mm and are typically much longer than hardwood fibers, which average about 1 mm in length. The smaller fibers are much stronger and explain why they are classified as hardwoods. Softwoods typically contain 23% to 33% lignin by weight while hardwoods are composed of 16% to 25% lignin. The additional lignin in softwoods serves to hold the much larger fibers together. Softwoods usually contain higher amounts of extractives while hardwoods contain additional cells called *pores* that have a larger diameter (20 to 300 μm)

and that are used for the movement of sap. Additional cells called *rays* are used in both hardwoods and softwoods to transport sap in the radial direction.

The combustion properties of wood are usually correlated to the proximate analysis, ultimate analysis, and the higher heating value of dried wood. The proximate analysis determines weight content of the volatile, char, and ash, while the ultimate analysis determines the weight fraction of carbon, hydrogen, oxygen, nitrogen, and sulfur. The volatile yield increases with temperature and heat flux by increasing the number of chemical bonds that are broken within the wood particle. The ultimate analysis remains fairly constant for wood, with slightly higher amounts of carbon in softwoods due to the increased carbon content in the lignin and the extractives. Wood consists of approximately 6% hydrogen (Petura 1979), 40% to 44% oxygen, and trace amounts of nitrogen and sulfur (Ragland, Aerts, and Baker 1991), and close to 50% carbon remaining. The higher heating value increases with carbon and hydrogen content, while decreasing with oxygen, nitrogen and ash. The respective quantities of cellulose, hemicellulose, lignin, extractives and ash will thus affect the higher heating value for a given species of wood. The higher heating value for softwoods varies from 20 to 22 MJ/kg while hardwoods vary from 19 to 21 MJ/kg. Reed (1987) presented the following empirical relationship for HHV based on percent weight composition of carbon, hydrogen, oxygen, nitrogen, and ash:

$$HHV = 0.341C + 1.322H - 0.12(O + N) - 0.153A + 0.0686 \text{ MJ / kg} \qquad [9]$$

This empirical relationship has proved applicable for a wide range of particles including biomass, charcoals, pyrolysis oils, and tars.

Chapter 3

Mathematical Description of Pyrolysis

The system of equations is developed for the computational model. This equation set describes the performance of a particle of wood undergoing pyrolysis. The particle is discretized into smaller regions, and the equations are applied to each smaller region. The mathematical system of equations is true regardless of the discretization of the computational domain. The discretization of the computational domain and the solution procedures are discussed in Chapter 4.

The physical particle is divided into smaller finite volumes. Each of these finite volumes consists initially of a solid region filled with virgin wood, bound liquid water, and gaseous regions that are initially filled with water vapor. The fraction of the finite volume occupied by gases increases as the amount of wood decreases during pyrolysis, and as water is vaporized from the particle. Two-dimensional wood pyrolysis can be described using a set of pyrolysis reactions and the differential equations for conservation of mass, species, momentum, and energy applied to the solid and gaseous regions. The conservation equations are

Conservation of Total Gas Mass

$$\frac{\partial m_G}{\partial t} + \oint \rho_G \vec{V} \bullet \hat{n} = \dot{\omega}_G \qquad [10]$$

Conservation of Momentum

$$\vec{V} = -\frac{\phi}{\mu}\frac{\partial p}{\partial \hat{n}} \qquad [11]$$

Conservation of Species

$$\frac{\partial m_I}{\partial t} + \oint \rho_I X_I \vec{V} \bullet \hat{n} = \dot{\omega}_I \qquad [12]$$

Conservation of Energy

$$\oint k \frac{\partial T}{\partial \hat{n}} + \oint h(T_\infty - T) + \oint \sigma\left(T_\infty^4 - T^4\right) - \oint \rho_G V c_G (T_n - T_i) + \sum \Delta h_I^o \dot{\omega}_I = \frac{\partial E}{\partial t} \qquad [13]$$

Conservation of Wood Mass

$$\frac{\partial m_W}{\partial t} = \dot{\omega}_W \qquad [14]$$

Conservation of Char Mass

$$\frac{\partial m_C}{\partial t} = \dot{\omega}_C \qquad [15]$$

Ideal Gas Equation

$$\rho_G = \frac{pW_G}{RT} \qquad [16]$$

Solid Production terms

$$\dot{\omega}_W = -(k_1 + k_2 + k_3) m_W \qquad [17]$$

$$\dot{\omega}_C = m_W k_3 + m_T k_5 \qquad [18]$$

Gas Production Terms

$$\dot{\omega}_G = m_W (k_1 + k_2) - m_T k_5 + m_M k_6 \qquad [19]$$

$$\dot{\omega}_T = m_W k_1 - m_T (k_4 + k_5) \qquad [20]$$

$$\dot{\omega}_{LG} = m_w k_2 + m_T k_4 \qquad [21]$$

$$\dot{\omega}_V = m_M k_6 \qquad [22]$$

The surface integrals indicate that indicate that the quantities are integrated over the surface of the particle. The gas velocity ($\vec{V}$) is out of the finite volume by convention and the $\hat{n}$ indicates a direction that is outward normal to the surface of the finite volume. V without the vector indicates the scalar value of the velocity in the $\hat{n}$ direction. Subscript I indicates a particular gas species. Subscript i indicates the finite volume for which the conservation equations are being evaluated and subscript n refers to the finite volume sharing a surface with finite volume i. The quantities ρ and X are the total gas density and the species gas mass fraction and may be evaluated at i or n depending on whether gas flow is into or out of the finite volume. Additional subscript notations are explained in the derivation of the conservation equations.

3.1 Pyrolysis Reactions

The pyrolysis scheme presented in Chapter 2 is repeated for use with the relevant conservation equations.

$$wood \xrightarrow{k1} tar$$

$$wood \xrightarrow{k2} light\ gas \qquad [5]$$

$$wood \xrightarrow{k3} char$$

$$tar \xrightarrow{k4} light\ gas \qquad [6]$$

$$tar \xrightarrow{k5} char$$

3.2 Conservation of Mass

Conservation of mass states that matter can not be created or destroyed, and that the total mass of a system remains constant unless matter enters or leaves the finite volume. The net rate of mass accumulation is defined as the rate of mass entering minus the rate of mass leaving the finite volume.

$$\frac{\partial m}{\partial t} = \dot{m}_{in} - \dot{m}_{out} \qquad [23]$$

Solids such as wood do not cross the boundaries of the finite volume, and the rate of loss the wood mass with respect to time must be equal to the rate of primary char and pyrolysis gas production.

$$\frac{\partial m_W}{\partial t} = \dot{\omega}_W = -(k_1 + k_2 + k_3)m_W \qquad [17]$$

where m_W is the mass of wood and k is the rate of reaction and subscripts 1-3 refer to the first three pyrolysis reactions (Eq 5) that convert wood to pyrolysis products. The negative sign indicates that the destruction of wood results in the creation of the pyrolysis products.

The rate of production of char mass must be equal to the rate of char mass produced by the primary pyrolysis reaction and the rate of char production from repolymerization of gaseous tar within the pores.

$$\frac{\partial m_C}{\partial t} = \dot{\omega}_C = k_3 m_W + k_5 m_T \qquad [18]$$

where m_C is the mass of char, m_T is the mass of tar, k_3 is the rate of reaction for conversion of wood to char and k_5 is the reaction rate of repolymerization of gaseous tar to char.

Conservation of mass must also apply for the total gas mass, where gases can leave or enter a finite volume.

$$\frac{\partial m_G}{\partial t} = \dot{m}_{G,in} - \dot{m}_{G,out} + \dot{\omega}_G \qquad [24]$$

where m_G is the total gas mass within the finite volume and subscript G refers to the total gas. The total gas production can be found by combining the gas terms from the primary and secondary pyrolysis set, as well as the moisture vaporization equation.

$$\dot{\omega}_G = m_W (k_1 + k_2) - m_T k_5 + m_M k_6 \qquad [19]$$

The rate of mass flow for the total gas can be computed from the density of the gas, the gas velocity, and the area through which the gas flows.

$$\dot{m}_{in} = \rho_{G,n} L V_{in} \qquad [25]$$

The density of incoming gases is equal to the gas density of the neighboring finite volume ($\rho_{G,n}$). For a two-dimensional model, the area is the length (L) of the shared side multiplied by a unit depth. The incoming velocity (V_{in}) is computed from solution of the momentum equation.

The conservation equations can be written more concisely as volume and surface integrals. The surface lengths are implied in the surface integrals as the quantities are evaluated over the entire surface. This code uses constant properties within a finite volume so the volume integrals are not shown. Quantities such as temperature, density and gas production rates are equal across the entire finite volume. Resistance to flow, thermal conductivity, and shrinkage are the only quantities that are evaluated at a surface as the average of the two neighboring cells, as is discussed in Chapter 4.

3.3 Conservation of Momentum

The gases in the particle move though the particle according to Darcy flow

$$V_{out} = -\frac{\phi}{\mu}\frac{\partial p}{\partial \hat{n}} \qquad [11]$$

where ϕ is the permeability of the particle, and μ is the viscosity of the gas and $\frac{\partial p}{\partial \hat{n}}$ is the pressure gradient normal to the surface. The inertial terms in the momentum equation are neglected, and the gas velocities across each surface can be directly computed from the pressure gradient across that surface, the permeability of the solid, and the viscosity of the gas. Gas flow between two finite volumes is calculated using the average resistance to flow $\left(\frac{\phi}{\mu}\right)$ between two finite volumes.

In solving for the gas flow, additional relationships are needed. The ideal gas equation is used in the solution of the gas flow.

$$\rho_G = \frac{pW_G}{RT} \qquad [26]$$

The fraction of the finite volume that is occupied by the gases is called to void fraction (ε) and changes based on the quantities of solid and liquid. The void fraction is found from the intrinsic density of wood (Siau 1984) of 1500kg/m^3. If the intrinsic density of char is equal the intrinsic density of wood the void fraction can be written as

$$\varepsilon = 1 - \frac{\rho_W + \rho_C}{1500} - \frac{\rho_M}{1000} \qquad [27]$$

3.4 Conservation of Species

Conservation of mass must also be true for each gas species.

$$\frac{\partial m_T}{\partial t} = \dot{m}_{T,in} - \dot{m}_{T,out} + \dot{\omega}_T \qquad [28]$$

$$\frac{\partial m_{LG}}{\partial t} = \dot{m}_{LG,in} - \dot{m}_{LG,out} + \dot{\omega}_{LG} \qquad [29]$$

$$\frac{\partial m_V}{\partial t} = \dot{m}_{V,in} - \dot{m}_{V,out} + \dot{\omega}_V \qquad [30]$$

Subscript T refers to tar, LG refers to light gases, and subscript V refers to water vapor. This can be written for species I in general as

$$\frac{\partial m_I}{\partial t} = \dot{m}_{I,in} - \dot{m}_{I,out} + \dot{\omega}_I \qquad [31]$$

where m_I is the mass of species I and $\dot{\omega}_I$ represents the rate of creation of species I.

The individual species production terms are found from the relevant pyrolysis and vaporization equations.

$$\dot{\omega}_T = m_W k_1 - m_T (k_4 + k_5) \qquad [20]$$

$$\dot{\omega}_{LHC} = m_w k_2 + m_T k_4 \qquad [21]$$

$$\dot{\omega}_V = m_M k_6 \qquad [22]$$

For each gas species, the rate of mass entering or leaving is equal to the total gas mass flow multiplied by the mass fraction of the species.

$$\dot{m}_{in} = \rho_{G,n} X_n L V_{in} \qquad [32]$$

$$\dot{m}_{out} = \rho_{G,i} X_i L V_{out} \qquad [33]$$

where X refers to the mass fraction of a species at finite volume i or neighboring finite volume n.

3.5 Conservation of Energy

Conservation of energy indicates that energy can not be created or destroyed. The rate of change of energy in a system is equal to the net rate of energy into the system plus the net rate of energy production.

$$\frac{\partial E}{\partial t} = \dot{Q}_{in} - \dot{Q}_{out} + Q_{production} \qquad [34]$$

The production term is really a transfer of stored potential (chemical) energy through molecular bonding that may add or subtract energy form the finite volume. For the pyrolysis system, energy enters or leaves the finite volume through radiation, conduction or convection. Energy is also be carried by gases traveling through the particle.

The energy carried into the finite volume by conduction is given by

$$\dot{Q}_{cond} = \oint k \frac{\partial T}{\partial \hat{n}} \qquad [35]$$

where k is the thermal conductivity and T is the temperature. Finite volume calculation of the temperature gradient is found in Chapter 4.

Incoming convective energy is applied to the surface of the particle

$$\dot{Q}_{conv} = \oint h\left(T_{h,\infty} - T\right) \qquad [36]$$

where h is the convective heat transfer coefficient and $T_{h,\infty}$ represents the free stream gas temperature.

The incoming radiative energy is also located at the surface of the particle and may

$$Q_{rad} = \oint \sigma \left(T_{\infty}^4 - T^4 \right) \qquad [37]$$

include absorption or emission coefficients. T_{∞} is the radiative source temperature. This expression is for radiation from a source at a fixed temperature.

The gases are assumed to heat up instantaneously to the solid surface temperature. Although gases exiting a finite volume do carry energy out of the finite volume, these gases are at the same temperature as the finite volume that they are leaving. As a result, they do not cause any temperature change within the finite volume. Each finite volume can be considered to be at its reference state. Gases entering the finite volume may be hotter or colder than this reference state, and may contribute to the change in energy of the finite volume.

$$\dot{Q}_{gas} = -\oint \rho_G V c_G \left(T_n - T_i \right) \qquad [38]$$

c_G is the specific heat of the gas. The negative sign indicates that incoming gases (V_{out} by convention) will cause energy storage if the incoming gases are hotter than the temperature in the finite volume receiving the incoming gas flow.

The individual pyrolysis reactions can be endothermic or exothermic and are included as a source term from the heat of formation of each pyrolysis product. The vaporization of liquid water is endothermic and is also included as a source term.

$$\dot{Q}_{source} = \sum \Delta h_I^o \dot{\omega}_I \qquad [39]$$

Combining all of the energy terms yields the net rate of energy into the particle which must be equal to the rate of storage of energy.

$$\dot{Q}_{in,net} = \oint k \frac{\partial T}{\partial \hat{n}} + \oint h \left(T_{\infty} - T \right) + \oint \sigma \left(T_{\infty}^4 - T^4 \right) - \oint \rho_G V c_G \left(T_n - T_i \right) + \sum \Delta h_I^o \dot{\omega}_I = \frac{\partial E}{\partial t} \qquad [40]$$

3.6 Shrinkage Development

The shrinkage equation relates the final particle dimension to the original dimension before pyrolysis.

$$f_C = \frac{L_{final}}{L_o} \qquad [41]$$

For a two-dimensional grid, there will be a shrinkage value in both the grain and the cross-grain direction. The amount of shrinkage of a finite volume is based on the overall shrinkage factors, and linearly on the fraction of wood remaining. The fraction of wood remaining (η) is found as

$$\eta = \frac{m_W}{m_{W,O}} \qquad [42]$$

where $m_{W,O}$ is the original mass of wood in the finite volume. In order to maintain the grid integrity, the edge shared by two adjacent finite volumes must shrink by the same amount for each finite volume. The amount of shrinkage for the edges of the finite volume must be based on the average shrinkage value of the neighboring finite volumes.

$$L_{a-b} = L^0_{a-b}\left(f_C + (1-f_C)\frac{\eta_i + \eta_n}{2}\right) \qquad [43]$$

L_{a-b} is the current distance of the edge shared by finite volume i and finite volume n and L^0_{a-b} is the original length of the edge. The shrinkage value f_C can be found from the orientation of L^0_{a-b} relative to the grain direction and the grain and cross-grain shrinkage values. If f_X is the grain direction shrinkage value and f_Y is the cross-grain shrinkage value, and L^0_{a-b} sits at an angle θ from the grain direction, f_C can be found as

$$f_C = \sqrt{(f_X \cos\theta)^2 + (f_Y \sin\theta)^2} \qquad [44]$$

As the finite volumes within the particle shrink at different rates, the shape of individual finite volumes and the shape of the overall particle changes. For example, the corners of a square particle will heat up and pyrolyze first, resulting in a rounded appearance at the corners of the particle where edge lengths shrink first (see Fig 13). The directional properties for shrinkage are based on the original orientation of the finite volume edges. If a finite volume becomes distorted in a particular direction due to two-dimensional shrinkage, the original grain direction of the finite volume is also distorted in the same direction.

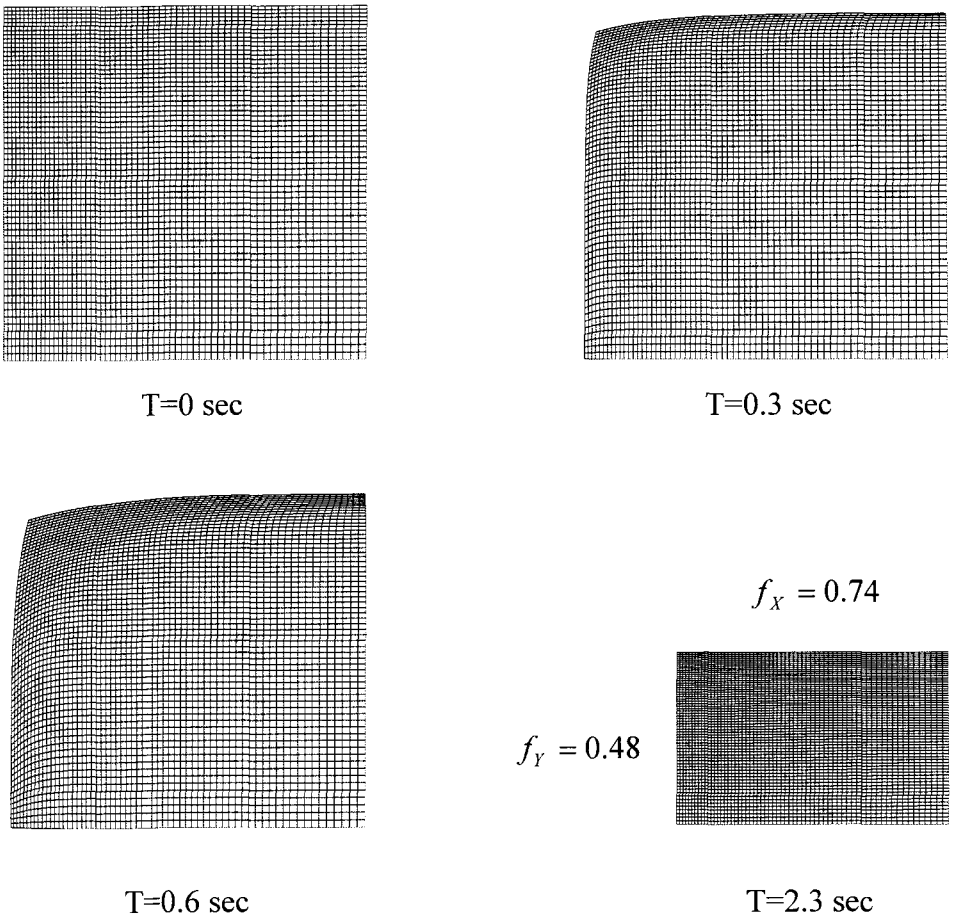

Fig 13. Shape Change of the Top-Left Quarter Section of a 2mm Particle at 1600K

Chapter 4

Numerical Model

The two-dimensional numerical differencing scheme presented here uses a finite volume method to solve the governing equations on an unstructured grid. The primary issues for the system are:

1. Grid Generation and Connectivity Information
2. Conservation Equation Formulation
3. Solution Procedure

4.1 Grid Generation and Connectivity Information

Unstructured grids are commonly used to describe systems that have complex geometries. The validation and computational model results presented in Chapter 5 and Chapter 6 use rectangular and square shaped particles. These geometries can easily be presented as a structured grid. The unstructured formulation was chosen to give the model additional capabilities to be able to handle complex two-dimensional geometries. The unstructured formulation will also allow changes in the particle connectivity that may be important to future models that incorporate the cracking of the solid particle. An unstructured formulation may also be necessary for future models that incorporate gas phase reactions with a shrinking particle, as new finite volumes may need to be added to replace the space originally occupied by the solid (unshrunk) particle.

Unstructured grids are produced by identifying the connectivity information (e.g. each finite volume, the neighbors of each finite volume, and the edges that are shared by the finite volume and its neighbors). Any structured grid can be converted into an unstructured

grid by providing the appropriate connectivity information. The computational model can accept any size or shape of grid as long as the appropriate connectivity information is given. Additionally, the finite volumes can consist of any size or shape as the equation formulations consist of volume and surface integrals. For two-dimensional particles with irregular shapes, it is easiest to divide the computational domain into triangular regions. Delauney triangulation is done by finding the set of triangular volumes from a point set that are closest to isosceles triangles. Isosceles triangles are desirable because they produce less error than triangles with a distorted aspect ratio. An example of Delauney triangulation is shown below in Fig 14.

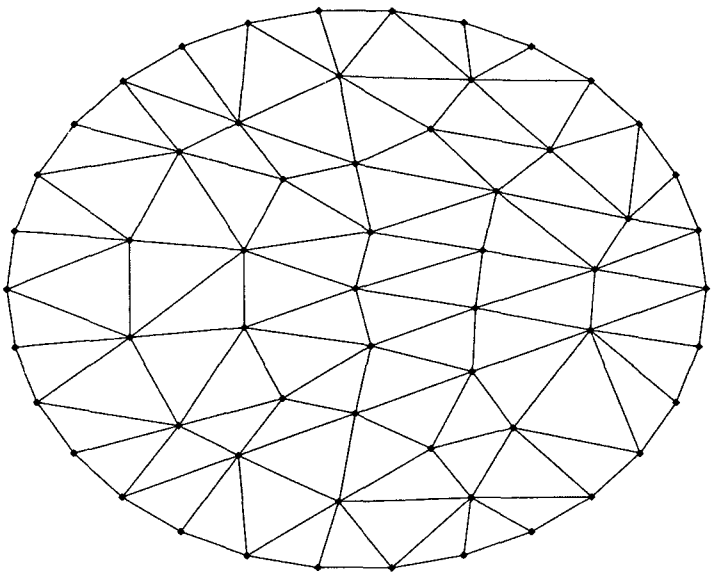

Fig 14. Delauney Triangulation of a Point Set

For the particle shown in Fig 14 and Fig 15, the connectivity information must be developed. A sample of the connectivity information is shown in Table 1. Each triangle

Tri	Pt1	Pt2	Pt3	Nbor1	Nbor2	Nbor3	Edge1	Edge2	Edge3
1	1	2	41	0	5	3	118	1	2
2	1	53	30	3	45	0	3	4	119
3	1	41	53	1	64	2	2	5	3
4	2	3	31	0	6	5	120	6	7
5	2	31	41	4	47	1	7	8	1

Table 1. Connectivity Information

contains a list of its triangle number, point set, neighbor set, and the edge set. Points, neighbors and edges are all arranged in counter-clockwise order to provide the relationship between the different sets. As an example, Pt 1 and Pt 2 make up edge 118, and triangle 1 does not have a neighbor (nbor=0) through edge 118. A neighbor value of 0 indicates that that edge is at the surface of the particle. Fig 15 shows the connectivity for of a portion of the particle from Fig 14 and corresponds to the information in Table 1.

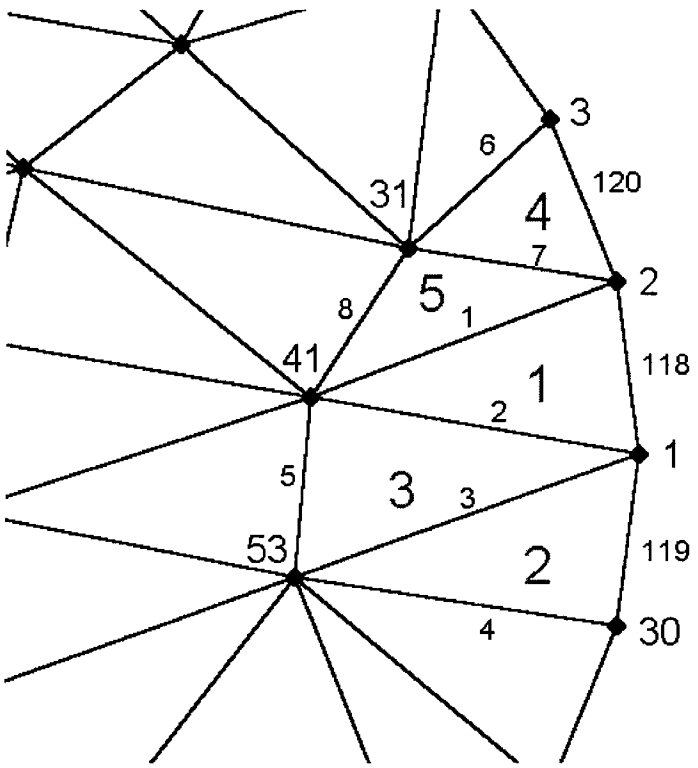

Fig 15. Selected Grid Information for the Particle in Fig 14

The unstructured formulation gives a lot of flexibility in the discretization of the particle. If each finite volume contains an integer that tells how many sides it has, the finite volumes can consist of any number of sides. The conservation equations have been developed as volume and surface integrals. To apply these conservation equations to an unstructured grid, the volume of each finite volume must be calculated as well as the gradients between neighboring finite volumes.

Gradients for temperature and pressure will be needed along each edge for surface integral calculations for heat transfer and velocity calculations. The temperature gradient along an edge of a triangle can be found by performing a surface integral around the two triangles containing the common edge. Resistance to flow ($\frac{\phi}{\mu}$) and thermal conductivity (k) are evaluated at edges at conditions that are the average of the neighboring two cells.

$$\frac{\phi}{\mu} = 0.5\left(\left.\frac{\phi}{\mu}\right|_i + \left.\frac{\phi}{\mu}\right|_n\right) \qquad [45]$$

$$k = 0.5(k_i + k_n) \qquad [46]$$

For an edge at the surface of the particle, the resistance to flow is the value of that finite volume. This type of non-orthogonal formulation is given in Tannehill, Anderson, and Pletcher (1997). An example for heat flux from 65 to 1 across the shared surface is given below and is shown in Fig 16..

$$\frac{\partial T}{\partial n} = \frac{1}{(A_{acdb})}\left[T_1(\hat{r}_{67-b}\cdot\hat{r}_{66-67}) + T_1(\hat{r}_{b-a}\cdot\hat{r}_{66-67}) + T_1(\hat{r}_{a-66}\cdot\hat{r}_{66-67})\right]$$

$$+\frac{1}{(A_{acdb})}\left[T_{65}(\hat{r}_{66-c}\cdot\hat{r}_{66-67}) + T_{65}(\hat{r}_{c-d}\cdot\hat{r}_{66-67}) + T_{65}(\hat{r}_{d-67}\cdot\hat{r}_{66-67})\right] \qquad [47]$$

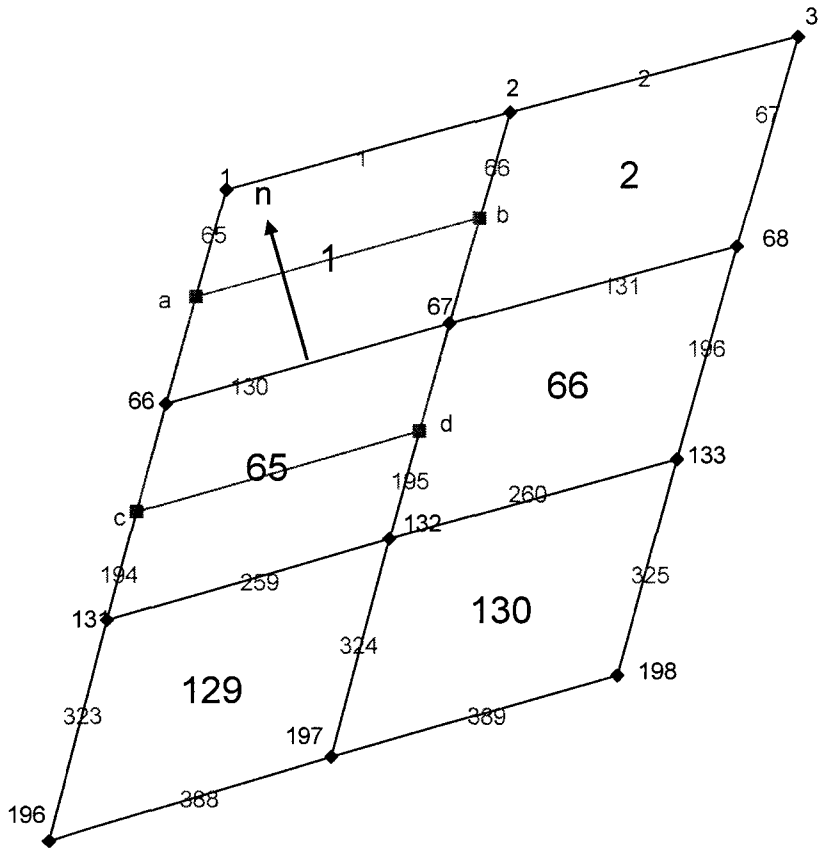

Fig 16. Gradient Calculations

4.2 Conservation Equation Formulation

The conservation equations from Chapter 3 are now written in a form that is more tractable for the solution techniques in section 4.3. The computational model solves for the primitive variables temperature, pressure, density, and molecular weight. Recall conservation of gas mass and conservation of momentum.

$$\frac{\partial m_G}{\partial t} + \oint \rho_G \vec{V} \bullet \hat{n} = \dot{\omega}_G \qquad [10]$$

$$\vec{V} = -\frac{\phi}{\mu}\frac{\partial p}{\partial \hat{n}} \qquad [11]$$

Conservation of mass can be combined with the momentum equation.

$$\frac{\partial m_G}{\partial t} - \sum_{j=1}^{k} \rho_G L \frac{\phi}{\mu} \frac{\partial p}{\partial \hat{n}} = \dot{\omega}_G \qquad [48]$$

where the gas masses are summed crossing each surface of a finite volume with k sides. The appropriate gas density depends on whether gas is leaving or entering the finite volume and can be more easily written as incoming or outgoing surfaces.

$$\frac{\partial m_G}{\partial t} - \sum_{out} \rho_{G,i} L \frac{\phi}{\mu} \frac{\partial p}{\partial \hat{n}} + \sum_{in} \rho_{G,n} L \frac{\phi}{\mu} \frac{\partial p}{\partial \hat{n}} = \dot{\omega}_G \qquad [49]$$

Outgoing flows use the gas density at i and incoming gas flows use the gas density from neighbor n. Recall that average values are used for resistance to flow.

$$\frac{\partial m_G}{\partial t} - 0.5 \sum_{out} \rho_{G,i} L \left(\frac{\phi}{\mu}\bigg|_i + \frac{\phi}{\mu}\bigg|_n \right) \frac{\partial p}{\partial \hat{n}} + 0.5 \sum_{in} \rho_{G,n} L \left(\frac{\phi}{\mu}\bigg|_i + \frac{\phi}{\mu}\bigg|_n \right) \frac{\partial p}{\partial \hat{n}} = \dot{\omega}_G \qquad [50]$$

Because the pressure gradient drives the gas flow through the particle, it is useful to rewrite the gas density terms from the ideal gas equation.

$$\frac{\partial (m_G)_i}{\partial t} - 0.5 \sum_{out} \left(\frac{PW_G}{RT} \right)_i L \left(\frac{\phi}{\mu}\bigg|_i + \frac{\phi}{\mu}\bigg|_n \right) \frac{\partial p}{\partial \hat{n}} + 0.5 \sum_{in} \left(\frac{PW_G}{RT} \right)_n L \left(\frac{\phi}{\mu}\bigg|_i + \frac{\phi}{\mu}\bigg|_n \right) \frac{\partial p}{\partial \hat{n}} = \dot{\omega}_G \qquad [51]$$

The rate of change with respect to time can be replaced by a Taylor series expansion to get the following expression of second order accuracy

$$\left. \frac{\partial m}{\partial t} \right|^{n+1} = \frac{1.5 m^{n+1} - 2.0 m^{n} + 0.5 m^{n-1}}{\Delta t} + O(\Delta t)^2 \qquad [52]$$

where the (n+1) superscript indicates the next time step, (n) indicates the current time step and (n-1) indicates the previous time step.

For a two-dimensional case, the gas mass can be found by multiplying the gas density by the finite volume area and the void fraction. Using the second order expression and rearranging gives the Pressure Evolution Equation for conservation of the total gas mass.

$$1.5\left(\frac{PW_G}{RT}\varepsilon A\right)_i^{n+1} - 0.5\sum_{out}\left(\frac{PW_G}{RT}\right)_i L\left(\frac{\phi}{\mu}\bigg|_i + \frac{\phi}{\mu}\bigg|_n\right)\frac{\partial p}{\partial \hat{n}} + 0.5\sum_{in}\left(\frac{PW_G}{RT}\right)_n L\left(\frac{\phi}{\mu}\bigg|_i + \frac{\phi}{\mu}\bigg|_n\right)\frac{\partial p}{\partial \hat{n}}$$

$$= \dot{\omega}_G + 2.0m_G^n - 0.5m_G^{n-1} \qquad [53]$$

For each species I, there must also be conservation of mass. The mass of species I is given by

$$m_I = \rho_I X_I \varepsilon A \qquad [54]$$

where X_I is the mass fraction of species I. The Pressure Evolution Equation can be written for each species.

$$1.5\left(\frac{PW_G X_I}{RT}\varepsilon A\right)_i^{n+1} - 0.5\sum_{out}\left(\frac{PW_G X_I}{RT}\right)_i L\left(\frac{\phi}{\mu}\bigg|_i + \frac{\phi}{\mu}\bigg|_n\right)\frac{\partial p}{\partial \hat{n}} + 0.5\sum_{in}\left(\frac{PW_G X_I}{RT}\right)_n L\left(\frac{\phi}{\mu}\bigg|_i + \frac{\phi}{\mu}\bigg|_n\right)\frac{\partial p}{\partial \hat{n}}$$

$$= \dot{\omega}_I + 2.0m_I^n - 0.5m_I^{n-1} \qquad [55]$$

The energy equation is given as

$$\oint k\frac{\partial T}{\partial \hat{n}} + \oint h(T_\infty - T) + \oint \sigma\left(T_\infty^4 - T^4\right) - \oint \rho_G V c_G (T_n - T_i) + \sum \Delta h_I^o \dot{\omega}_I = \frac{\partial E}{\partial t} \qquad [13]$$

The rate of storage is

$$\frac{\partial E}{\partial t} = mc_P\frac{\partial T}{\partial t} \qquad [56]$$

where mc_P is the total storage capacity of the fine volume and includes the storage capacity of the wood, char, water, and gases. The energy equation can be rearrange to solve for the rate of temperature change which is the Temperature Evolution Equation.

$$\frac{\partial T}{\partial t} = \frac{\oint k \frac{\partial T}{\partial \hat{n}} + \oint h(T_\infty - T) + \oint \sigma(T_\infty^4 - T^4) - \oint \rho_G V c_G (T_n - T_i) + \sum \Delta h_l^o \dot{\omega}_l}{mc_P} \quad [57]$$

4.3 Solution Procedure

The temperature and pressure equations are coupled because they both depend on the variables T, P, ρ, and W_G. During pyrolysis, temperature and pressure change faster than the other variables. The molecular weight changes slowly, and the density of the gas is largely a function of the gas temperature and pressure. In developing a solution procedure, it makes sense to first solve for the temperature evolution equation.

The temperature evolution equation is influenced by the gas flow through the finite volume, the heat of formation of new pyrolysis gases, and the thermal mass of the particle. The solid particle has over 600 times the thermal mass of the gases, and even large changes in gas mass have little influence on the resulting temperature profile. For the same reason, gas flow through the particle has little influence on the temperature evolution equation. Gas production rates are small for a given time step, and the heat of formation of pyrolysis gases is small.

The temperature evolution equation can be solved once initial conditions are set and an external heat flux is applied to the surface of the particle. Note that the temperature

gradient with respect to time is an exact formulation if all of the quantities are known at a given time.

$$\frac{\partial T}{\partial t} = \frac{\oint k \frac{\partial T}{\partial \hat{n}} + \oint h(T_\infty - T) + \oint \sigma(T_\infty^4 - T^4) - \oint \rho_G V c_G (T_n - T_i) + \sum \Delta h_I^o \dot{\omega}_I}{mc_P} \quad [58]$$

At time zero, all of the property values are specified. The temperature gradient at time zero can be directly calculated for each finite volume. This temperature gradient can be used to calculate a guess (T^*) for the temperatures at the next time step.

$$T^* = T^n + \frac{\partial T}{\partial t}\Delta t \quad [59]$$

Temperature dependent properties such as the specific heat of wood and char, and the heat of formation from pyrolysis gas production are updated. The guess for the rate of temperature change at time (n+1) is computed $\left.\frac{\partial T}{\partial t}\right|^{n+1}$ using T^* and the updated property values. The guess for the new (n+1) temperatures is then found as

$$T^* = T^n + 0.5\left(\frac{\partial T}{\partial t}^n + \frac{\partial T}{\partial t}^{n+1}\right)\Delta t \quad [60]$$

The iterative value (T^*) is plugged into the temperature evolution equation until T^* converges. This is the converged value for T^{n+1} from the initial temperature evolution equation, noting that the gas velocities, gas mass, and the heat of pyrolysis are based on lagged gas values. The solution procedure assumes that the temperature gradient varies linearly with respect to time, and is equivalent to Crank-Nicolson formulation, which has second order accuracy.

$$T^{n+1} = T^n + 0.5\left(\frac{\partial T^n}{\partial t} + \frac{\partial T^{n+1}}{\partial t}\right)\Delta t + O(\Delta t)^2 \qquad [61]$$

The main advantages of this formulation is that properties that vary are already included in the formulation and errors are not introduced by using average values between time steps. The temperature equation is diagonally dominant and unconditionally stable. It is currently solved using Guass-Seidel iteration with an accuracy of 10^{-8} kPa.

Once the temperatures have been solved, the pressure evolution equation is solved for the total gas flow. The pressure equation is a non-linear equation, is not diagonally dominant (in general) and requires a solution procedure on an unstructured grid. The pressure equation is solved using the updated temperature, gas production, and property values from the solution of the temperature evolution equation.

$$1.5\left(\frac{PW_G}{RT}\varepsilon A\right)_i^{n+1} - 0.5\sum_{out}\left(\frac{PW_G}{RT}\right)_i L\Delta t\left(\frac{\phi}{\mu}\bigg|_i + \frac{\phi}{\mu}\bigg|_n\right)\frac{\partial p}{\partial \hat{n}} + 0.5\sum_{in}\left(\frac{PW_G}{RT}\right)_n L\Delta t\left(\frac{\phi}{\mu}\bigg|_i + \frac{\phi}{\mu}\bigg|_n\right)\frac{\partial p}{\partial \hat{n}}$$

$$= \dot{\omega}_G \Delta t + 2.0m_G^n - 0.5m_G^{n-1} \qquad [62]$$

For gases leaving the control volume, the density of the gases leaving the control volume is the same as the density within the control volume.

$$F = 1.5\left(P_i W_{G,i} / RT_i\right)\varepsilon A - 2.0m^n + 0.5m^{n-1}$$

$$+1000 \cdot dt \cdot \left(\frac{W_{G,i}}{RT_i}\right)\left(\frac{\varphi_i}{\mu_i} + \frac{\varphi_n}{\mu_n}\right)\left(Z_i P_i^2 - Z_n P_i P_n\right) - \dot{\omega}_G \cdot dt = 0 \qquad [63]$$

where Z_i and Z_n are the coefficients of i and n in the gradients computed between the two finite volumes, and the factor of 1000 is from expressing pressures in kPa. Gases entering the control volume enter with the density of the neighboring control volume.

$$F = 1.5\left(P_i W_{G,i} / RT_i\right)\varepsilon A - 2.0m^n + 0.5m^{n-1}$$
$$+1000 \cdot dt \cdot \left(\frac{W_{G,n}}{RT_n}\right)\left(\frac{\varphi_i}{\mu_i} + \frac{\varphi_n}{\mu_n}\right)\left(Z_i P_i P_n - Z_n P_n^2\right) - \dot{\omega}_G \cdot dt = 0 \qquad [64]$$

The pressure evolution equation is solved using a Newton-GMRES procedure. Newton's method can be written in matrix form as

$$F'(x_n) \cdot \Delta x_n = -F(x_n) \qquad [65]$$

In the solution procedure used for this code, the pressure evolution equation is assumed to be a function of only pressure, using the most current property values available. Effects of changes in molecular weight are ignored at this point in the solution procedure. The pressure equation can be written for every finite volume in the grid (n equations for a grid with n finite volumes). To apply Newton's method, the derivative of the pressure equation is taken with respect to each variable. If F_i represents the pressure equation at i, F' would be written as

$$\mathrm{F}'(x_i) = \frac{\partial F_i}{\partial x_1}\ \frac{\partial F_i}{\partial x_2}\ \frac{\partial F_i}{\partial x_3}\ \frac{\partial F_i}{\partial x_4}\quad \cdots \quad \frac{\partial F_i}{\partial x_n} \qquad [66]$$

The function and its derivative are evaluated using the most current (iterative) property values available to solve for changes in the pressure field. For a gas leaving the control volume,

$$F'(P_i) = 1.5(W_{G,i} / RT_i)\varepsilon A + 1000 \cdot dt \cdot \left(\frac{W_{G,i}}{RT_i}\right)\left(\frac{\varphi_i}{\mu_i} + \frac{\varphi_n}{\mu_n}\right)(2Z_i P_i - Z_n P_n) \quad [67]$$

$$F'(P_n) = 1000 \cdot dt \cdot \left(\frac{W_{G,i}}{RT_i}\right)\left(\frac{\varphi_i}{\mu_i} + \frac{\varphi_n}{\mu_n}\right)(-Z_n P_i) \quad [68]$$

If repeated for each finite volume, F' would in general be an n x n matrix. For finite volumes using quadrilaterals, the pressure equation would depend on the pressure at i as well as the pressure at the four neighbors. For quadrilaterals, the pressure gradient can be written as an n x 5 matrix, where the first value is the derivative of the pressure evolution equation at i with respect to the pressure at i, and the next four terms are the derivative of the pressure evolution equation at i with respect to the neighboring pressures. Newton's method forms a linear matrix equation using the $F'(x_i)$ matrix and the $F(x_i)$ known values.

The solution of this matrix requires a sparse, unstructured matrix solver. The generalized minimum residual algorithm (GMRES) was used with restart to solve for the changes in pressure. This algorithm takes an n-dimensional space and finds the closest answer (minimum residual) in a particular initial search direction (usually the steepest descent). Subsequent search directions are perpendicular to previous search directions, ensuring a solution if n search directions (levels) were used in the algorithm. The computational cost becomes high as the number of levels is increased. To speed up the solution, the procedure can be applied to a lesser number of levels (~10) and the updated guesses can be used as the initial guess (restart). Although it is mathematically possible for the restart procedure to stagnate for a limited number of problems, the GMRES with restart procedure converged for all of the cases performed in developing this thesis. One advantage

of this procedure is that the error in the answer is explicitly computed in the algorithm at each step.

Thus a Newton-GMRES procedure is employed to solve the non-diagonally dominant pressure equation. In this procedure, the pressure is solved to a specified tolerance (GMRES) based on F and F' (Newton). The changes in pressure predicted in the GMRES algorithm and used to update the pressure terms, and Newton's procedure is repeated with GMRES until the pressure terms converge to a specified tolerance (10^{-9} kPa).

It is not necessary to compute the accuracy of temperature and pressure to computer precision at each time step. To ensure conservation of mass in the gas phase, it is desirable to solve for gas densities to a high precision. After the solution of the temperature and pressure, the density of each species and the total gas density is solved to computer precision using the Newton-GMRES procedure. Thus, while there may be a small amount of error in the temperature and pressure profile, conservation of mass is exact to computer precision based on those profiles. This ensures that matter is not created or destroyed within the computational domain. After the density has been solved, the molecular weights can be updated according to the ideal gas equation. If the change in molecular weight is greater than 10^{-9}, the pressure, density and molecular weight are recomputed until convergence occurs. If desired, the temperature routine can be updated based on the new gas velocities and densities until all of the variables converge to a specified tolerance, although lagging the gas terms in the temperature equation produces very little error, as the gas fluxes become relatively stable within the particle and have only a small influence on the temperature profile at a given time step.

The solution procedures were verified by a number of methods during the development of the code. As an example, the pressure equation is initially diagonally dominant, and the pressure equation can be solved by simple Guass-Seidel iteration. Comparison with the Newton-GMRES procedure shows the same pressure values. Agreement between the two procedures supports the correct implementation of the matrix values and derivatives. The GMRES procedure was tested by solving a known linear matrix. Conservation of mass momentum and energy were checked manually within the finite volumes. The correct implementation of the numerical code was supported by the nearly identical results running the code with different time steps, varying grid sizes, and using both triangular and quadrilateral finite volumes.

Chapter 5

Validation

There are a limited number of pyrolysis experiments that have been performed using large particles (≥ 1 cm). Some works include experiments for a 2-cm diameter moist cylinder (Lee, Chaiken, Singer 1976), a 1-cm diameter cylinder (Chan, Kelbon, and Krieger 1985), 0.95-cm diameter cylinders (Tinney 1965), several spheres ranging from 2 to 5.6-cm in diameter (Balboa, Millera, Murillo 1993), 1-cm cubes (Bonnefoy et al), 0.125cm, 0.25cm, and 0.5cm rectangular sections (Hoerning 1999), and 15-cm by 15-cm by 6.4-cm blocks (Tran and White 1992). Some of these models blow inert gases over the surface of the particle to prevent oxidation reactions. Nitrogen was used by Lee, Balboa, and Hoerning and helium was used by Chan to prevent surface oxidation reactions. In the works of Tran and White, over-fire air was added to complete combustion for gas analysis. These researchers have used different geometries, flow-fields, and species of wood for their analysis and have taken varying degrees of data. Most pyrolysis experiments do not include all of the data needed to completely describe the system. In particular, the gas flow field around the particle is often formed by buoyant or unspecified flow conditions.

Validation for this computational model uses the work of Hoerning (1999). Hoerning studied the pyrolysis of hybrid poplar wood samples in an inert environment. Wooden particles within a furnace were pyrolyzed while nitrogen carrier gas was blown across the surface to prevent oxidation reactions. The rate of nitrogen gas flow was controlled and recorded. In his experiments, rectangular particles ranged in size from

⅛ x 1 x 1 in^3 to ½ x 1 x 1 in^3 with the dimension perpendicular to the gas flow varying. The particle was suspended from a precision balance and furnace temperatures were varied from 800°C to 1400°C for each particle size. The poplar particles were stored in a controlled environment, allowing controlled moisture contents for each particle size and temperature to be used within the furnace. Transient temperature and mass data were recorded, along with net gas products. The particles sizes were measured before and after pyrolysis, allowing multi-dimensional shrinkage data to be taken. The gas flow of nitrogen was constant during each run, and was increased with furnace temperature to keep external gas temperatures below 600°C and prevent any gas phase reactions from occurring outside of the particle before the gases could be collected for analysis.

The experimental setup used by Hoerning provides a well-defined system in which particle shape, size, moisture content, and external temperature are varied and biomass pyrolysis performance is measured. The forced external flow field and the extent of data taken allow many of the experimental conditions to be applied to the computational model. The primary limitation of the two-dimensional computational model is that it describes the experimental system of Hoerning in two dimensions. In a two-dimensional model, there is a difference between the actual ratio of particle surface area to particle volume (in three dimensions) and the ratio that is produced by the two-dimensional model.

The smallest particle used in Hoernings experiments is a ⅛ x 1 x 1 in^3 particle where the particle surface is ⅛ inch x 1 inch in the directions perpendicular to the nitrogen gas flow. In the two dimensional computational model, this particle is described as the ⅛ x 1 inch surface perpendicular to the flow direction, and convection at the surface of the two-

dimensional particle is determined by using the average convection coefficient along the length of the particle. The average convection coefficient is evaluated by calculating the average convection coefficient for a 1-inch flat plate with the measured nitrogen free stream velocity. When the furnace temperature was 800°C, the gas temperature was measured as 500°C. At 1100°C and 1400°C, the flow rate was adjusted to get a free stream gas temperature of 600°C. In the computational model, convection occurs at the surface of the particle using the flat plate convective heat transfer coefficient and the measured free stream gas temperature. 98% of the radiation from the furnace surface is assumed to reach the particle, based on the high view factor from the furnace to the particle, the high emissivity of char, and a mostly transparent external gas media with forced flow and external gas temperatures below 600°C. Shielding of the particle by participating gas media is not included in the model.

There have been a wide range of property values that have been used in computational models. These property values are often chosen to most closely match experimental results. In this work, the property data such as specific heat, conductivity, and the pyrolysis reaction rates are those recorded by experiment. Some material properties vary with species. Density and conductivity can vary by a factor of two, depending on the species of wood. The permeability of the wood to gas flow can vary by a factor of 100 depending on the particle species. The products of pyrolysis also vary depending on wood species, with hardwoods producing more volatile products. This computational model is applicable to any species of wood as long as property data is used that is appropriate for a given species of wood. The following sections highlight the property data used in this computational model.

The thermal conductivity of dry wood increases with temperature and density. The thermal conductivity of wood rises approximately 10% for every 50K rise in temperature (Ragland, Aerts, Baker 1991). Moisture adds to the thermal conductivity of wood, but is less than the conductivity of water because of the wood-water bond. The thermal conductivity of wet wood is given as a function of the specific gravity and the moisture content on a dry basis by the Forest Products Handbook (1987) as

$$k_{wetwood} = s.g.(1.39 + 0.028M) + 0.165 \frac{Btu \cdot in}{hr \cdot ft^2 \cdot °F} \qquad [69]$$

$$k_{wetwood} = s.g.(0.20 + 0.004M) + 0.024 \frac{W}{m \cdot K} \qquad [70]$$

The thermal conductivity of the char is given by Lee, Chaiken, and Singer (1976)

$$k_{char} = 0.105 \frac{W}{m \cdot K} \qquad [71]$$

The thermal conductivity of char increases during pyrolysis because additional energy is transported by radiation through pores and by radiation through cracks in the char layer. At high temperatures radiation is the dominant mode of heat transfer within the char layer.

As the particle devolatilizes, the thermal conductivity can be found from the fraction of original wood remaining (η).

$$k = \eta k_{wood} + (1 - \eta) k_{char} \qquad [72]$$

The specific heat of wood increases with temperature, but is constant with respect to wood species or density. TenWolde et al. (1988) reviewed over 120 observations of specific heat in a survey of wood and wood paneling in buildings and recommends the following correlation for wood temperatures between 280K and 420K

$$c_W = 3.867(T - 273.2) + 103.1 \quad \frac{J}{kg \cdot K} \qquad [73]$$

The specific heat of wet wood is higher than that obtained by adding the contribution of dry wood and water because of the energy needed to break the wood-water bond. This effect increases with moisture content and temperature (Forest Products Laboratory 1987), but is small and is not included in this model. All but three of the specific heat observations were taken at temperatures between 300K and 340K, leaving some uncertainty in the specific heat of wood at pyrolysis temperatures. Most computational models for wood pyrolysis use specific heat values that are between 2.2 and 2.5 kJ/kg-K (Kung 1974, Krieger-Brockett and Glaister 1988, Di Blasi 1993a, Melaaen and Gronli 1997). In this work, the correlation of TenWolde is extended to 600K, which results in a specific heat for wood of 2.4 kJ/kg-K at 600K. The specific heat of water is 4.18 kJ/kg-K at 60°C. The specific heat of char is assumed to be the same as that of graphite (Ragland, Aerts, and Baker 1991). A curve fit by Stull (1971) gives the following relationship for the specific heat of graphite

$$c_C = 1390 + 0.36T \quad \frac{J}{kg \cdot K} \qquad [74]$$

The specific heat of some pyrolysis gases are listed below

water vapor	2.0 kJ @ 400K
carbon dioxide	1.1 kJ @ 600K
methane	3.2 kJ @ 600K
ethane	3.0 kJ @ 600K
butane	2.9 kJ @ 600K.

Due to the global nature of the pyrolysis reaction set, the exact composition of the pyrolysis gases is not known. The specific heat of the pyrolysis gases should lie somewhere between these values, depending on the percentage of each pyrolysis gas. A specific heat of 2.4 kJ/kg-K is used for the total pyrolysis gases in this model.

$$c_G = 2400 \frac{J}{kg \cdot K} \qquad [75]$$

The permeability of wood can vary with species and direction. A permeability of 1 Darcy is used for wood in the validation of this model. Char is assumed to be one hundred times more permeable than wood.

The two-dimensional computational model has shown that the pyrolysis of wood is insensitive to many of these property variables, such as specific heat, thermal conductivity of wood, porosity, and the specific heat of the wood or the char. As an example, doubling the pyrolysis reaction rates for a thermal wave particle will cause an increase in pyrolysis times of less than 5%. The most important variable in determining the rate of pyrolysis is the rate at which heat is transferred through the external char layer. Computational modelers have recognized that radiation becomes the dominant mechanism of heat transfer within the particle at high temperatures (>600C). Researchers have traditionally accounted for radiation by using the work of Panton and Rittman (1971) in which an equivalent conductivity term is developed from amount of radiation transfer and added to the conduction term to find the total equivalent conductivity.

$$k_{eff} = k_{cond} + k_{rad} \qquad [76]$$

$$k_{rad} = \frac{\varepsilon}{1-\varepsilon}\sigma d_p 4T^3 \qquad [77]$$

where d_p is the pore diameter, ε is the fraction of the wood occupied by gases, and σ is the Stefan-Boltzmann constant.

The equivalent radiation term depends linearly on the pore diameter and the particle temperature raised to the third power. This formulation can cause the radiative conductivity from one finite volume to a neighboring finite volume to be up to twenty times that of a blackbody because radiation does not have to travel directly from one location to an adjacent location, and the radiative conductivity must be higher than that of a blackbody to account for the additional energy transport.

Using a constant thermal conductivity, the two-dimensional computational model predicts that small particles (1/8 x 1 x 1) at high temperatures (1400°C) are about 25% faster than experimental results and that large particles (1/2 x 1 x 1) at low temperatures (800°C) take about 30% longer than the measured pyrolysis time when using constant char conductivity. If the char conductivity increases with temperature, the discrepancy becomes larger, because the char conductivity will be higher at elevated temperatures, and the predicted pyrolysis times of the high temperature runs will even farther off from the measured pyrolysis times. Using the formulation of Panton and Rittman makes the predicted pyrolysis times even farther off because the equivalent conductive coefficient will be higher at high temperatures than at low temperatures.

The discrepancy between the computational model and the experimental data can be examined by varying values in the computational model to determine what factors are important in determining pyrolysis times. The discrepancy in pyrolysis times across the range

of particle sizes could not be explained by changing property values such as specific heat or the rate of the pyrolysis reactions in the computational model. The difference between the predicted pyrolysis times and the actual pyrolysis times can only be explained if there are important phenomena that have not been included in the numerical model. Cracking of the char surface is known to be an important process and has not been included in this computational model. As the particle pyrolyzes, cracks form at the surface to alleviate stresses within the solid particle. These cracks allow external radiation to radiate directly into cooler regions within the particle. These cracks typically extend all the way into the active pyrolysis layer and grow with the char layer as the particle pyrolyzes. When an external load is applied, the rate of cracking will increase because the additional stresses can only be relieved by the cracking of the char layer. One example of the effect of cracking is that loaded wooden beams show a larger rate of char growth than unloaded beams because loaded beams have additional crack surfaces and additional energy is transported directly to the crack surfaces in the loaded beam. Increasing char conductivity changes the ratio between the amount of energy that is transported through the particle and the amount of energy that is stored in the particle at a given time step. In a particle model that does not compute crack formation, crack formation can be thought of as a process that increases the conductivity of the char, allowing more of the applied external heat flux to be transported into the particle. Char conductivity from cracking will increase with the size of the char layer as the cracks continue to grow. The following formulation for char conductivity was developed using this computational model, based on the fact that char conductivity must increase in some manner with the size of the char layer.

$$k_{char} = 0.105 + 1400(L_{char})^{1.4} \quad \text{W/m K} \qquad k_{char,\max} = 0.605 \quad \text{W/m K} \qquad [78]$$

where the length of the char layer is in meters.

The length of the char layer was calculated as the distance from the surface of the particle to the location where 90% of the original mass of wood remains. This formulation assumes that the effect of char cracking is independent of temperature and of the shape of the particle. It is likely that the shape of the particle, the permeability, and the moisture content have an influence on the stresses developed within the particle and on the cracking process that relieves these stresses. Although the exact nature of crack formation is not known at this time, this formulation is consistent with assuming that the primary importance of cracking is to allow external radiation to penetrate directly into the particle.

If the material properties used in the computational model are correct, a two-dimensional model should predict pyrolysis times that are too slow because a three-dimensional particle has a larger surface area to volume ratio. With a larger surface area relative to the mass of the particle, a three-dimensional particle would pyrolyze faster. The surface area to volume ratios are shown in Table 2 for 1D, 2D, and 3D particles with their initial (no shrinkage) and final (shrinkage included) dimensions.

Table 2 shows that one-dimensional or two-dimensional computational models will predict pyrolysis times that are too slow when correct physical property data is used because the surface area will be too small relative to the energy storage capacity of the particle. The maximum char conductivity, as measured in the laboratory should be somewhat less than the two-dimensional computational model value of 0.605 W/m-K due to the increased surface area of three-dimensional particles.

Initial

1/8 Inch Particle			
	1D	2D	3D
L1	0.125	0.125	0.125
L2	-	1	1
L3	-	-	1
SA	2 dx	2.25	2.5
Vol	0.125 dx	0.125	0.125
SA/Vol	16	18	20
% Error	**-20%**	**-10%**	**0%**

1/4 Inch Particle			
	1D	2D	3D
L1	0.250	0.250	0.250
L2	-	1	1
L3	-	-	1
SA	2 dx	2.5	3
Vol	0.25 dx	0.25	0.25
SA/Vol	8	10	12
% Error	**-33%**	**-17%**	**0%**

1/2 Inch Particle			
	1D	2D	3D
L1	0.500	0.500	0.500
L2	-	1	1
L3	-	-	1
SA	2 dx	3	4
Vol	0.5 dx	0.500	0.500
SA/Vol	4	6	8
% Error	**-50%**	**-25%**	**0%**

Final

1/8 Inch Particle			
	1D	2D	3D
L1	0.06	0.06	0.06
L2	-	0.86	0.86
L3	-	-	0.86
SA	2 dx	1.84	1.686
Vol	0.125 dx	0.125	0.125
SA/Vol	16	14.72	13.4848
% Error	**19%**	**9%**	**0%**

1/4 Inch Particle			
	1D	2D	3D
L1	0.1625	0.1625	0.1625
L2	-	0.86	0.86
L3	-	-	0.86
SA	2 dx	2.045	2.038
Vol	0.25 dx	0.25	0.25
SA/Vol	8	8.18	8.1528
% Error	**-2%**	**0%**	**0%**

1/2 Inch Particle			
	1D	2D	3D
L1	0.4	0.4	0.4
L2	-	0.89	0.89
L3	-	-	0.89
SA	2 dx	2.58	3.0082
Vol	0.5 dx	0.500	0.500
SA/Vol	4	5.16	6.0164
% Error	**-34%**	**-14%**	**0%**

Table 2. 1D, 2D and 3D Surface Area to Volume Ratios

The conservation equations developed in Chapter 3 were solved on a two-dimensional unstructured grid using a Fortran computer code. The particle was divided into finite volumes, and the energy equation was solved using Guass Seidel iteration. The momentum equation is solved using a Newton-GMRES solution procedure. The number of finite volumes was typically limited to less than 5,000 for the two-dimensional grid due to the amount of computational time required for solving the system using unstructured

(iterative) solution procedures. Profiles of mass loss versus time and temperature versus show grid independent solutions using less than 5,000 finite volumes. For large particles at high temperatures, more resolution may be needed to completely eliminate small peaks in the pressure profile caused by the rise in pressure of individual finite volumes, particularly in finite volumes near the particle surface. This additional resolution is not needed for predicting pyrolysis time or pyrolysis products.

The predicted pyrolysis times for a 1/8 x 1 in^2 particle had less than 5% error for furnace temperatures of 800°C, 1100°C and 1400°C. The total mass of the particle verse time for the experimental results and for the computational model results are shown in Fig 17 and in Table 3. The shape of the mass loss curves match up closely with the experimental mass loss curves at each temperature. The computational pyrolysis times are calculated as the time when 99% of the wood has been converted to char. At 800°C, the computational model

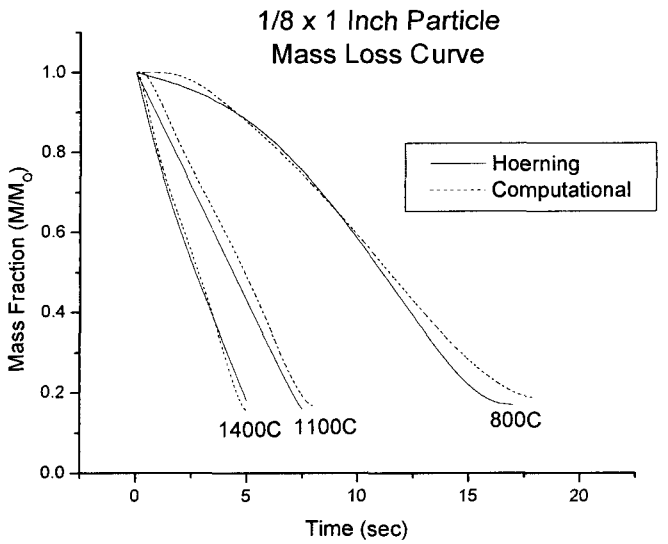

Fig 17. 2D Validation of a 1/8 x 1 x 1 Inch Particle

	Computational Pyrolysis Time	Hoerning Pyrolysis Time	Percent Difference
800C	17.3	16.5	4.8%
1100C	7.75	7.5	3.3%
1400C	5.02	5	0.4%

Table 3. Pyrolysis Times for a 1/8 x 1 x 1 Inch Particle

predicts a time 4.8% slower than the experimental value. At 1100°C, the model is 3.3% slower than experimental data and at 1400°C, the model is 0.4% slower than experimental data. Using the formulation, the char conductivity ranges from 0.105 to 0.275 W/m-K as the char layer grows to the center of the particle. Using the formulation of Patton, the radiation portion of char conductivity would have to be over 5 times as much at 1400°C as 800°C. The increased conductivity at high temperatures in the formulation of Patton causes the 1400°C pyrolysis time to be shorter relative to the 800°C run, and causes over 25% error between the pyrolysis times of a 1/8 inch particle at 800°C and at 1400°C. The numerical model suggests that char conductivity must be nearly the same at 800°C, 1100°C, and at 1400°C. For the 1/8 inch particle, a one-dimensional model will initially have 20% less surface area than the actual (3D) particle. When pyrolysis is complete and the particle has shrunk to its final dimensions, the one-dimensional model will have 19% more surface area than the actual particle. For the 1/8 inch particle, these results offset each other for 1D and 2D models. The net pyrolysis times can be determined using 1D, 2D, or 3D models when one of the three dimensions is small (1/8 inch or less). For small particles, although the total pyrolysis time will be correct, one-dimensional or two-dimensional models will predict that the initial rate

of mass loss is too slow, but will have a more rapid rate of mass loss near the end of devolatilization. This effect is more pronounced in one-dimensional models than for two-dimensional models.

For the ¼ x 1 in^2 particle, the numerical model was within 16% of the measured pyrolysis times for all of the furnace temperatures. The results for the ¼ inch particle are shown in Fig 18 and in Table 4.

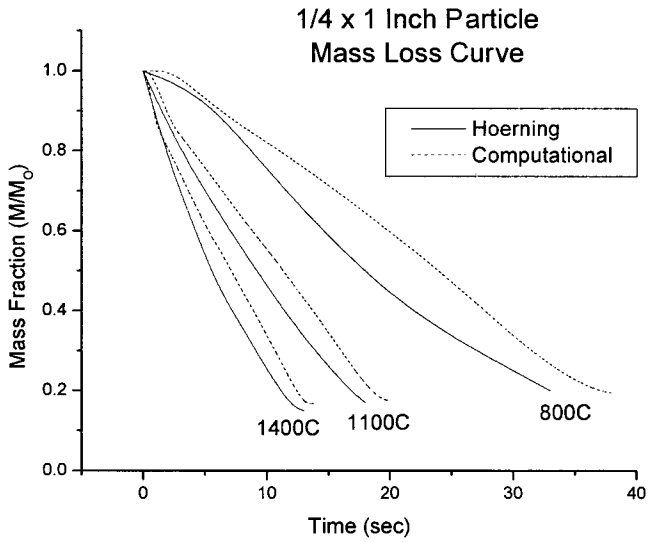

Fig 18. 2D Validation of a 1/4 x 1 x 1 Inch Particle

	Computational Pyrolysis Time	Hoerning Pyrolysis Time	Percent Difference
800C	38.16	33	15.6%
1100C	19.67	18	9.3%
1400C	13.32	13	2.5%

Table 4. Pyrolysis Times for a 1/4 x 1 x 1 inch Particle

The maximum char conductivity of 0.605 W/m-K is reached at a char length of approximately 1/8 inch, which is the distance to the center of a ¼ inch particle. In each case, the numerical model predicted that pyrolysis took longer than the measured pyrolysis time. The volume and surface area begin to be important for ¼ x 1 in^2 particles, as the two-dimensional model predicts that pyrolysis times are too slow. While the two-dimensional model does a better job of finding the correct ratio of surface area to volume than a one-dimensional model, it does not include the three-dimensional effects of shrinkage. At high temperatures, pyrolysis occurs more quickly near the surface, and the high temperature particle has a smaller surface area for most of pyrolysis than low temperature particles, even if the total shrinkage (fc) values are similar. This effect is only partially accounted for in a two-dimensional particle, and may account for the fact that the low temperature runs are too slow by 15.6%. If radiative char conductivity varies with temperature to the third power, there will be a 50% difference between the 800°C and 1400°C runs, indicating that char cracking is likely a more important process than radiation within the wood pores.

For the ½ x 1 in^2 particle, the pyrolysis times were within 12.7 % of the experimental pyrolysis times. The ½ inch particle is shown in Fig 19 and Table 5. The char conductivity ranged from 0.105 W/m-K to a maximum value of 0.605 W/m-K when the char layer reached half way to the center of the particle. The initial rate of mass loss was slower than the experimental results, which is consistent with the smaller surface area in the two-dimensional model than for the actual particle. As the char layer grows, cracks continue to form and grow, and the conductivity of the char layer increases. It is likely that the maximum value of 0.605 W/m-K in the computational model is higher than the actual

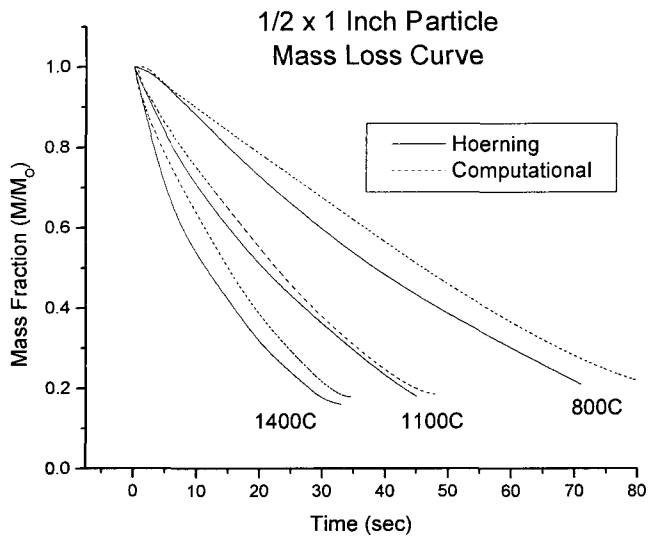

Fig 19. 2D Validation of a ½ x 1 x 1 Inch Particle

	Computational Pyrolysis Time	Hoerning Pyrolysis Time	Percent Difference
800C	80	71	12.7%
1100C	50	48	4.2%
1400C	32	31.5	1.6%

Table 5. Pyrolysis Times for a ½ x 1 x 1 inch Particle

(three-dimensional) value. The two-dimensional model underestimates the surface area of the ½ x 1 x 1 in^3 particle by about 25%, and the value of char conductivity used in the model is probably higher than the actual value. Using a larger value of conductivity in a two-dimensional model helps to reduce the error in pyrolysis times for particles that would be better modeled in three dimensions.

The two-dimensional model was able to predict pyrolysis times within 15% for all particle sizes and temperatures. The model worked best for the 1/8 inch particle, where errors in surface area from the two-dimensional discretization before and after shrinkage were each off by 10%, and tended to cancel each other out. The predicted pyrolysis times were off by a maximum of 15% for the ¼ inch particle. Errors in the total surface area of the particle were caused by the two dimensional representation of the particle, and caused the predicted pyrolysis times to be slower than experimental values. For the ½ inch particles, the pyrolysis times were within 13%, and also tended to be slower than the measured pyrolysis times. The effect of underestimating the surface area by a two-dimensional representation of the particle is likely offset by overestimating the conductivity of the char layer for ½ x 1 x 1 in^3 particles. At low temperatures, the computational model was farther off than for high temperatures. This may be caused by the effects of shrinkage in three dimensions, or because high temperature particles have higher gas fluxes which will shield the particle from some of the external radiation.

This computational model shows why many computational modelers have had difficulty applying their computational models to more than one experiment. Errors in the surface area of the particle with respect to time make it difficult for computational modelers to match experimental results using the measured property values. The numerical model typically will have to use a higher value for char conductivity to obtain similar pyrolysis times to experimental results because they have underestimated the surface area of the particle. These computational models may work well for a given set of conditions, but can not be applied to the wide range of conditions that exist in combustion situations.

The two-dimensional computational model demonstrates the importance of particle shape, size, and temperature in the pyrolysis process. The results indicate that char cracking is a primary mechanism by which heat is transferred into the particle, and that char conductivity may be less dependant on temperature the previous modelers have assumed. More research is needed to determine the exact nature in which char cracking affect the pyrolysis process. While some three-dimensional effects cannot be accounted for in the two-dimensional model, it does a much better job of accounting for all of the important phenomena than do the existing one-dimensional models. The current model can be used to solve for three dimensional particles, but was not validated on this basis due to the time needed to solve the problem on a three dimensional grid.

Chapter 6

Results

The two-dimensional computational model was used to predict the performance of single particles of dry wood for a fixed external temperature of 800K, 1200K, 1600K and 2000K. In order to examine the importance of particle size and shape, square particles were varied in size from 0.1 mm x 0.1 mm to 5 cm x 5 cm. Rectangular particles were also tested for each case with an aspect ratio of 2:1 and were tested for both a horizontal grain direction and a vertical grain direction. The conductivity was assumed to be 1.8 times larger in the grain direction. The shrinkage data (where available) was obtained from Hoerning (1999). For particle sizes and temperatures outside of the range of the data of Hoerning, shrinkage factors were assumed. The walls of the transport vessels in the grain direction are composed structural components containing lignin, and these structural components limit the amount of shrinkage in the grain direction. By contrast, there are many empty channels in the cross-grain direction which result in a more shrinkage in the cross-grain direction when wood is pyrolyzed into char. Shrinkage was treated as being preferential in the direction perpendicular to the grain by a factor of two. At conditions where the shrinkage factor is 0.9 (10% shrinkage) in the grain direction, the shrinkage factor would be 0.8 (20% shrinkage) in the cross-grain direction. This shrinkage formulation is consistent with the measurements taken by Hoerning. The shrinkage factor in the model varied from 0.8 to 0.4 in the cross-grain direction (and 0.9 tp 0.7 in the grain direction), depending on the particle size and the temperature. At 2000K, for very small particles, the shrinkage factor was 0.4. The amount of shrinkage decreases as the temperature is decreased and as particle size is increased, due to

the lower pyrolysis temperatures in larger particles. The shrinkage parameters used for the model runs are given in Table 6.

Length	Temperature (K) with grain				Temperature (K) against grain			
mm	800	1200	1600	2000	800	1200	1600	2000
0.1	0.750	0.710	0.700	0.700	0.500	0.420	0.400	0.400
0.2	0.760	0.720	0.700	0.700	0.520	0.440	0.400	0.400
1	0.770	0.730	0.715	0.700	0.540	0.460	0.430	0.400
2	0.780	0.760	0.740	0.720	0.560	0.520	0.480	0.440
4	0.830	0.825	0.820	0.815	0.660	0.650	0.640	0.630
5	0.845	0.840	0.835	0.830	0.690	0.680	0.670	0.660
10	0.900	0.900	0.900	0.900	0.800	0.800	0.800	0.800
20	0.900	0.900	0.900	0.900	0.800	0.800	0.800	0.800
40	0.900	0.900	0.900	0.900	0.800	0.800	0.800	0.800
50	0.900	0.900	0.900	0.900	0.800	0.800	0.800	0.800
100	0.900	0.900	0.900	0.900	0.800	0.800	0.800	0.800

Table 6. Shrinkage Parameters Used For Model Results

The performance of a wood particle during pyrolysis can vary depending on whether thermally thin, thermally thick, or thermal wave conditions exist within the particle. For a two-dimensional particle, differences in size, shape, and directional properties may make it difficult to determine the thermal regime under which pyrolysis occurs. As an example, if a large thin (1 mm x 50 cm x 50 cm) wooden slab exposed to a low pyrolysis temperature (800K) on all sides, it would be considered under thermally thin conditions in the 1 mm direction and under thermal wave conditions in the 50 cm directions, based on the Biot number (hD/k) in each direction. In this simple case, the characteristic length is in the 1 mm direction and the wooden slab could be modeled as a thermally thin, one-dimensional, 1 mm particle. For particle sizes where the particle dimensions differ but are of similar magnitude, the characteristic dimension(s) becomes less clear.

Previous computational modeling work has shown that most pyrolysis occurs under thermally thick or thermal wave conditions. While simple models may be used in the extreme cases of a thermally thin or a thermal wave particle, detailed models are needed when both external and internal heat transfer are important. In the thermal wave regime, a particle could be modeled using a reacting front that moves through a particle to obtain pyrolysis times. This type of model may be applicable to a one-dimensional reacting front, but can not predict the pressures within the particle or pyrolysis residence times. For multi-dimensional particles, it is much more difficult to apply a simple reacting front model when there is a reaction front on each surface of the particle, different properties in each direction, and an interaction between the reacting fronts on each surface of the particle. It is likely that the strict thermal wave regime only exists for truly one-dimensional cases. Because the anisotropy of the particle complicates analysis, a number of particle sizes, shapes, and temperatures will be examined in detail to determine what can be learned from a two-dimensional pyrolysis model.

6.1 Square Particles

The smallest particle computed by the model was a 0.1 mm x 0.1 mm particle. With an external temperature of 800K, the rate of internal heat transfer is much faster than the rate of external heat transfer, and a lumped capacitance model could be used with a pyrolysis scheme to analyze the pyrolysis performance. The rate of mass loss predicted by the detailed model is shown in Fig 20 and the rate of release of pyrolysis gases from the surface of the particle is shown in Fig 21. The rate of mass loss is highest near the beginning of pyrolysis

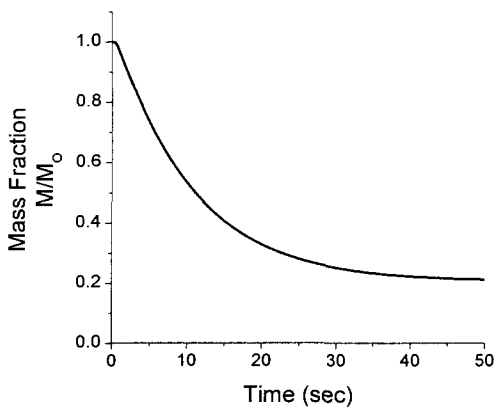

Fig 20. Solid Mass Fraction Remaining for a 0.1 mm x 0.1 mm Particle at 800K

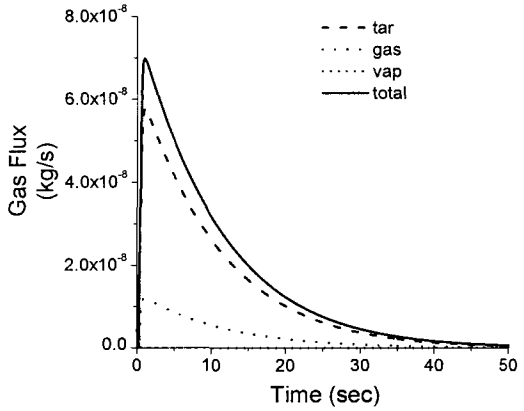

Fig 21. Surface Gas Fluxes for a 0.1 mm x 0.1 mm Particle at 800K

when more virgin wood is available to pyrolyze. The slope of the mass loss curve decreases as time continues because the amount of wood available for pyrolysis continues to drop. The mass loss curve indicates that the mass of the particle does not drop much after 30 seconds, indicating that pyrolysis is completed after around 30 seconds. At the end of pyrolysis, 21% of the original mass of the particle remains in the form of char.

The maximum release of pyrolysis gases occurs after 1.05 seconds of pyrolysis, when the particle heats up to pyrolysis temperatures. The production of pyrolysis gases is limited by the rate of pyrolysis reaction and the amount of wood remaining. This is an example of kinetically controlled pyrolysis, where the rate of pyrolysis is controlled by the rate of the pyrolysis reaction and the amount of wood available of pyrolyze. The release of gases peaks at $6.98*10^{-8}$ kg/s with tars accounting for $5.78*10^{-7}$ kg/sec and light gases accounting for $1.20*10^{-7}$ kg/s. The rate of release of tar is initially 5 times higher than rate of release of light

hydrocarbons and the proportion of tars continues to dominate, with 1.5 times as much tar being releases near the end of pyrolysis.

The temperature and pressure profiles are shown at various time steps in Fig 22 for the 0.1 mm x 0.1 mm particle at 800K. The figure shows temperature and pressure profiles for the bottom left quarter of the particle after 0.3 seconds, 0.65 seconds, and 5 seconds, respectively. For all particle profiles, the particle dimensions are given in millimeters. After 0.3 seconds, the particle has heated up to a temperature of around 679K. The particle has a nearly constant temperature, with only a 2K temperature difference within the particle. The pressure is 100.010 kPa at the center of the particle, with pressure dropping towards the outer (left and bottom) surfaces of the particle. The total gas flux from the particle after 0.3 seconds is $1/10^{th}$ the maximum gas flux recorded for the 0.1 mm x 0.1mm particle at 800K.

The particle reaches a temperature of 723 K after 0.65 seconds, and rises only 7K further to 730K after 5 seconds. The maximum pressure in the particle is 100.021 kPa, which occurs at 0.5 seconds (not shown). The pressure at the center of the particle drops after 0.5 seconds, with a value of 100.018 kPa at 0.65 seconds. Interestingly, the maximum gas fluxes from the particle occur at 1.05 seconds, when the peak pressure is only 100.010 kPa. These results would seem to indicate that the pressurization of the particle is caused by the temperature increases within the particle and gas production during the first 0.5 seconds of pyrolysis and that the peak flux of pyrolysis gases occurs after the peak pressure, while there is rapid depressurization within the particle.

If a similar 0.1 mm x 0.1 mm particle is heated with an external temperature of 1600K, the particle will perform much differently. The initial amount of radiation to the

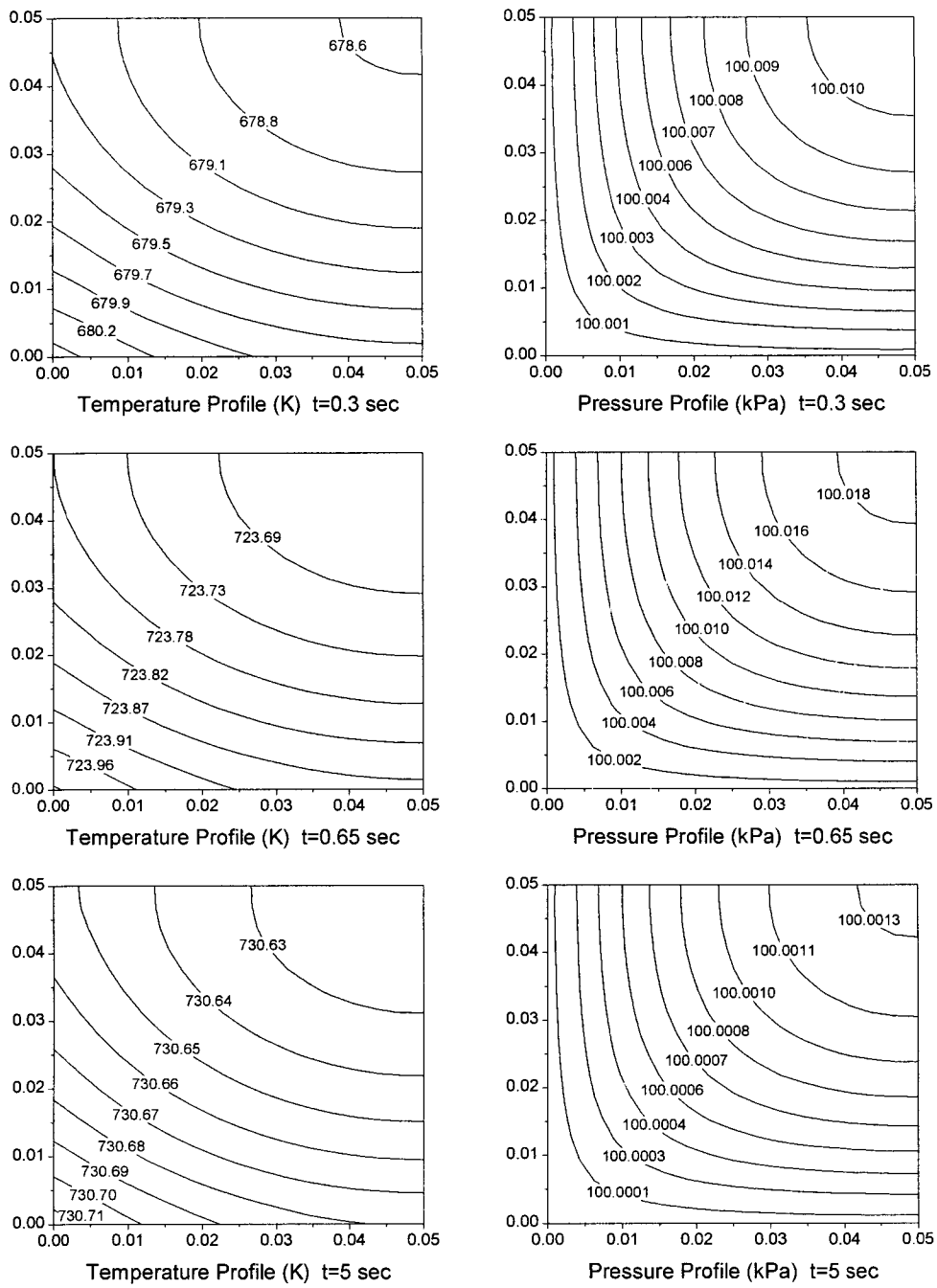

Fig 22. Temperature and Pressure Profiles for a 0.1 mm x 0.1 mm Particle at 800K

surface of the particle will be approximately 16 times higher for the 1600K external source because radiation depends on temperature to the fourth power. Although the particle will heat up quickly with such a high external heat flux, the external heat flux also drives the particle to much higher pyrolysis temperatures than in the previous example. The mass loss curve and pyrolysis gas release curve are shown in Fig 23 and 24.

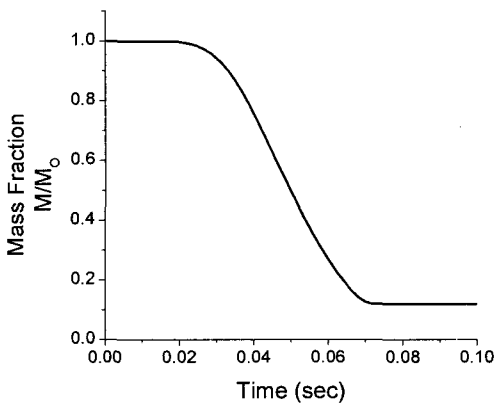

Fig 23. Solid Mass Fraction Remaining for a 0.1 mm x 0.1 mm Particle at 1600K

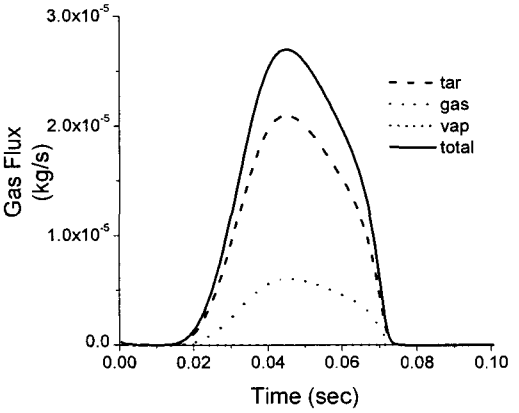

Fig 24. Surface Gas Fluxes for a 0.1 mm x 0.1 mm Particle at 1600K

For the first 0.025 seconds of pyrolysis, there is very little production of pyrolysis gases because the particle has to heat up to pyrolysis temperatures. The rate of mass loss begins rapidly and remains nearly constant until pyrolysis finishes after around 0.07 seconds. In the previous case with an external temperature of 800K, the amount of gas production decreased as the amount of wood decreased. With an external temperature of 1600K, the pyrolysis temperatures continue to rise even after rapid pyrolysis begins. As temperatures

continue to rise, the increase in the rate of pyrolysis gas production offsets the reduction in the amount of wood remaining in the particle to produce a somewhat linear mass loss curve.

After only 0.015 seconds, the rate of gas production for the 1600K particle is equal to $1.2x10^{-7}$ kg/s, the maximum rate of gas production at 800K. The gas release continues to rise to a rate of $2.7x10^{-5}$ kg/s at 0.045 seconds. The peak gas release rate for a 0.1 mm x 0.1 mm particle at 1600K is 200 times higher than the peak rate for the same particle at 800K.

The temperatures and pressures for the 0.1 mm x 0.1 mm particle at 1600K are shown in Fig 25. The highest pressure within the particle happens at 0.03 seconds, prior to the maximum rate of release of pyrolysis gases from the particle. At 0.03 seconds, the gas flux from the particle is only 1/3 of the maximum gas flux that occurs at 0.045 seconds. Temperatures and pressures are shown at 0.03 seconds, 0.0375 seconds, and 0.045 seconds to demonstrate what is happening during this period of pyrolysis. The temperature profiles show that there is about an 80K temperature difference within the particle during this portion of pyrolysis, with the highest temperature at the corners of the particle. The pressure profiles show that the pressure at the center of the particle drops from 101.62 kPa at 0.03 seconds, to 101.44 kPa at 0.0375 seconds, and to 100.99 kPa at 0.045 seconds. The pressure near the surface of the particle drops from 100.09 kPa to 100.06 kPa during this same time period. The increase in gas fluxes from 0.03 seconds to 0.045 seconds can not be a result of an increased pressure gradient. Fig 26 shows the resistance to gas flow within the particle. The resistance to flow within the particle is based on the amount of wood and char. The regions in the particle that have a higher resistance to flow have a higher fraction of wood remaining. Recall that char is 100 times more permeable than wood. Wood was assumed to have a resistance to flow of 1 Darcy and char 0.01 Darcy. If a char particle and a wood particle had

the same pressure gradient, the char particle would have a gas flux that is 100 times higher than the wood particle. Fig 26 shows that the resistance to flow drops by a factor of 3 at the surface of the particle from 0.03 to 0.045 seconds, which means that the permeability of the wood increases by a factor of 3. The threefold increase in the release of pyrolysis gases from 0.03 seconds to 0.045 seconds happens because the permeability of the particle increases by a factor of three at the surface during the same time period. At 0.03 seconds, the production of pyrolysis gases is highest at the corners of the particle, where temperatures are at 1000K, and nearly 80% of the wood still remains. The center of the particle still has 95% wood, but produces less pyrolysis products because it is at a temperature of 920K. At 0.0375 seconds, the corners of the particle are at 1040K and still have 50% wood remaining. The maximum rate of gas production is still at the corners of the particle, but the gas production has increased within the particle. The central surface region is at about 1006K and has 70% wood remaining. Further within the particle, temperatures are closer to 997K, but 80% of the wood still remains. The rate of gas production in various regions of the particle is a function of both temperature and the amount of wood remaining, and is based on the way in which pyrolysis occurs. The rate of production of pyrolysis gases is important to the pressurization of the particle. The surface of the particle heats up from 300K to 900K in about 0.01 seconds. This temperature increase would cause the pressure to increase by a factor of three if no gases were allowed to escape from the surface of the particle. With a gas production rate of

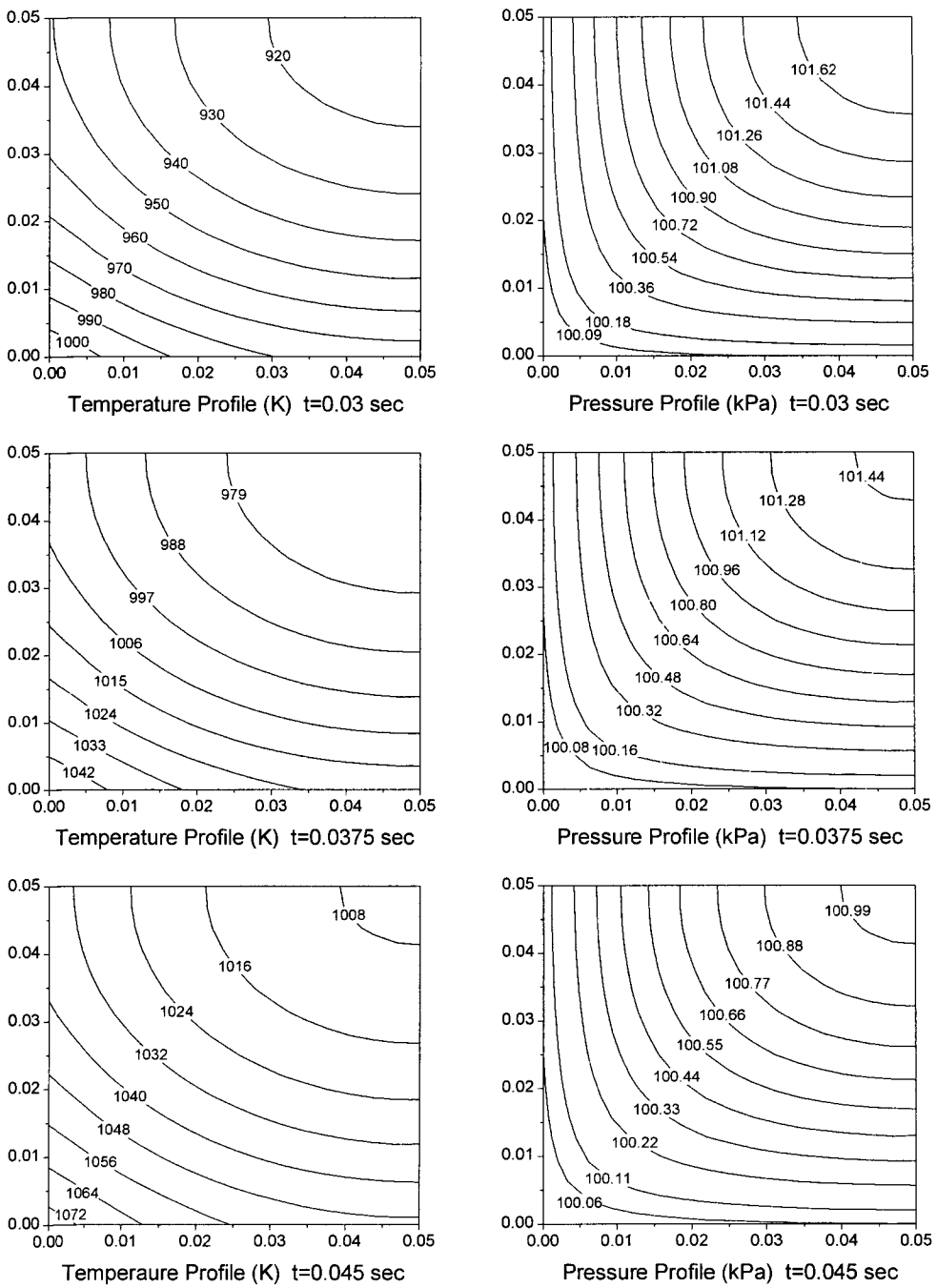

Fig 25. Temperature and Pressure Profiles for a 0.1 mm x 0.1 mm Particle at 1600K

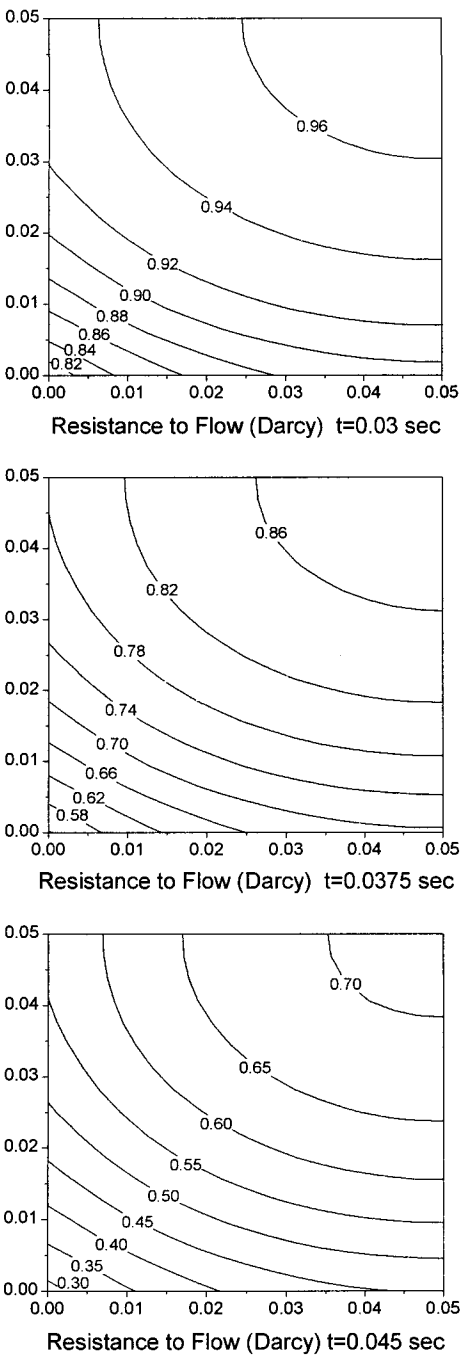

Fig 26. Resistance to Flow for a 0.1 mm x 0.1 mm Particle at 1600K

0.01 kg/s, the surface of the particle would produce 10^{-4} kg of gas in 0.01 seconds. The whole particle contains less than 10^{-8} kg of gas. In the same 0.01 second time period, if no gases were allowed to escape the production of pyrolysis gases would increase the pressure of the particle by a factor of 10,000. An order of magnitude analysis indicates that while rapid increases in temperature and pressure often occur in the same regions of the particle, gas production is the primary mode of pressurization within small particles. Fig 27 shows that the initial pressurization of the particle is caused by heat flux at the surface, because pyrolysis gases are not yet being produced. The large rise in pressure is caused by the production of pyrolysis gases within the particle.

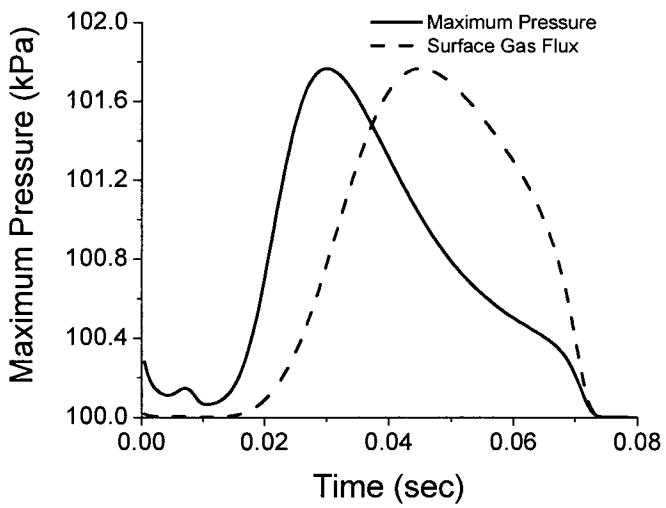

Fig 27. Particle Pressurization vs. Surface Gas Flux

These results indicate that for the pyrolysis of fine powders with low heating rates the particle remains at a nearly constant temperature. The amount of time required to heat the particle is negligible, because the steady state temperature of the particle and the rate of the pyrolysis reactions determine the pyrolysis process. It is important to understand the kinetics

of the wood particle for fine powders at low pyrolysis temperatures. The particle pressurizes in response to the heating of the particle and the gas production in pyrolysis regions. The permeability of the particle also begins to increase due to conversion of wood to char. These two factors cause pressure to drop rapidly. The rate of gas production from the particle reaches a maximum after the particle begins to depressurize, when continued conversion of the surface of the particle increases the permeability near the surface. At low temperatures, the maximum rate of pyrolysis gas production is 1.5 times the rate of gas production when the particle is at its highest pressure.

For powders at high temperatures, there are limited temperature gradients within the particle. The heat up time of these particles can account for over 1/3 of the total pyrolysis time, indicating that both the thermal capacity of the particle and the pyrolysis kinetics are important for pyrolysis. Pressurization happens in a similar manner to the low temperature particle, with peak pressures at the center of the particle. The pressurization of the particle is much higher because of elevated temperatures, and the faster conversion to char near the surface of the particle causes the maximum gas flux to increase from the rate at peak pressurization by over a factor of 3. When temperature gradients exist within the particle, the rate of production of pyrolysis gases can vary from region to region depending on the amount of wood and the temperature at each location. A 2 mm x 2 mm particle is a relatively coarse sawdust particle.

The mass loss and gas flux curves for a 2 mm x 2 mm particle at 800K are shown in Fig 28 and Fig 29. The mass loss curve for the 2 mm x 2 mm particle shows that there is a delay of around 7 seconds while the particle heats up. The mass loss curve for the 2 mm particle at 800K appears to be about half way between the shape of the exponential decay of

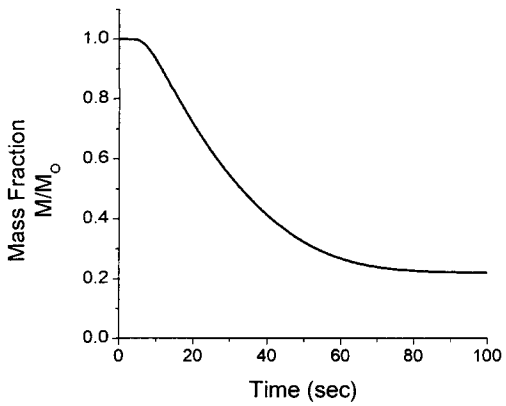

Fig 28. Solid Mass Fraction Remaining for a 2 mm x 2 mm Particle at 1600K

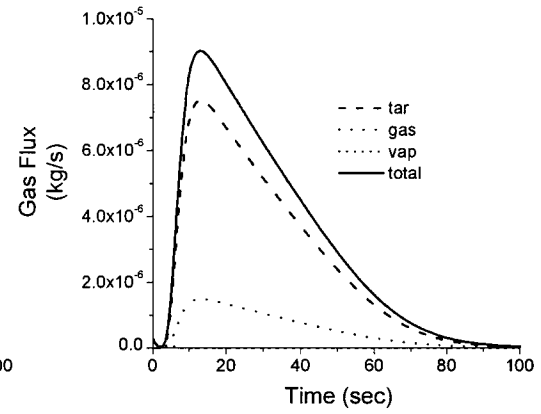

Fig 29. Surface Gas Fluxes for a 2 mm x 2 mm Particle at 1600K

the 0.1 mm particle at 800K and the more linear shape of the mass loss curve of the 0.1 mm particle at 1600K. The initial delay in mass loss shows that the heat up time is somewhat important, accounting for over 10% of the total pyrolysis time. The more linear mass loss curve indicates that either there are temperature gradients within the particle and/or the pyrolysis temperature is increasing as the amount of wood decreases. The pyrolysis gas flux curve shows a peak production of pyrolysis gases of $9x10^{-6}$ kg/s after 13 seconds. The tar production dominates initially by a factor of 5 and is only less than the light hydrocarbon (gas) production after 100 seconds, when the rate of release of pyrolysis gases is negligible.

The temperature and pressure graphs for the 2 mm x 2 mm particle at 800K are shown in Fig 30. Once again, the profiles show only the bottom left quarter of the particle due to particle symmetry, with particle dimensions in millimeters. The particle has a temperature variance of around 20K at 10 seconds and 6K after 40 seconds. The pressure is highest at the center and reaches a maximum at 6.8 seconds and then begins to drop. The

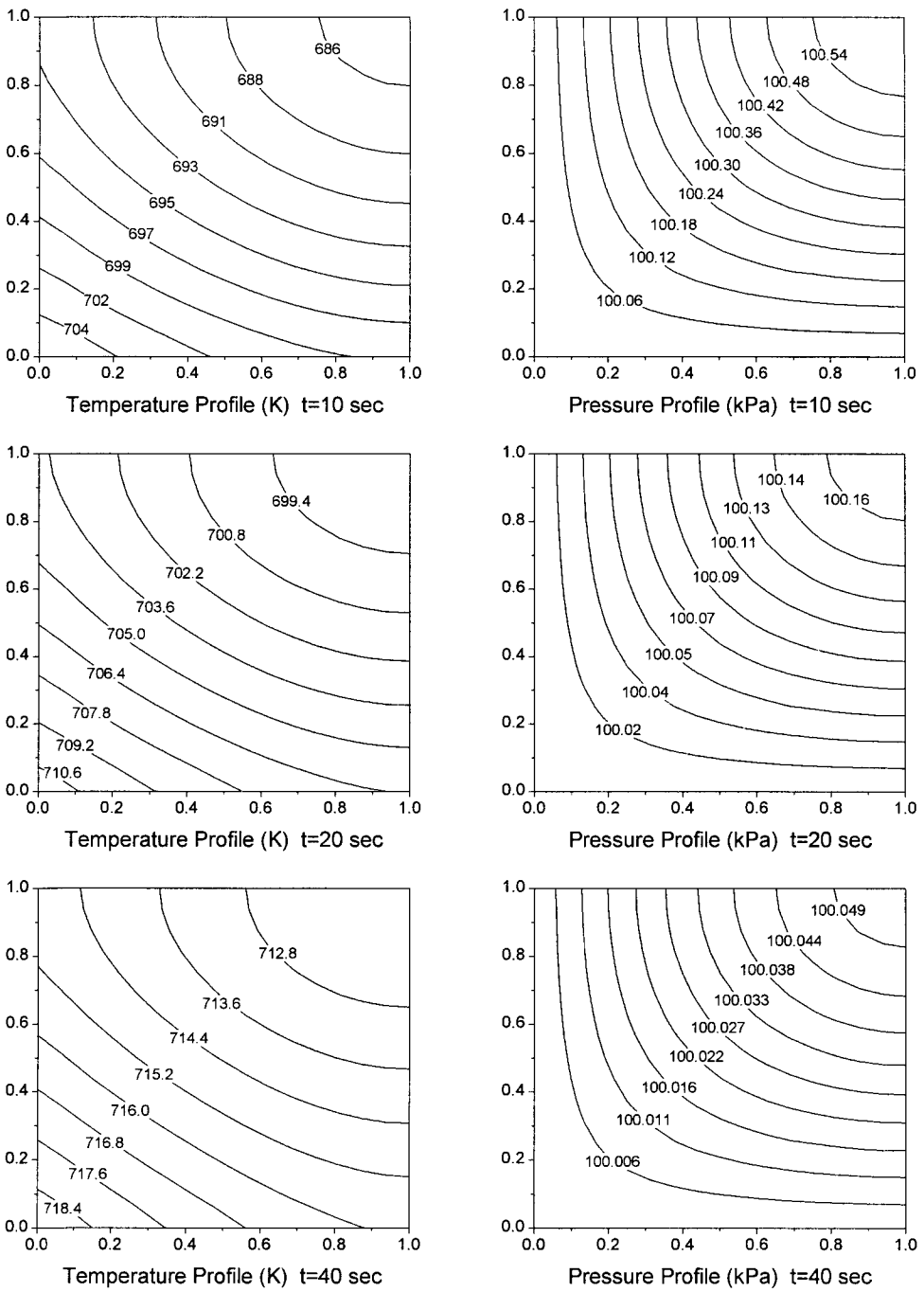

Fig 30. Temperature and Pressure Profiles for a 2 mm x 2 mm Particle at 800K

pressure is the highest while gas fluxes are less than 50% of their maximum. This case is very similar to the 0.1 mm x 0.1 mm case, in that the particle is thermally thin and the pyrolysis time depends on the rate of kinetic reaction. The main difference is that the 2 mm x 2 mm particle has 20 times the surface area but has 400 times as much volume. The heat up time thus becomes important, and most pyrolysis occurs at around 700K, which is 30K cooler than the 0.1 mm x 0.1 mm particle. The total pyrolysis time takes about 50% longer than the 0.1 mm x 0.1 mm particle at the same temperature due to the lower pyrolysis temperature and the additional time required to heat the particle. The mass loss and gas flux figures for a 2 mm x 2 mm particle at 1600K are shown in Fig 31 and Fig 32.

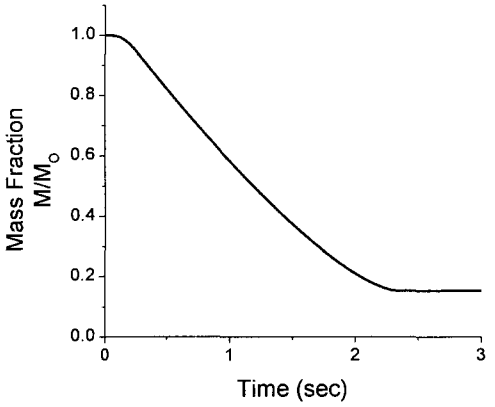

Fig 31. Solid Mass Fraction Remaining for a 2 mm x 2 mm Particle at 1600K

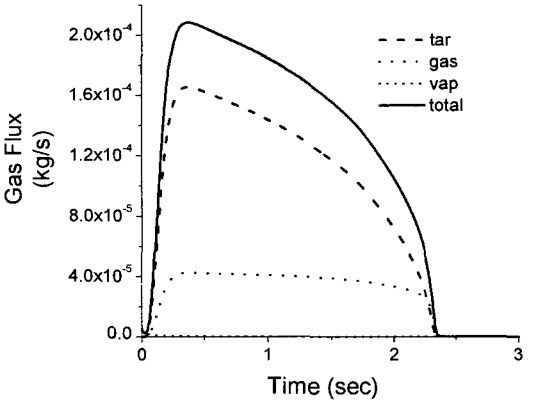

Fig 32. Surface Gas Fluxes for a 2 mm x 2 mm Particle at 1600K

The mass loss curve shows a relatively short delay of a few tenths of a second followed by a nearly linear rate of devolatilization, with the completion of pyrolysis after a little more than 2 seconds. The peak in gas production from the particle occurs after 0.38

seconds of heating. The rate of gas release from the particle decreases steadily for most of pyrolysis with a rapid drop in the total gas fluxes for the last quarter of pyrolysis. The production of tars follows the shape of the total gas flux curve while the light gases production remains nearly constant. The tar production dominates by 4:1 after 0.1 seconds and by 2:1 after 2 seconds.

The temperature and pressure profiles for the 2 mm x 2mm particle at 1600K are shown in Fig 33. The broad peak in the production of pyrolysis gases and the linear mass loss curve are caused by the temperature gradient within the particle. At 1600K, the 2 mm x 2 mm particle has temperature gradients of over 600K at 0.5, 1.0, and the linear mass loss curve are caused by the temperature gradient within the particle. At 1600K, the 2 mm x 2 mm particle has temperature gradients of over 600K at 0.5, 1.0, and 2.0 seconds. Initially, the highest pressures within the particle lie about two thirds of the way from the center of the particle to each of the corners. When the gas fluxes are at their highest (~0.5 sec), the highest pressures have moved to midway between each of the corners of the particle and the center of the particle. The peak pressure is in regions of the particle between 650K and 750K. By 1 second, which is about 50% of the total pyrolysis time, the peak pressure has moved to the center of the particle, with a center temperature of 680K. The peak pressure continues to rise at the center of the particle with a peak pressure of 105.12 kPa at 1.44 seconds and then begins to drop slowly. The performance of the 2 mm x 2 mm particle is different from the 0.1 x 0.1 mm particle. For the 2 mm particle at 800K, there is a delay while the particle heats up, and pyrolysis happens at a 30K cooler temperature. The mass loss curve is no longer a first-order decay curve, indicating that there are 20K temperature differences within the particle and that the particle is heating up during pyrolysis. The peak in gas fluxes comes shortly after

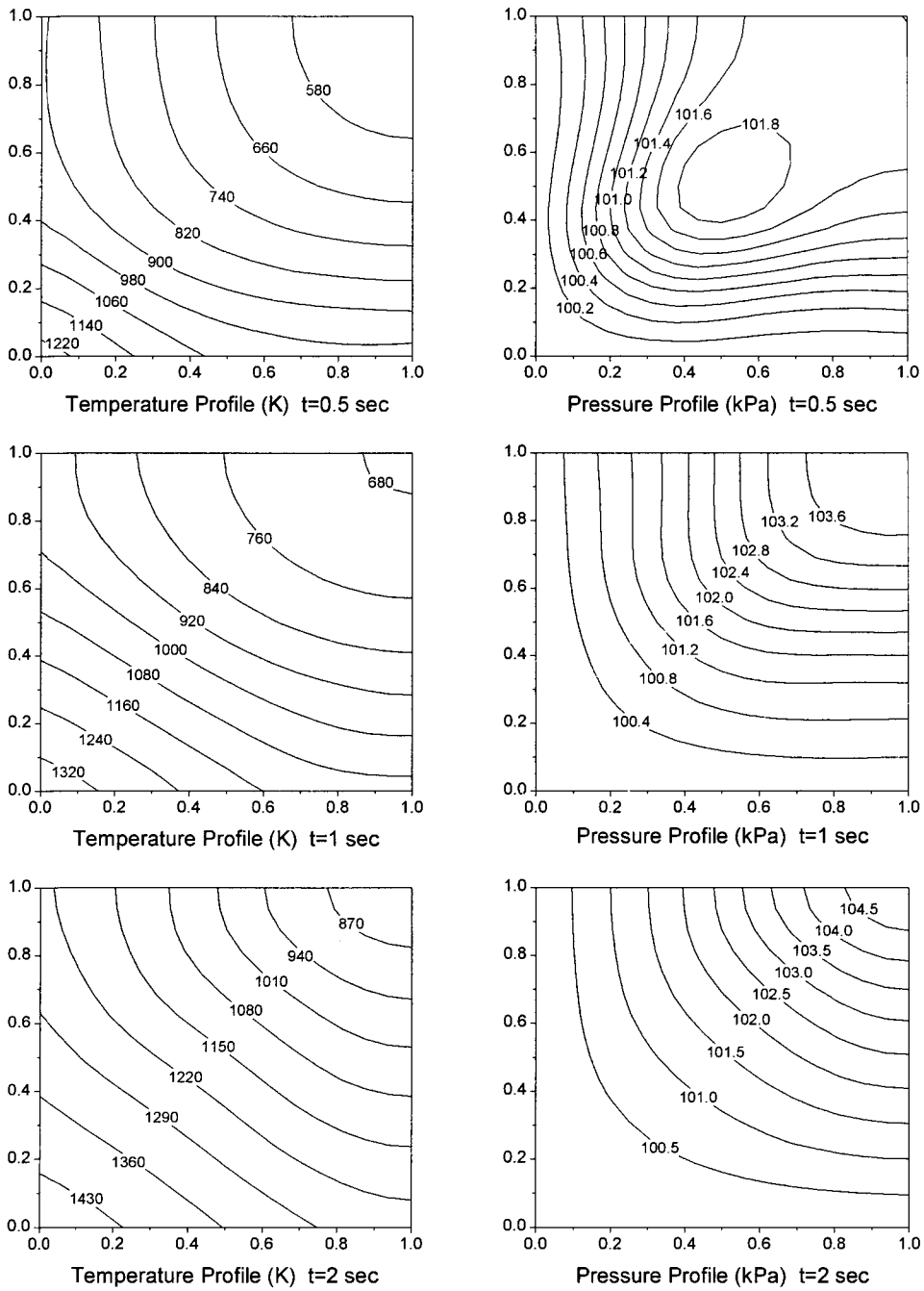

Fig 33. Temperature and Pressure Profiles for a 2 mm x 2 mm Particle at 1600K

the initial delay due to particle heating, with a slightly broader gas flux peak. At 1600K, the delay due to heating of the particle is less important than for the 0.1 x 0.1 mm particle. The gas fluxes peak after a short delay and drop gradually. The 2 mm x 2 mm particle shows a left centered peak with only a short delay, while the 0.1 mm x 0.1 mm particle at 1600K has a large delay followed by a nearly symmetrical peak in gas production. The pressure in the 2 mm x 2 mm particle at 1600K continues to rise after the peak gas fluxes, and peaks some time later in pyrolysis.

Wood chips are often preferred in pyrolysis systems because less mechanical work is required to produce larger particles. Fig 34 and Fig 35 show the performance of a 1 cm x 1 cm particle at 800K.

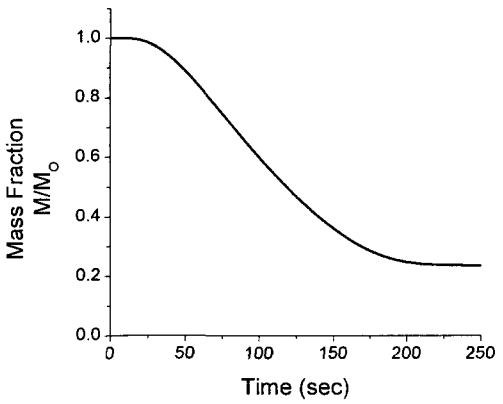

Fig 34. Solid Mass Fraction Remaining for a 1 cm x 1 cm Particle at 800K

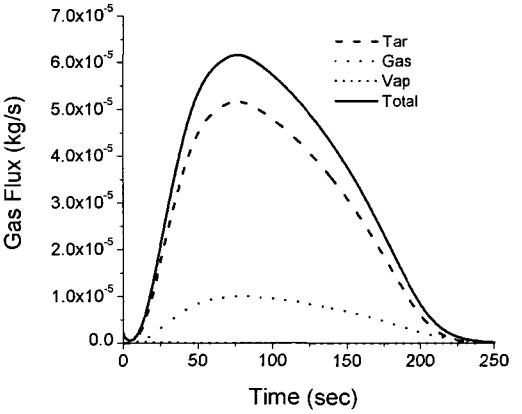

Fig 35. Surface Gas Fluxes for a 1 cm x 1 cm Particle at 800K

It takes about 25 seconds for the 1 cm x 1 cm particle at 800K to heat up to pyrolysis temperatures. For most of pyrolysis, the mass loss rate is fairly linear, with a slower rate of

devolatilization at the beginning and end of pyrolysis. The gas fluxes peak at 77 seconds, with a gas flow of $6*10^{-5}$ kg/s. The shape of the gas flux curve for the 1 cm x 1 cm particle is much more symmetrical than it was for smaller particles at 800K and, of the figures shown, most closely resembles the 0.1 mm x 0.1 mm particle at 1600K. Recall that the 0.1 mm x 0.1 mm particle had pyrolysis temperatures increasing above 1000K with an 80K temperature gradient across the particle. The linear mass loss rate and nearly symmetrical gas flux peak were caused by the fact that pyrolysis temperatures were increasing with time.

The temperature and pressure profiles for the 1 cm x 1 cm particle at 800K are shown at 50, 100, and 150 seconds in Fig 36. The 1 cm x 1cm particle has a temperature difference of around 80K at 50 seconds and a temperature difference of 25K at 150 seconds. At 150 seconds, the average pyrolysis temperature is 30K higher than at 50 seconds. The pyrolysis temperature increases with time and offsets the reduction in wood within the particle to produce a linear shaped mass loss curve. The particle pressure peaks at 102.0 kPa at 45 seconds and then begins to drop. The way the particle is pressurized, the maximum pressure within the particle, and the depressurization of the particle all closely resemble the 0.1 mm x 0.1 mm particle at 1600K.

The mass loss rate and the gas fluxes are shown for 1 cm x 1 cm wood chips at 1600K in Fig 37 and Fig 38. The wood chips exhibit a larger mass loss rate during the initial portion of pyrolysis. This is a result of the large heat flux to the virgin wood near the surface of the particle. The mass loss rate is fairly linear after this initial period, with the mass loss rate dropping slightly at the end of pyrolysis. The drop in rate of mass loss happens because less virgin wood is available at the center of the particle.

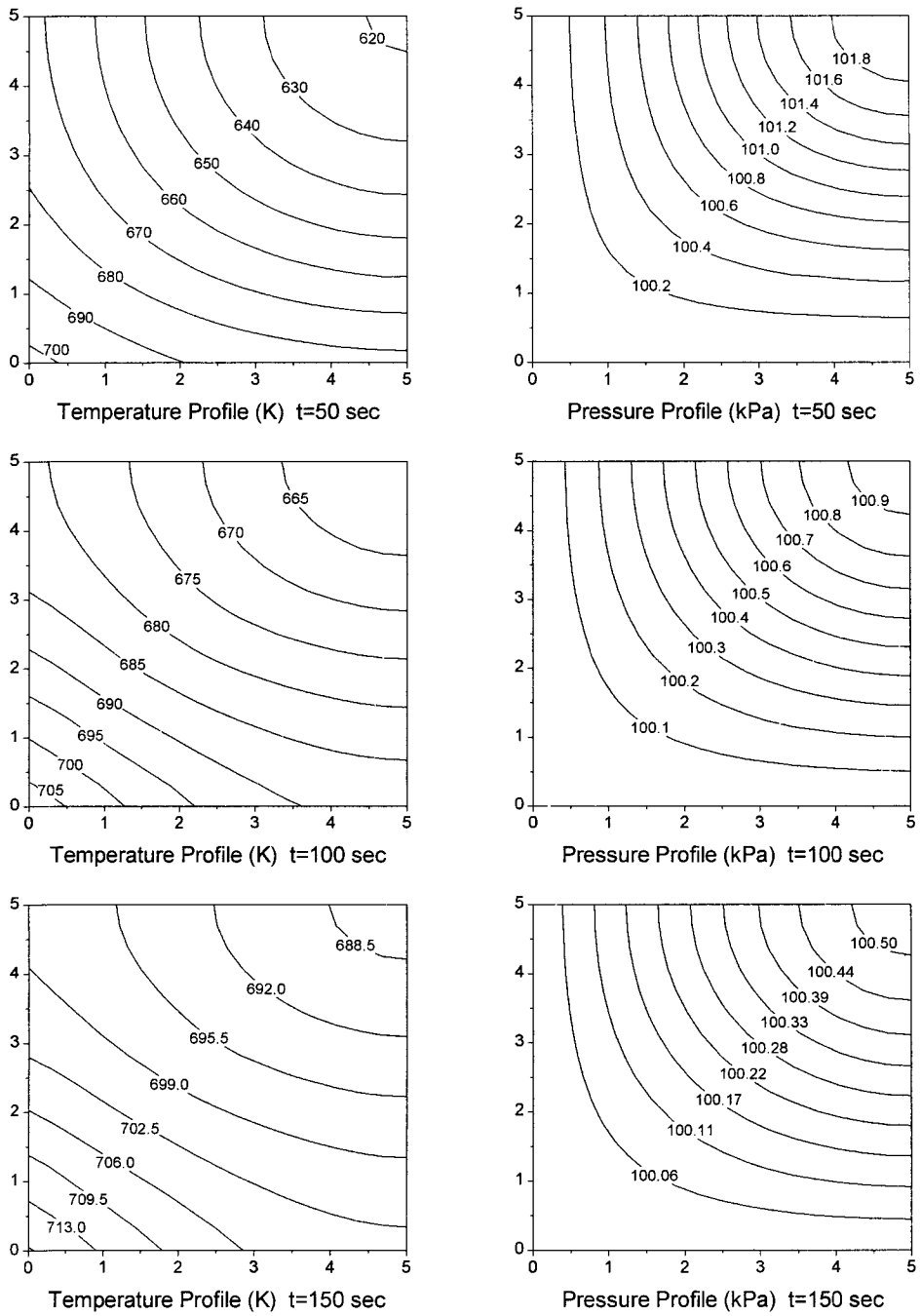

Fig 36. Temperature and Pressure Profiles for a 1 cm x 1 cm Particle at 800K

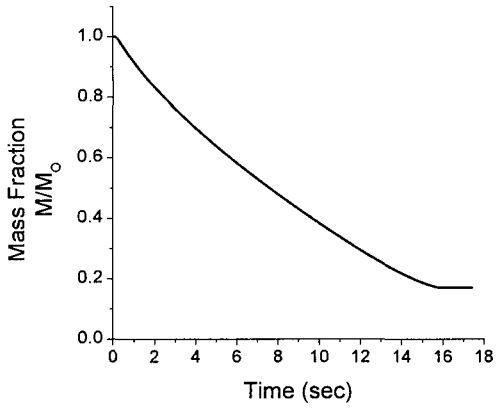

Fig 37. Solid Mass Fraction Remaining for a 1 cm x 1 cm Particle at 1600K

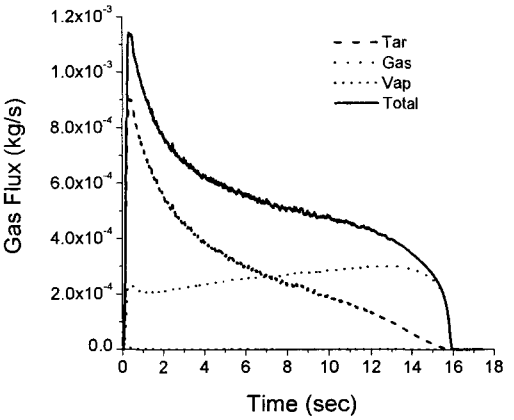

Fig 38. Surface Gas Fluxes for a 1 cm x 1 cm Particle at 1600K

The temperature and pressure profiles are shown in Fig 39. After 1 second of pyrolysis, regions within 1 mm of the surface are above 600K and are undergoing pyrolysis reactions. The peak pressure at 1 second is located at the corners of the particle, 1 mm from each surface. At 6 seconds, the particle has developed a fairly linear temperature profile, with an increase in the temperature gradient across the 600K-800K temperature regions. This region is located about 3 mm from the surface of the particle and corresponds to the peak pressure 6 seconds after heating. At 12 seconds, the center of the particle is being pyrolyzed, and the maximum pressure is located at the center of the particle.

The previous six examples demonstrate how pyrolysis performance will differ depending on the particle size and the external temperature. Intuition into the two dimensional nature of the pyrolysis can be gained by looking at the mass loss, gas flux, temperature and pressure profiles. These results show that the rate of particle mass loss and the rate of gas fluxes from the particle depend on both particle size and temperature. The

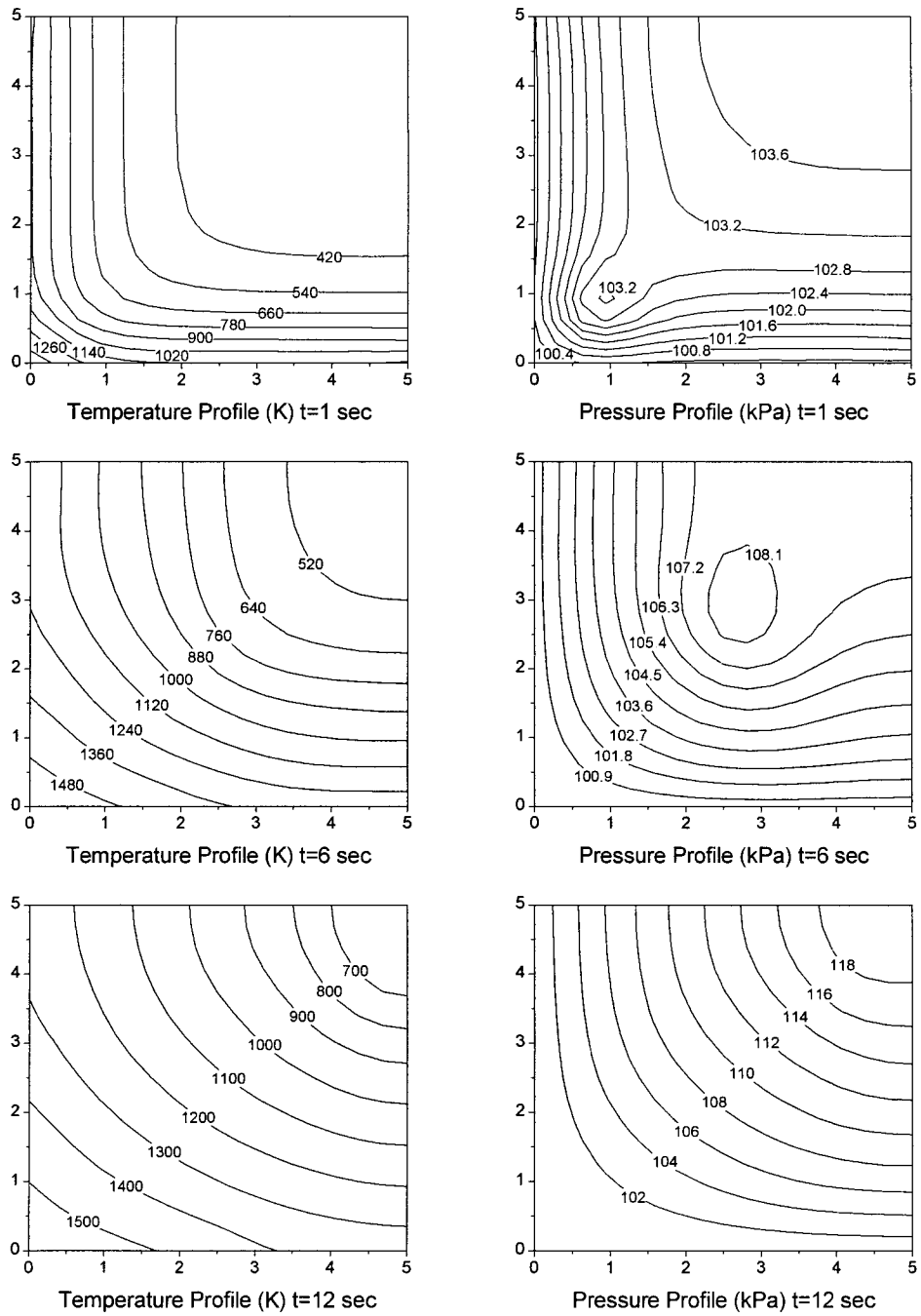

Fig 39. Temperature and Pressure Profiles for a 1 cm x 1 cm Particle at 1600K

cases with a limited temperature gradient all showed peak pressurization prior to the peak rate of gas fluxes from the particle, and the peak pressure was measured at the center of the particle. The cases with large temperature gradients showed that the peak pressure within the particle occurred only after the maximum rate of gas fluxes from the particle. For these cases the peak pressures were initially located between the corners of the particle and the center of the particle, with the peak pressure moving to the center of the particle during later portions of pyrolysis. The particle pressurization is linked to the total gas fluxes from the particle and the permeability of the particle near the surface. In all cases, the maximum gas flux rate did not correspond to the peak pressurization of the particle.

6.2 Rectangular Particles

The model runs were repeated using rectangular particles with an aspect ratio of 2:1 to determine the importance of particle shape. Fig 40 and Fig 41 compare the mass loss and total gas flux curves at 800K for a 0.1 mm x 0.1 mm particle and for a 0.2 mm x 0.1 mm particle, where the grain direction is in the 0.2 mm direction. In all cases the grain direction is the first reported dimension. The mass loss curves remain nearly identical for the 0.1 mm x 0.1 mm particle and the 0.2 mm x 0.1 mm particle at 800K. The rate of gas production from the rectangular particle is nearly double that of the smaller particle. The two particles perform identically, except that the rectangular particle has twice the initial mass and will release twice as much gas at any given time, with both particles completing pyrolysis at the same time. For ground sawdust or powders, the particle is kinetically controlled. The particle shape and size do not influence the pyrolysis time in the kinetically controlled pyrolysis

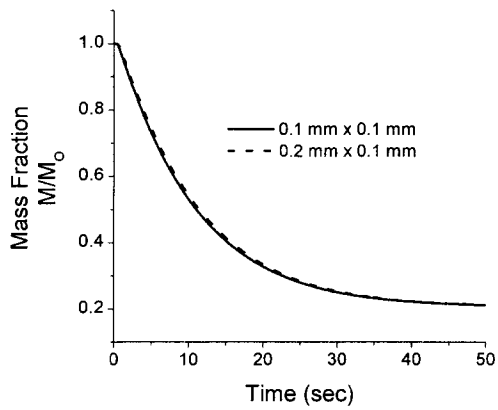

Fig 40. Solid Mass Fraction Remaining for a Square and Rectangular Grain-Direction Particle at 800K

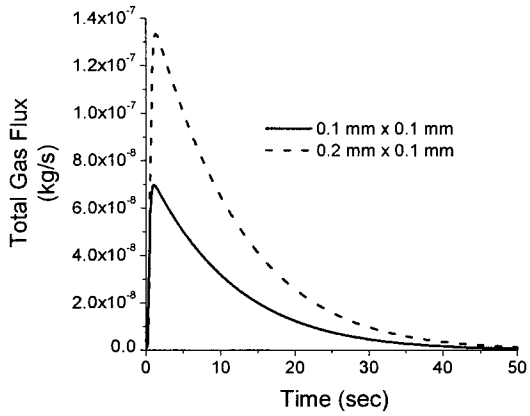

Fig 41. Surface Gas Fluxes for a Square and Rectangular Grain-Direction Particle at 800K

regime, with the rate of pyrolysis determining the total pyrolysis time. The temperature and pressure profiles are shown in Fig 42 for the bottom left quarter of the 0.2 mm x 0.1 mm particle at 800K at various time steps. At 0.3 seconds, the temperature gradient is about 20K/mm in the grain direction and 34 K/mm in the cross grain direction, which would be expected with a conductivity that is 1.8 times higher in the grain direction. The square particle had a temperature gradient of 18 K/mm in the grain direction and 28K/mm in the cross grain direction. The rectangular particle has a peak pressure at 0.65 seconds, with a peak gas flux at 1.35 seconds. The particle has only small temperature differences (less than 3K) and the particle continues to heat up during the first 5 seconds of pyrolysis. The computational model predicts that pyrolysis doesn't begin at any significant amount until the particle has reached 650K (~380°C), even with a relatively low heating rate. The rectangular

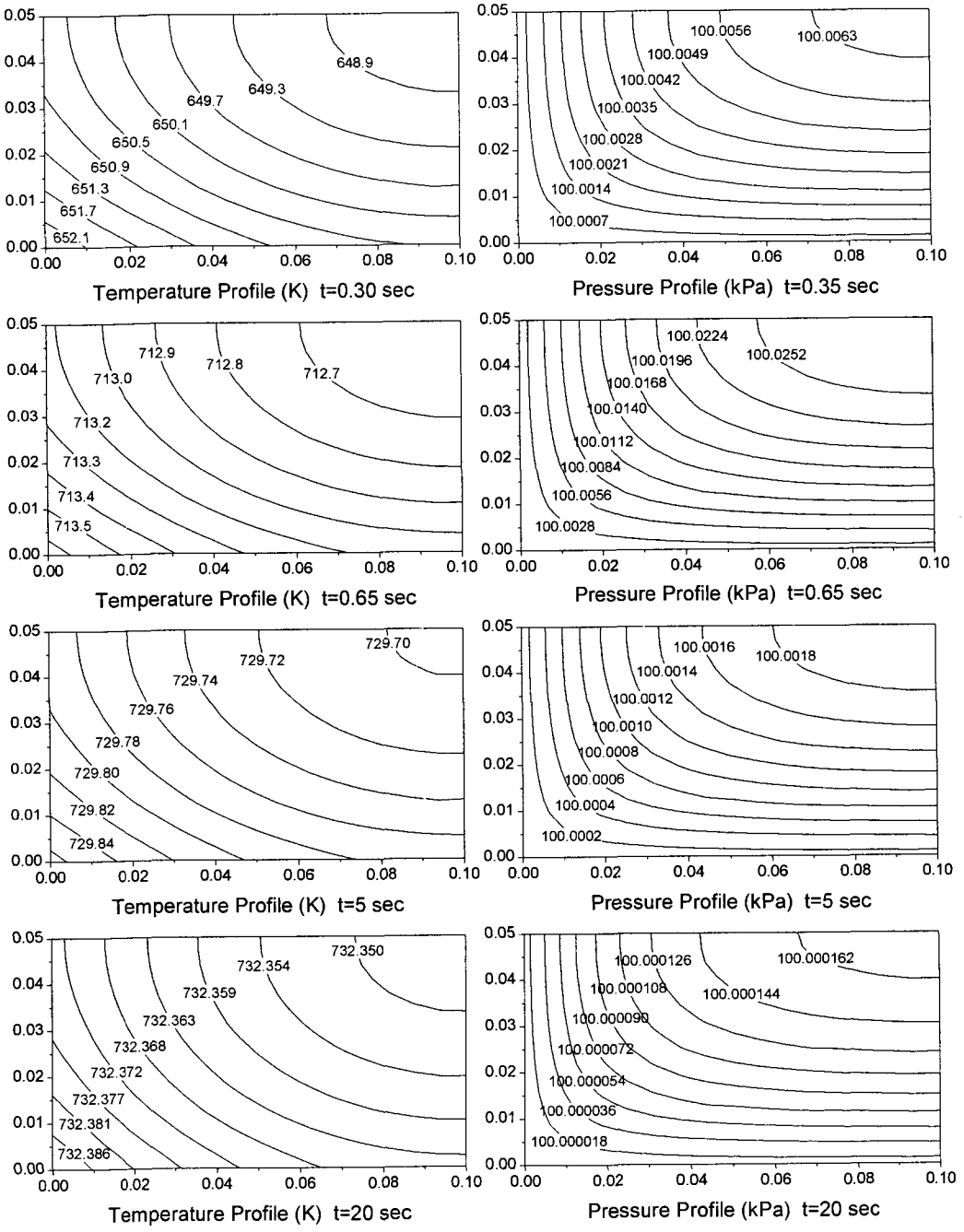

Fig 42. Temperature and Pressure Profiles for a 0.2 mm x 0.1 mm Particle at 800K

particle experiences very little pressurization, with a pressure of 100.0063 kPa at the center of the particle after 0.3 seconds of pyrolysis. At 0.65 seconds, the pressure at the center of the particle is 100.0252 kPa and corresponds with the maximum particle pressure. After 5 seconds, there is only a 0.14K temperature difference within the particle with an average particle temperature of around 729.8K. At 5 seconds, the particle has approximately 60% wood remaining ($\eta = 0.6$), indicating that the resistance to gas flow has decreased to 64% of its original value, with the peak pressure at the center of the particle dropping to 100.0018 kPa. The total gas fluxes from the particle have dropped by less than 30% from 0.65 seconds to 5 seconds, while the peak pressure has dropped by factor of 14. The rapid depressurization of the particle occurs because the particle temperature is no longer rising at any significant rate, there is a decrease in the rate of gas production, and there is an increase in the permeability near the surface. The particle temperature has only risen to 732.3K after 20 seconds of pyrolysis. Increased permeability and reductions in pyrolysis gas production cause the peak pressure to drop by another factor of 10 to a value of 100.000162 kPa after 20 seconds.

For a 0.1 mm particle at 1600K, there are differences in the pyrolysis time of the square and the rectangular particle, as shown in Fig 43 and Fig 44. The 0.2 mm x 0.1 mm particle has a larger delay while the particle is heated up. This happens because the surface area to volume ratio of the square particle is 4/3 the surface area to volume ratio of the rectangular particle. The square particle has more surface area relative to the amount of wood mass that needs to be heated. The square particle takes a little less than 0.03 seconds to heat up and the rectangular particle takes about 0.04 seconds to heat up. The rectangular particle completes

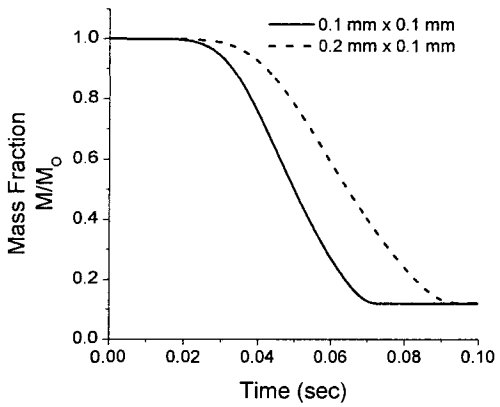

Fig 43. Solid Mass Fraction Remaining for a Square and Rectangular Grain-Direction Particle at 1600K

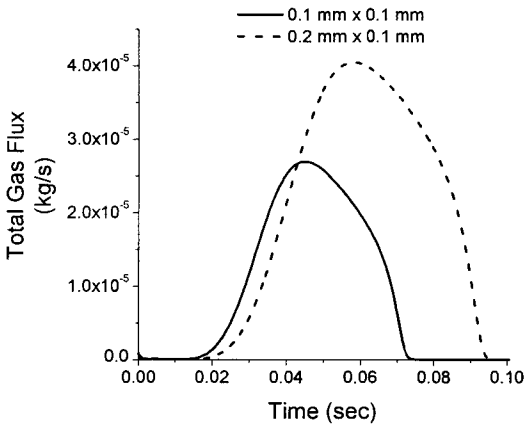

Fig 44. Surface Gas Fluxes for a Square and Rectangular Grain-Direction Particle at 1600K

pyrolysis after around 0.09 seconds, while the square particle gets done in 0.07 seconds. The rectangular particle takes roughly 4/3 as long to heat up and 4/3 as long to pyrolyze once it reaches pyrolysis temperatures. Because the rectangular particle takes longer to pyrolyze, the peak gas fluxes are only 1.5 times larger for the rectangular particle, even though it has twice the mass of the square particle.

The temperature and pressure profiles for the 0.2 mm x 0.1 mm particle at 1600K are shown in Fig 45. The square and rectangular particles have a similar maximum pressure (101.77 kPa and 101.82 kPa, respectively). The square particle has it peak pressure at 0.03 seconds and the rectangular particle has its peak pressure at 0.0393 seconds. The square particle has maximum surface gas fluxes after 0.045 seconds and the rectangular particle

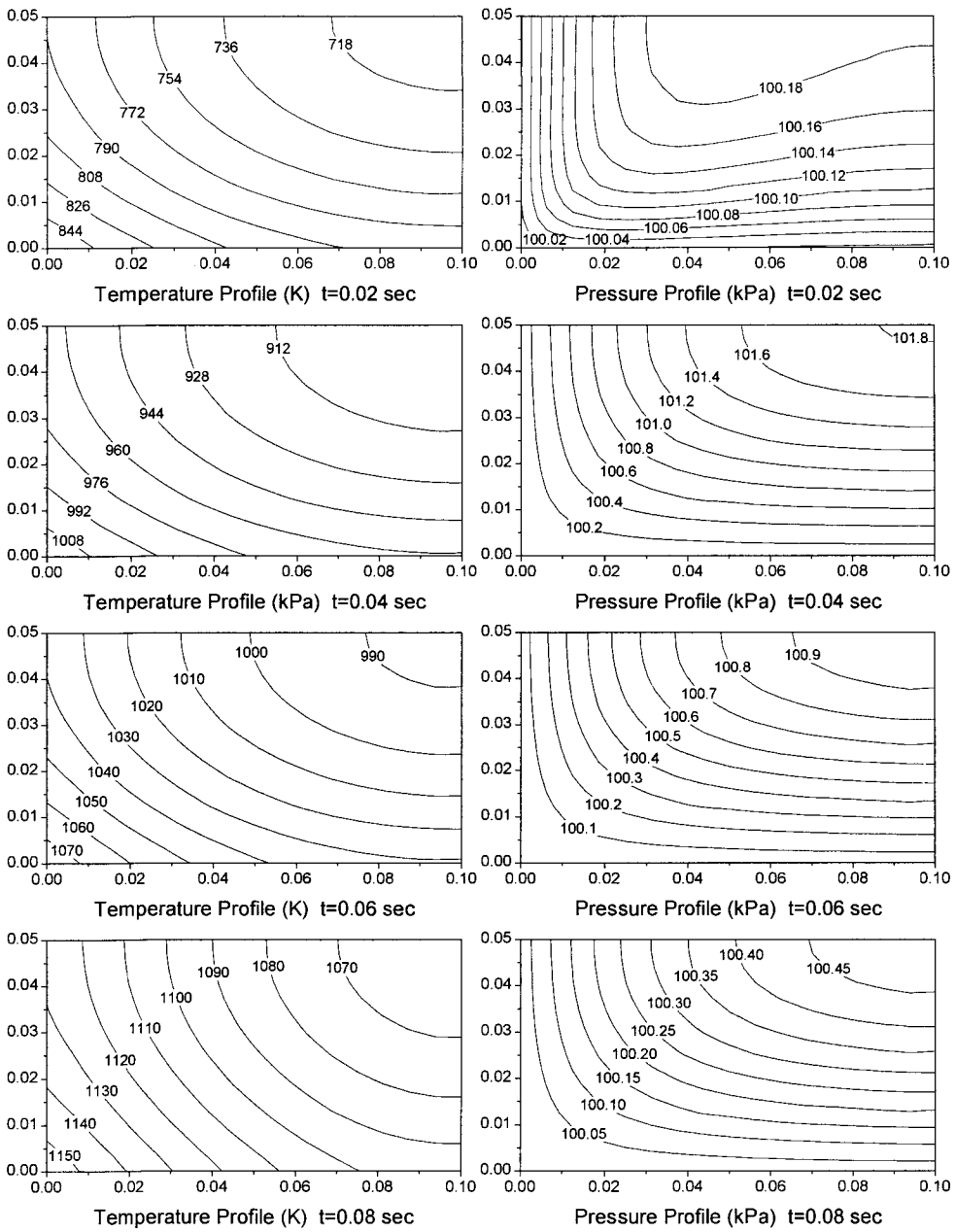

Fig 45. Temperature and Pressure Profiles for a 0.2 mm x 0.1 mm Particle at 1600K

after 0.058 seconds. The time to peak pressure and maximum gas flux are slowed for the rectangular particle because of the increased pyrolysis time.

The 2 mm rectangular particle differs subtly from the square 2 mm particle at 800K. Fig 46 and Fig 47 show the mass fractions and the gas fluxes for the square and the rectangular particle. The rectangular particle takes only a little longer to pyrolyze. There is a few second delay in the peak gas flux measurement, and a slightly broader peak in the release of pyrolysis gases. The peak gas fluxes are 70% higher for the rectangular particle than for the square particle.

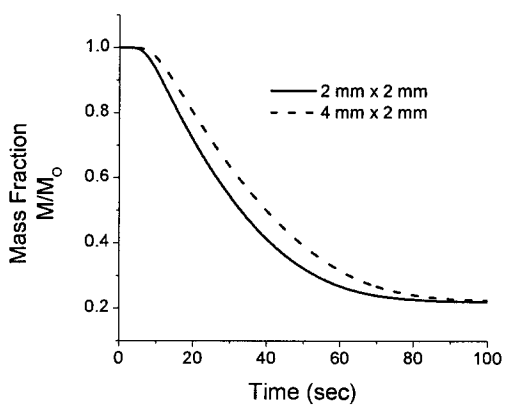

Fig 46. Solid Mass Fraction Remaining for a Square and Rectangular Grain-Direction Particle at 800K

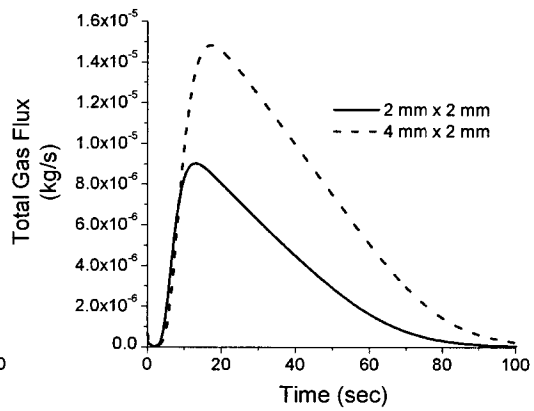

Fig 47. Surface Gas Fluxes for a Square and Rectangular Grain-Direction Particle at 800K

Temperature profiles (Fig 48) show a thermally thin particle with slightly increasing pyrolysis temperatures. Pressure profiles show a peak pressure prior to the maximum rate of gases from the particle.

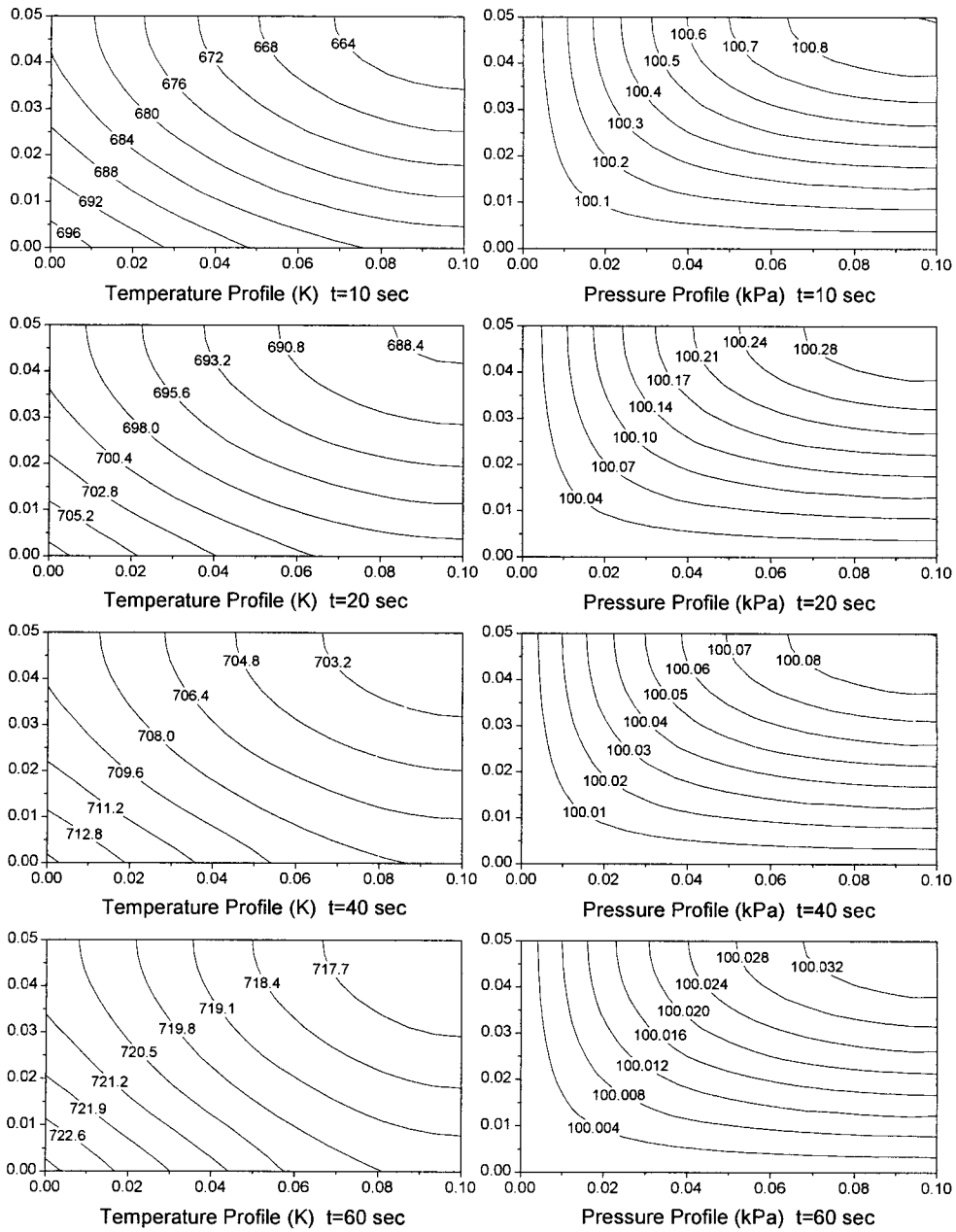

Fig 48. Temperature and Pressure Profiles for a 4 mm x 2 mm Particle at 800K

The solid mass fraction and rate of total gas fluxes from the surface of the particle are shown for both the 2 mm x 2 mm particle and the 4 mm x 2 mm particle at 1600K in Fig 49 and Fig 50. The rectangular particle shows a slower pyrolysis time and takes 25% longer to pyrolyze. The reduction in the surface area to volume ratio causes the rectangular particle to pyrolyze more slowly. The rectangular particle has a 50% increase in peak pyrolysis gas fluxes and has a sharper peak in gas flux production during the first second of pyrolysis.

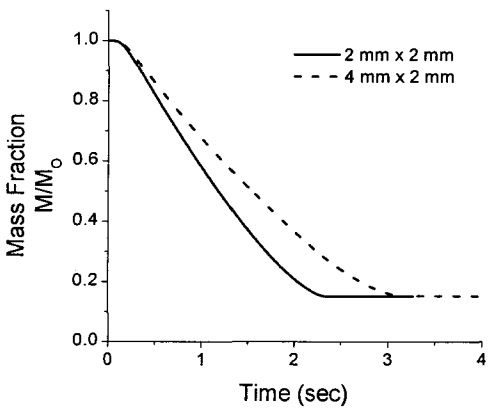

Fig 49. Solid Mass Fraction Remaining for a Square and Rectangular Grain-Direction Particle at 1600K

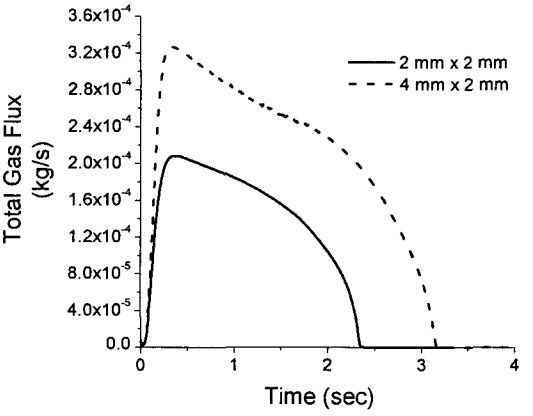

Fig 50. Surface Gas Fluxes for a Square and Rectangular Grain-Direction Particle at 1600K

The temperature and pressure profiles for the 4 mm x 2 mm particle are shown in Fig 51. The rectangular particle has temperatures that are almost 100K cooler than the square particle at the center after 0.5 seconds (compare with Fig 32 at 0.5 seconds). The peak pressure is 0.5 mm from each corner for both particles after 0.5 seconds. By 1.5 seconds, the peak pressure has moved to 1 cm from the corners for the square and the rectangular particle.

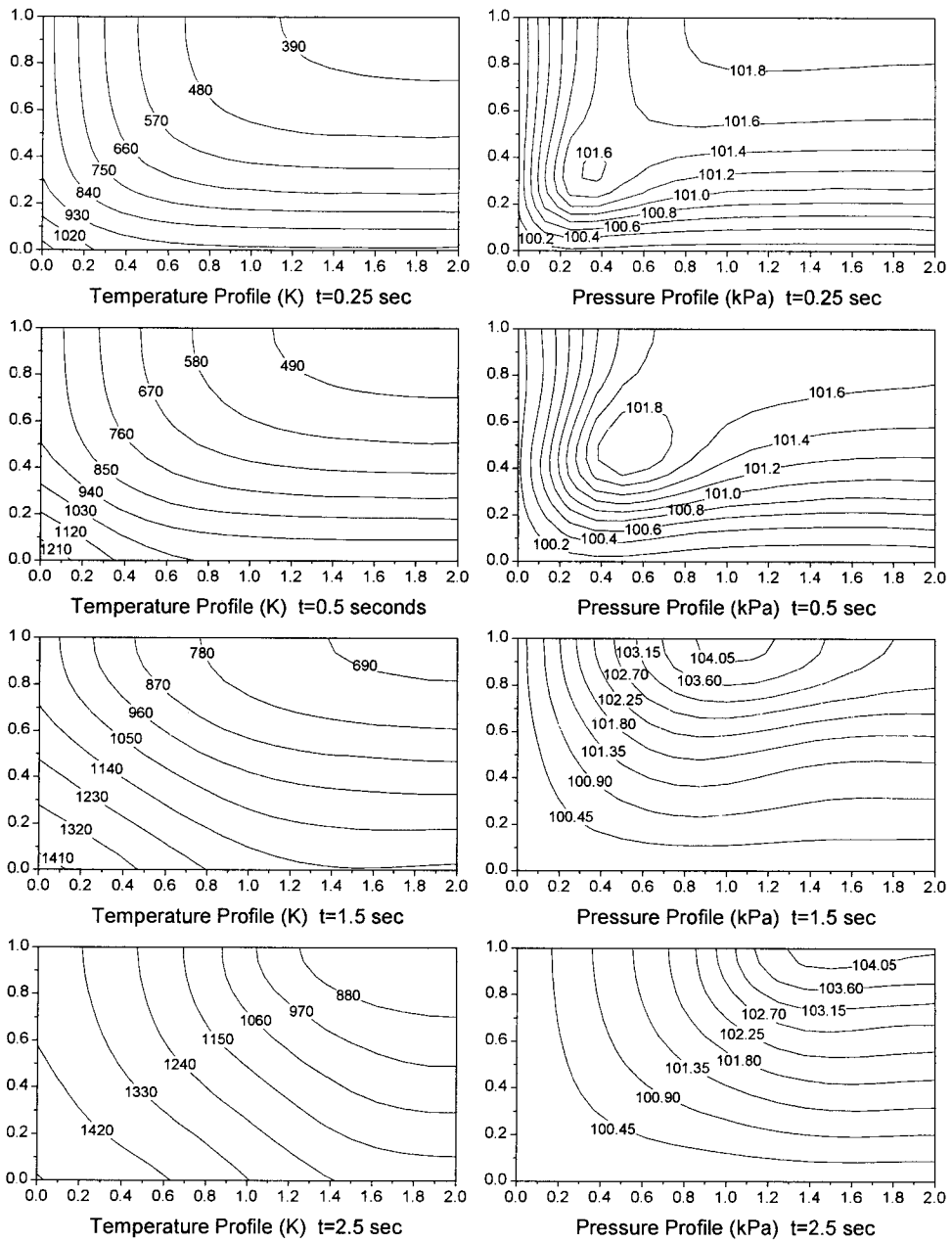

Fig 51. Temperature and Pressure Profiles for a 4 mm x 2 mm Particle at 1600K

For the square particle, the peak pressure is now at the center, while the rectangular particle has a peak pressure that is in the center in the 2 mm direction (cross-grain), but only half way between the corners and the center in the grain direction. The peak pressure of the rectangular particle only moves to the center of the particle after 2.5 seconds of pyrolysis. In each case, the peak pressure is located in regions of the particle between 640K and 750K, and is driven by the release of pyrolysis gases.

Fig 52 and 53 compare the rate of mass loss and the gas fluxes released from the surface of the 1 cm x 1 cm and the 2 cm x 1 cm particle at 800K. Once again, the rectangular particle takes longer to pyrolyze because of a reduced surface area to volume ratio. Peak gas fluxes are 50% higher for the rectangular particle. Both particles have a peak gas flux at approximately $1/3^{rd}$ of the way through pyrolysis, with the rectangular gas flux peak coming about 25 seconds after the peak gas flux for the square particle. The temperatures and pressures of the 2 cm x 1 cm particle at 800K are shown in Fig 54.

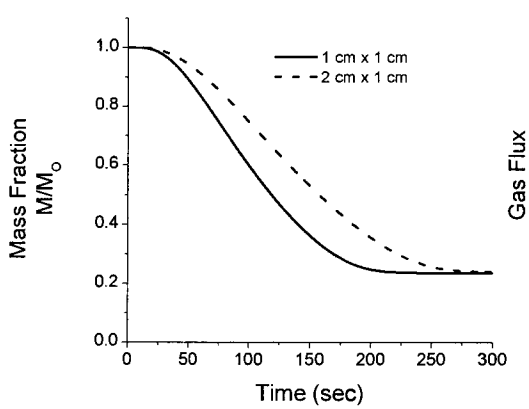

Fig 52. Solid Mass Fraction Remaining for a Square and Rectangular Grain-Direction Particle at 800K

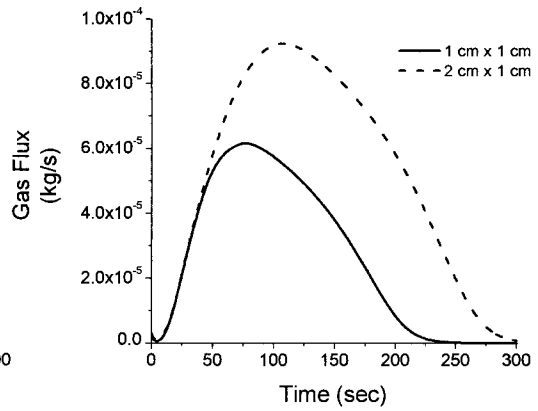

Fig 53. Surface Gas Fluxes for a Square and Rectangular Grain-Direction Particle at 800K

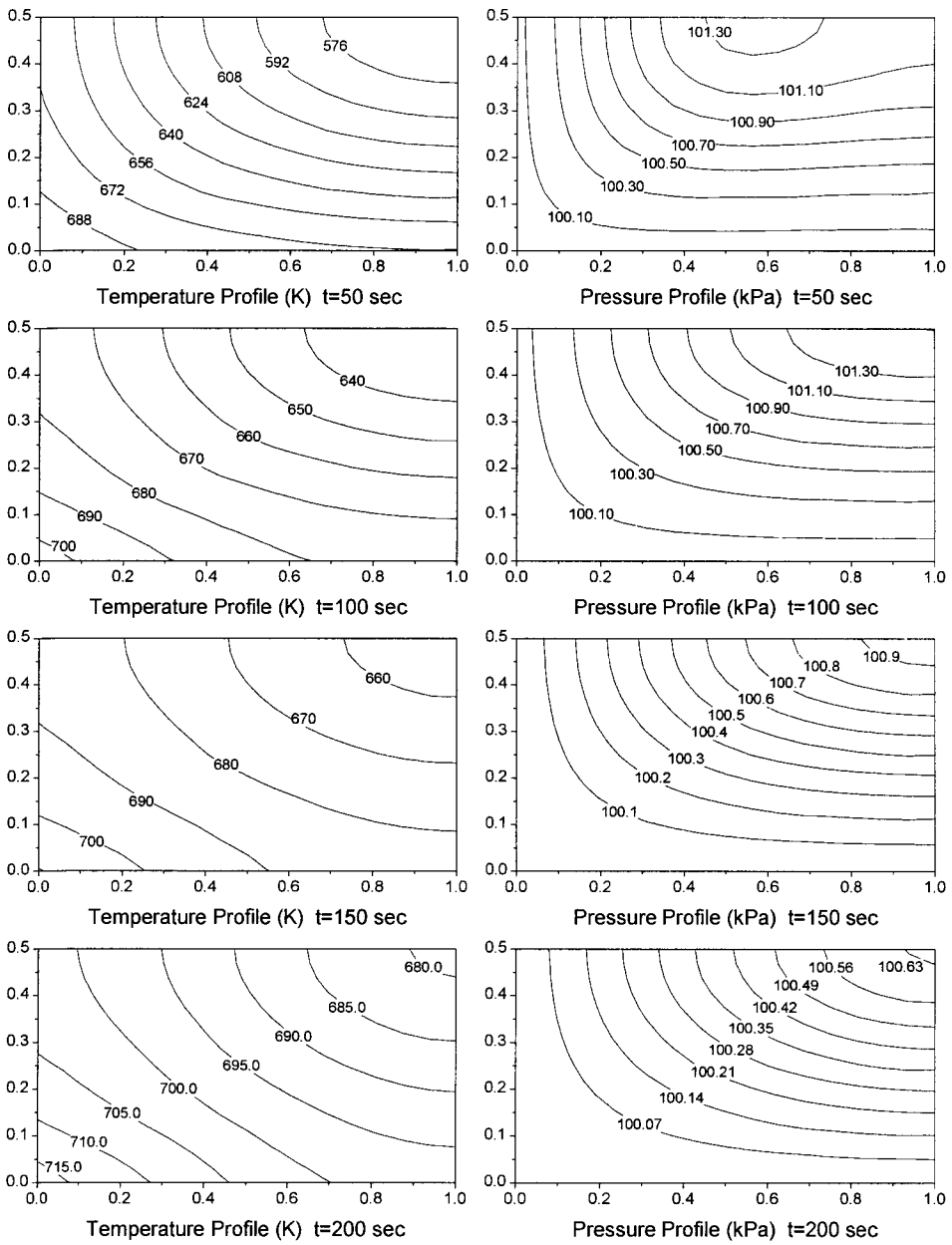

Fig 54. Temperature and Pressure Profiles for a 2 cm x 1 cm Particle at 800K

The rate of mass loss and the gas fluxes for the 1 cm x 1 cm particle and the 2 cm x 1 cm particle at 1600K are compared in Fig 55 and Fig 56.

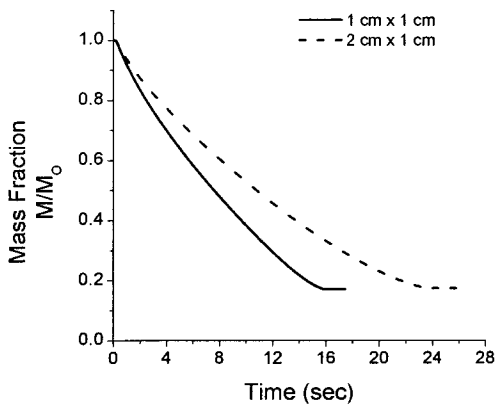

Fig 55. Solid Mass Fraction Remaining for a Square and Rectangular Grain-Direction Particle at 1600K

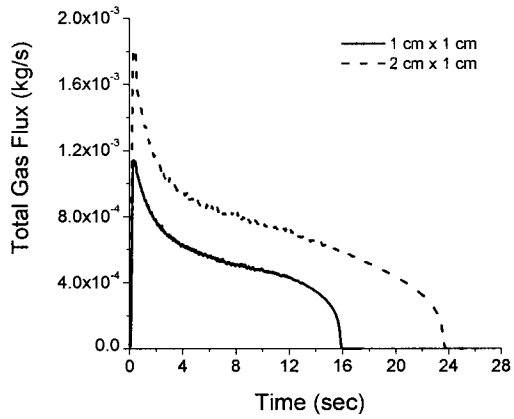

Fig 56. Surface Gas Fluxes for a Square and Rectangular Grain-Direction Particle at 1600K

The rectangular particle takes about 50% longer to pyrolyze. The gas flux for the rectangular particle has a similar shape to the square particle, with a 50% higher peak gas flux during the initial portion of pyrolysis. The temperatures and pressures for the rectangular particle are shown in Fig 57.

The rectangular particle pyrolyzes in a manner that is somewhat similar to the square particle. Initially, pyrolysis occurs only at the surface of the particle. The peak pressure is located at the corner of the particle. As the pyrolysis region moves inward, the pressurization of the rectangular particle responds differently to the advancing pyrolysis region than does the square particle. The peak pressure for the rectangular particle tends to move towards the

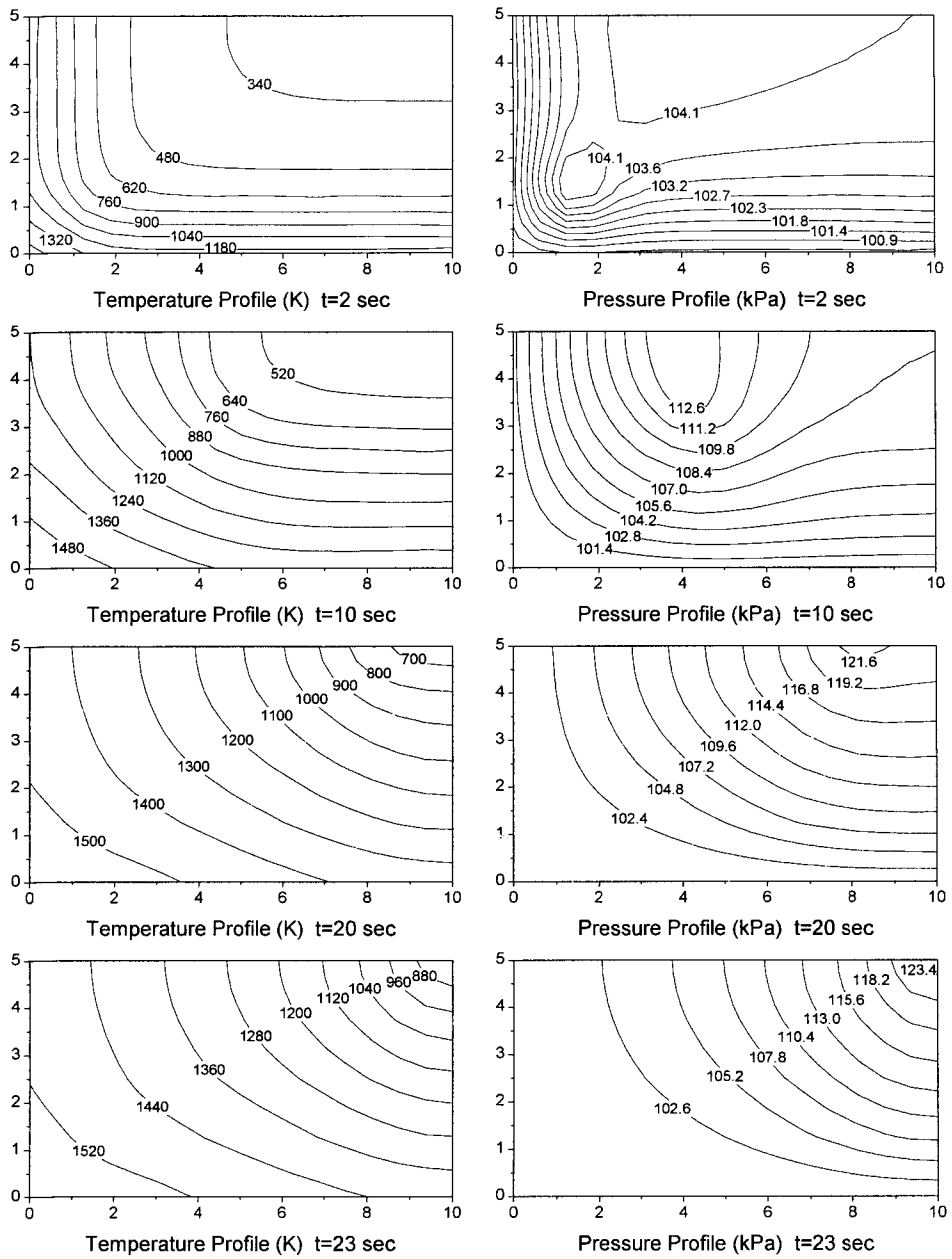

Fig 57. Temperature and Pressure Profiles for a 2 cm x 1 cm Particle at 1600K

center of the particle in the shorter dimension. At 10 seconds, the peak pressure is located 4 to 5 mm from each corner. This puts the peak pressure at the center of the particle in the 1 cm direction, but not in the 2 cm direction. The peak pressure corresponds to the active pyrolysis region only in the 1 cm direction.

6.3 Grain Direction

The next step in examining pyrolysis with the two-dimensional model was to investigate the importance of grain direction on the pyrolysis process. The rectangular particle runs were repeated with the grain running in the direction of the smaller of the two sides. Fig 58 and Fig 59 show that the total pyrolysis time and the rate of gas fluxes at the

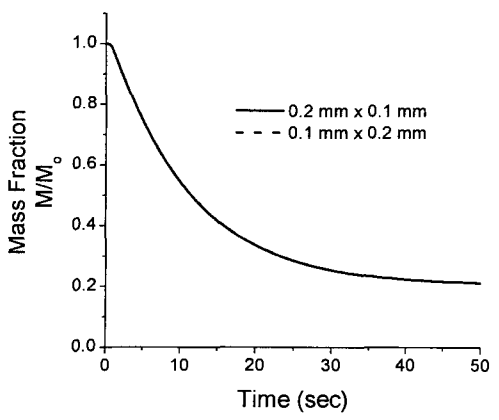

Fig 58. Solid Mass Fraction Remaining for a Grain Direction and a Cross-Grain Direction Rectangular Particle at 800K

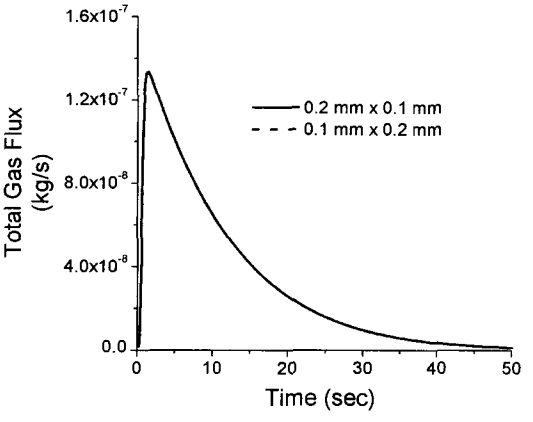

Fig 59. Surface Gas Fluxes for a Grain Direction and a Cross-Grain Direction Rectangular Particle at 800K

surface of the 0.1 mm particle at 800K are independent of the grain direction. The grain direction also has little effect on the temperature profiles for small particles at low temperature, shown in Fig 60.

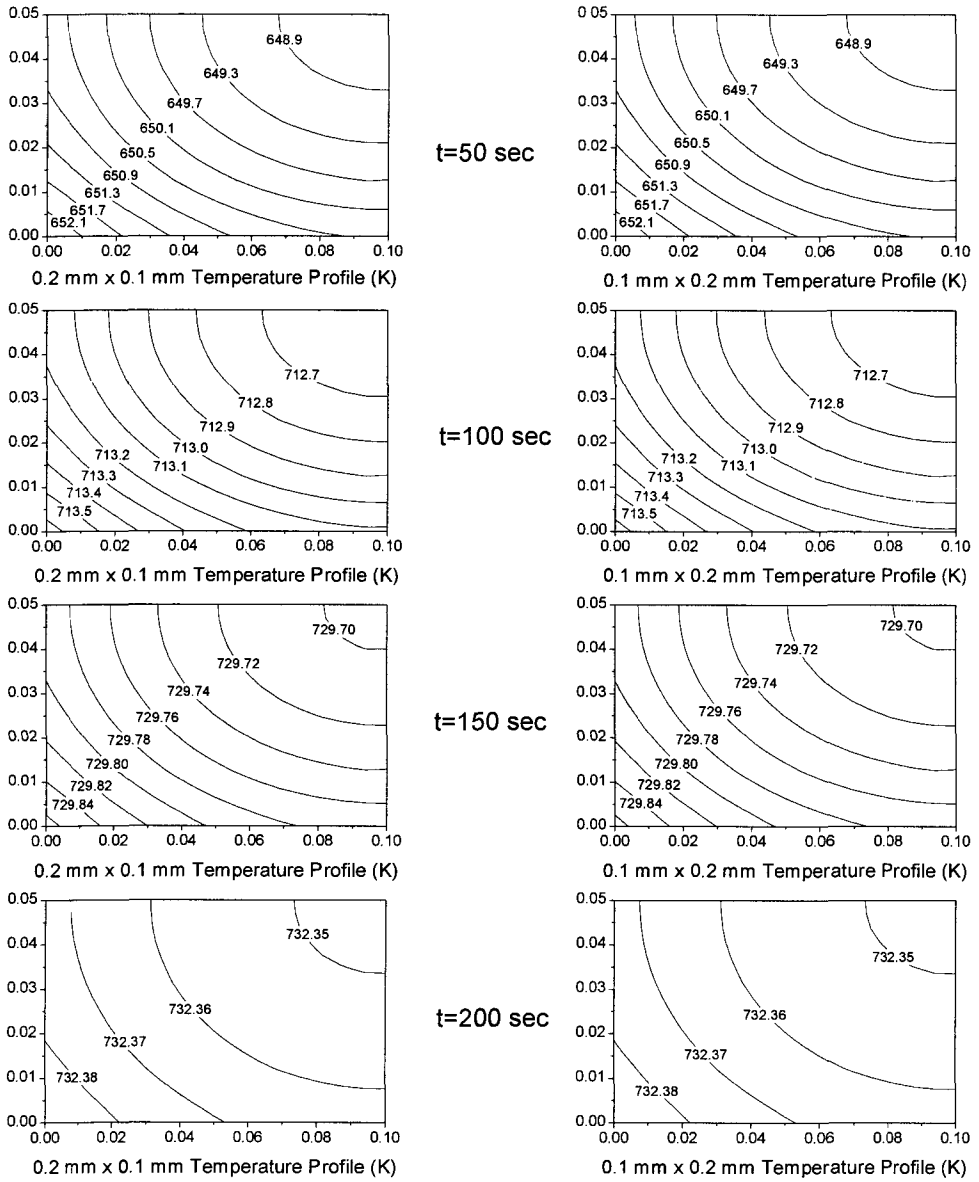

Fig 60. Temperature Profiles for a Grain Direction (0.2 mm x 0.1 mm) Particle and for a Cross-Grain Direction (0.1 mm x 0.2 mm) Particle at 800K

The results for a particle at 1600K with the grain direction in the 0.1 mm direction are shown in Fig 61 and Fig 62. The 0.1 mm x 0.2 mm particle takes longer to pyrolyze than the 0.2 mm x 0.1 mm particle, despite the fact that the conductivity is 1.8 times larger in the 0.1 mm direction. This may seem to be contrary to the notion that an increased rate of internal heat transfer in the smaller dimension should speed up pyrolysis. The difference between the two cases is that there is a preferential direction for shrinkage. The 0.1 mm x 0.2 mm particle has a larger reduction in surface area because shrinkage is larger in the cross-grain (0.2 mm) direction. While the conductivity of the particle does not matter, the shrinkage does matter because it reduces the surface area for the external radiant heat flux. The effect of grain direction on the temperature profiles is shown in Fig 63.

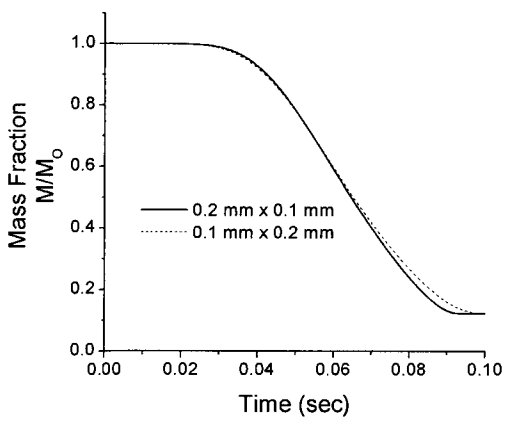

Fig 61. Solid Mass Fraction Remaining for a Grain Direction and a Cross-Grain Direction Rectangular Particle at 1600K

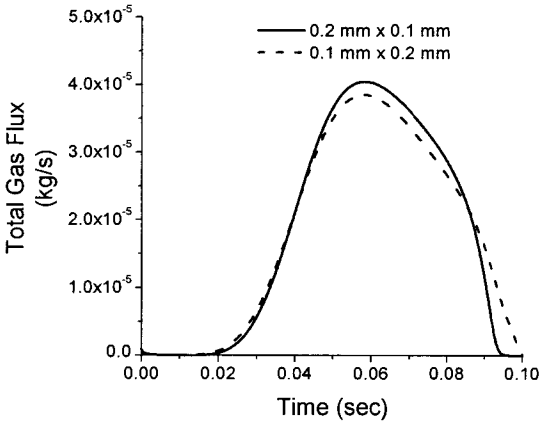

Fig 62. Surface Gas Fluxes for a Grain Direction and a Cross-Grain Direction Rectangular Particle at 1600K

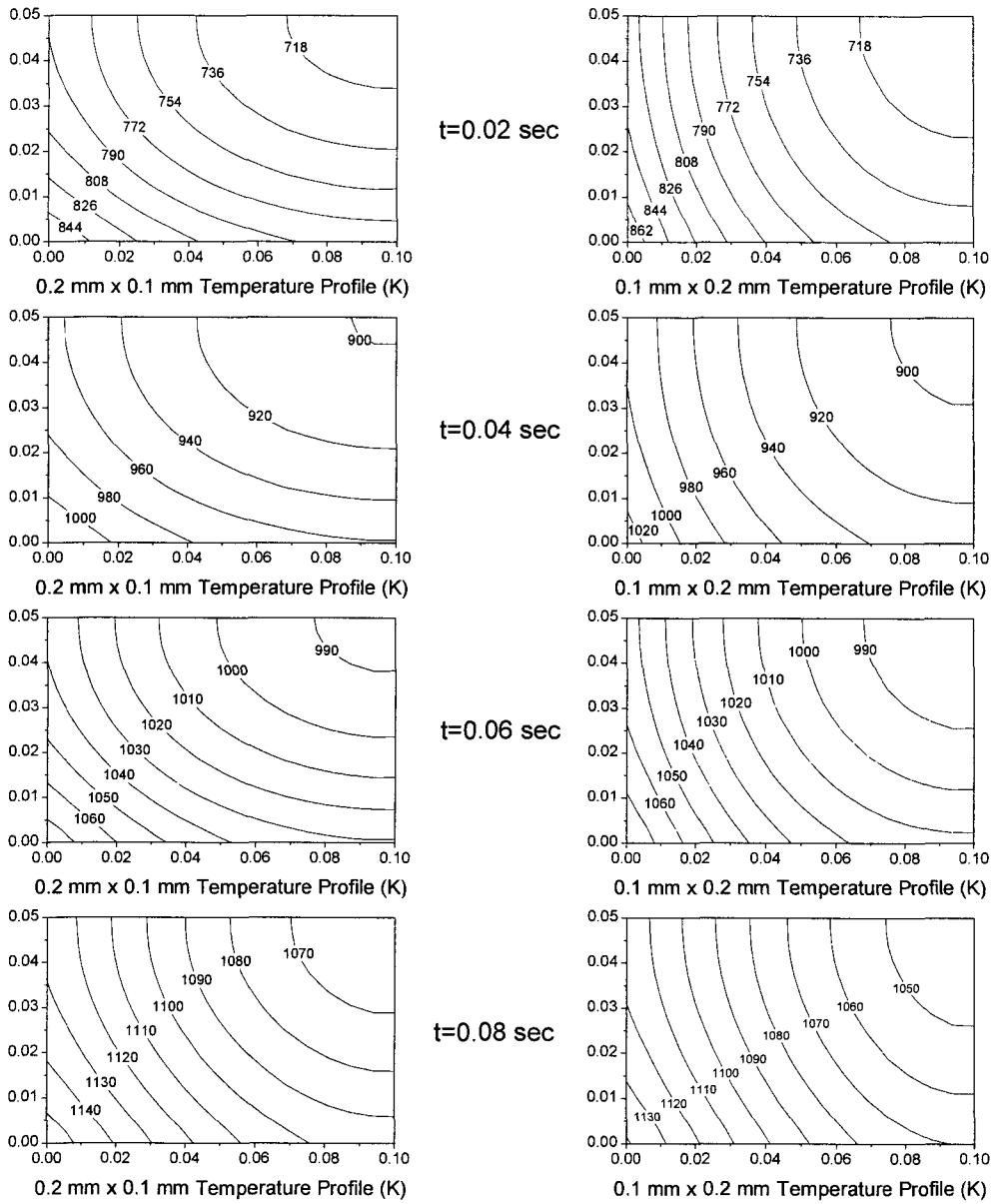

Fig 63. Temperature Profiles for a Grain Direction (0.2 mm x 0.1 mm) Particle and for a Cross-Grain Direction (0.1 mm x 0.2 mm) Particle at 1600K

Grain direction does not seem to matter for the 2 mm particle at 800K. Fig 64 and 65 compare the performance of the 4 mm x 2 mm particle and the 2 mm x 4 mm particle. For low temperatures and small particles, the amount of shrinkage is relatively small. The decrease in pyrolysis time from the reduction in surface area in the 4 mm direction due to shrinkage is offset by the increased conductivity in the 2 mm direction. For this particle, shrinkage and conductivity have a small but opposite effect.

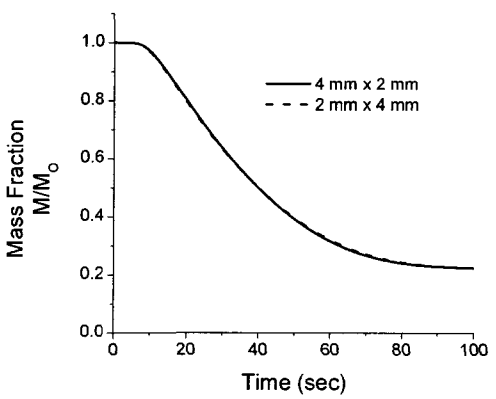

Fig 64. Solid Mass Fraction Remaining for a Grain Direction and a Cross-Grain Direction Rectangular Particle at 800K

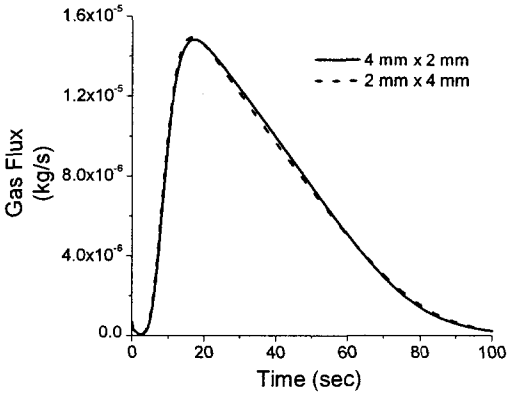

Fig 65. Surface Gas Fluxes for a Grain Direction and a Cross-Grain Direction Rectangular Particle at 800K

The mass fraction and gas fluxes for 2 mm rectangular particles at 1600K are shown in Fig 66 and Fig 67. At 1600K, the rate of internal heat transfer within the particle becomes more important. There is more shrinkage at 1600K than at 800K. The 4 mm x 2 mm particle has a 26% reduction in surface area and the 2 mm x 4 mm particle has a 30% reduction in surface area due to shrinkage. The 4 mm x 2 mm particle has a larger shrinkage in the 2 mm

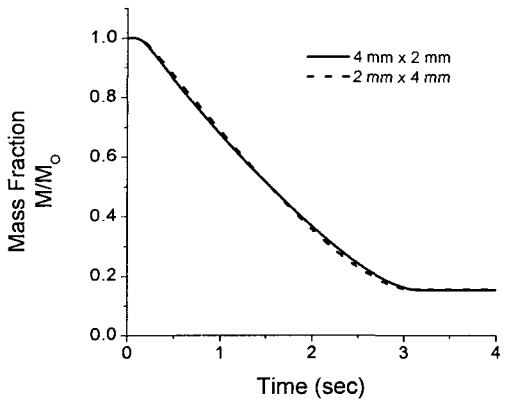

Fig 66. Solid Mass Fraction Remaining for a Grain Direction and a Cross-Grain Direction Rectangular Particle at 1600K

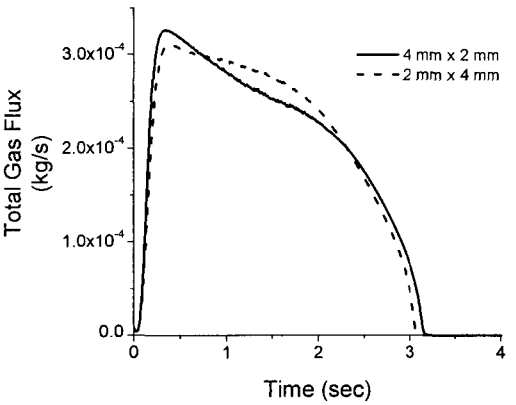

Fig 67. Surface Gas Fluxes for a Grain Direction and a Cross-Grain Direction Rectangular Particle at 1600K

direction. The 4 mm x 2 mm particle has a larger total surface area and has more shrinkage in the smaller dimension, both of which should speed up pyrolysis. The gas flux curve shows the opposite, that the 2 mm x 4 mm particle will pyrolyze faster. This indicates that the increased conductivity in the 2 mm direction is more important than the difference in surface area or the increased heat transfer within the particle due to shrinkage. The temperature profiles are shown in Fig 68.

The 4 mm x 2 mm particle has a higher peak gas flux than the 2 mm x 4 mm particle. The temperature profiles show that the 4 mm x 2 mm particle initially has higher surface temperatures along the longer (4mm) edge of the particle than does the 2 mm x 4 mm

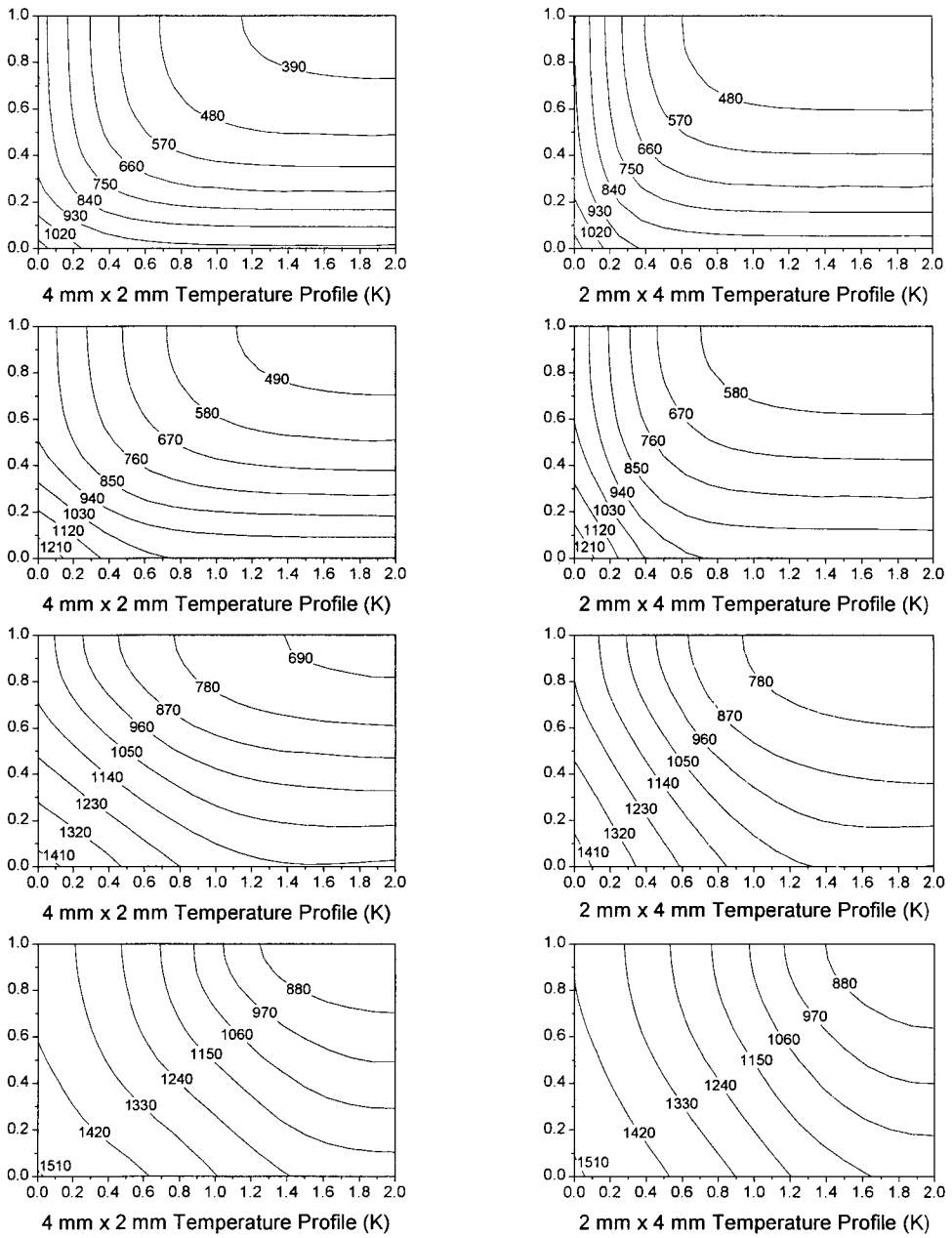

Fig 68. Temperature Profiles for a Grain Direction (4 mm x 2 mm) Particle and for a Cross-Grain Direction (2 mm x 4 mm) Particle at 1600K

particle. During the first 0.5 seconds of pyrolysis, the 4 mm x 2 mm particle will have higher peak gas fluxes because of higher temperatures along the 4 mm surface of the particle. The 2 mm x 4 mm particle has a higher conductivity in the 2 mm direction and the 4 mm x 2 mm particle has a higher conductivity in the 4 mm direction. The 2 mm x 4 mm particle has lower surface temperatures along the 4 mm length and the 4 mm x 2 mm particle has lower surface temperatures along the 2 mm length. The 2 mm x 4 mm particle receives more radiant heat flux because of lowered surface temperatures along the 4 mm length. The increased conductivity in the 2 mm direction causes more heat transfer to the center of the particle, raising the temperature at the center of the particle. The lowered surface temperatures along the 4 mm side and the increased heat transfer in the 2 mm direction cause a more rapid pyrolysis than the 4 mm x 2 mm particle, despite a larger reduction in surface area and less shrinkage in the 2 mm direction.

In particles the size of wood chunks, the internal properties of the wood particle become more important than for smaller particles. The mass fraction over time and the rate of gas flux are shown in Fig 69 and Fig 70 for a 1 cm x 2 cm particle at 800K.

The mass fraction drops gradually initially and then drops at a linear rate for most of pyrolysis. The rate of mass loss decreases towards the end of pyrolysis. There is only a small difference with grain direction, with the rectangular particle with the grain direction in the 1 cm direction pyrolyzing a little bit earlier. The gas fluxes from the surface of the particles are also similar, with the 1 cm x 2 cm particle observing a slightly higher peak gas flux. The 1 cm x 2 cm particle has a 17% reduction in surface area while the 2 cm x 1 cm particle has a 13% reduction in surface area. For large particles at low temperature, the decrease in pyrolysis time due to grain direction is slightly more important the loss of surface area due to

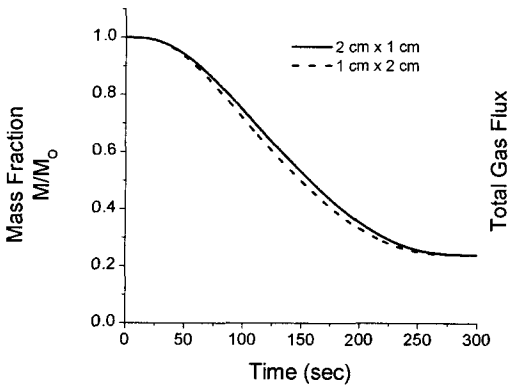

Fig 69. Solid Mass Fraction Remaining for a Grain Direction and a Cross-Grain Direction Rectangular Particle at 800K

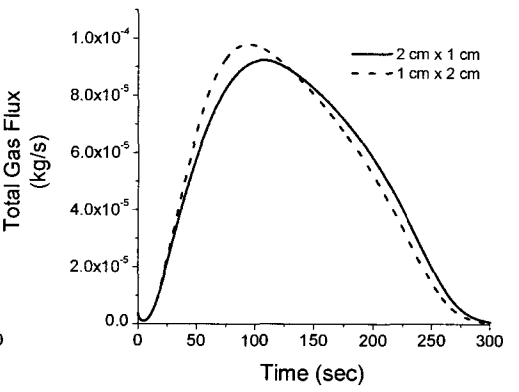

Fig 70. Surface Gas Fluxes for a Grain Direction and a Cross-Grain Direction Rectangular Particle at 800K

shrinkage.

The temperature profiles of the 1 cm rectangular wood chunks are shown in Fig 71. The 1 cm x 2 cm particle has a higher temperature at the center of the particle, with a slightly lower temperature along the 2 cm surface and a slightly higher temperature along the 1 cm surface.

For large particles at high temperatures, the rate of internal heat transfer is the controlling factor for pyrolysis. It would be expected that directional properties would be the most significant under large particles at high temperature. The mass fraction and the gas fluxes for 1 cm rectangular particles at 1600K are shown in Fig 72 and Fig 73.

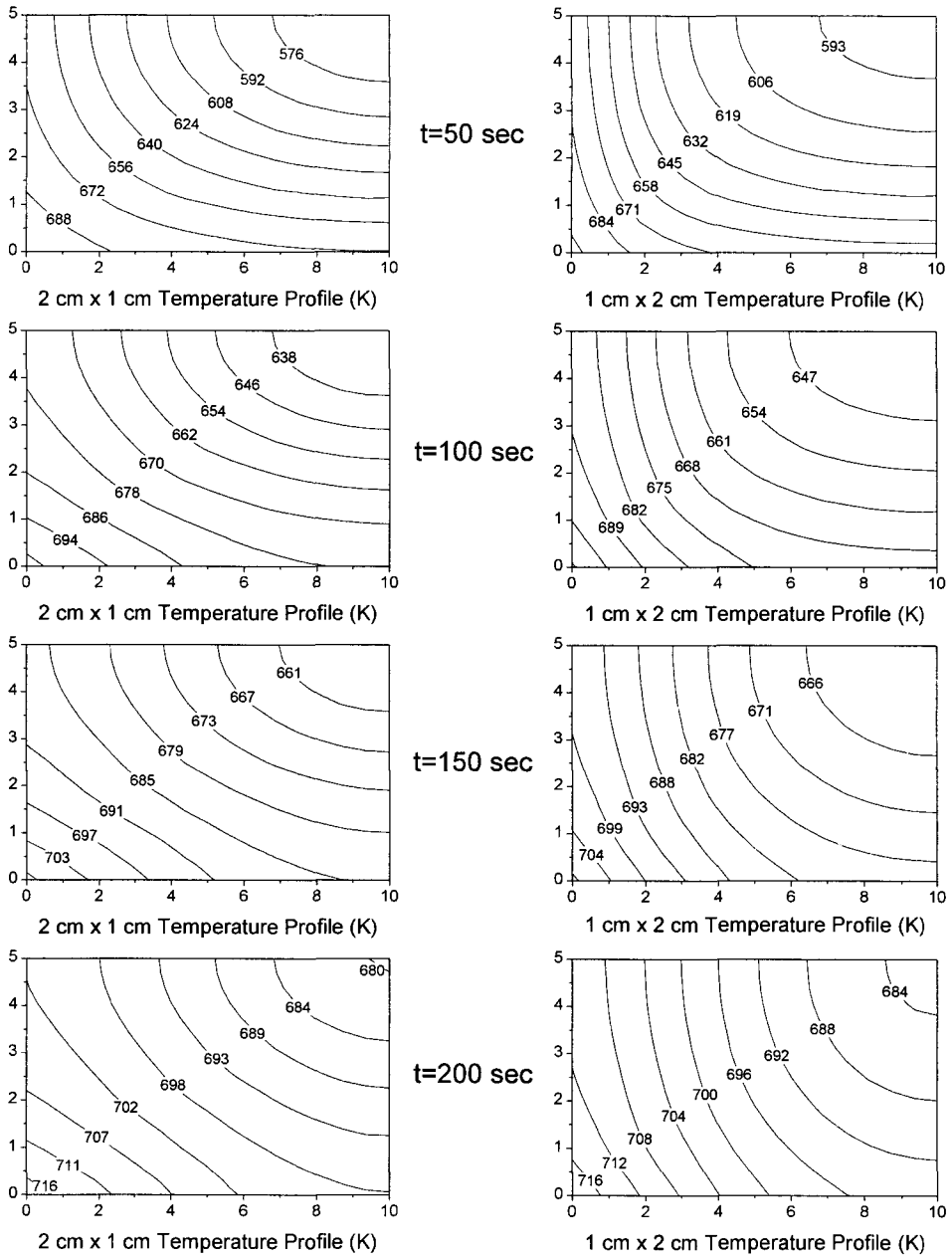

Fig 71. Temperature Profiles for a Grain Direction (2 cm x 1 cm) Particle and for a Cross-Grain Direction (1 cm x 2 cm) Particle at 800K

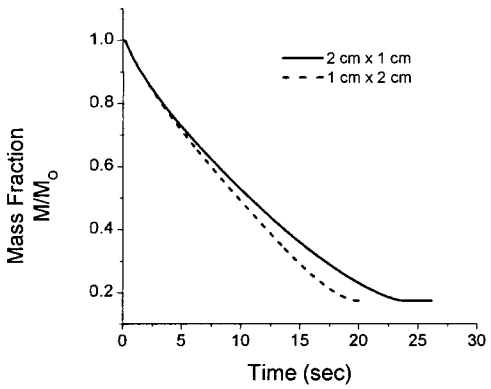

Fig 72. Solid Mass Fraction Remaining for a Grain Direction and a Cross-Grain Direction Rectangular Particle at 1600K

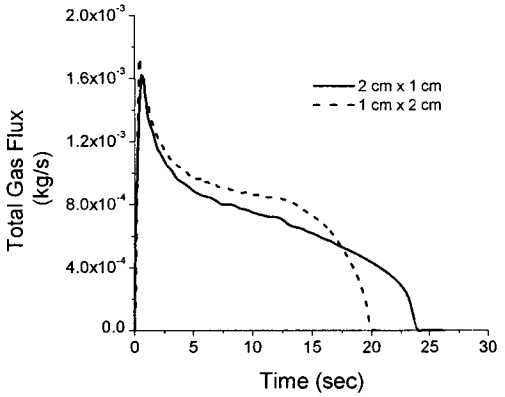

Fig 73. Surface Gas Fluxes for a Grain Direction and a Cross-Grain Direction Rectangular Particle at 1600K

The increased conductivity in the 1 cm direction reduces the total pyrolysis time by about 18%. The rate of gas flux is similar from each rectangular particle is similar during the first few seconds of pyrolysis. As the interior of each particle is heated, the increased conductivity in the 1 cm direction causes the release of pyrolysis gases to increase. Fig 74 demonstrates how the temperature profiles of the 1 cm rectangular particles at 1600K differ with the grain direction.

While the rate of mass loss and the gas fluxes appear similar during the first few seconds of pyrolysis, the temperature profiles show that the particles a responding differently to the external heat flux. After 2 seconds, the 2 cm x 1 cm particle is about 100K hotter on the 2 cm surface and is about 100K cooler on the 1 cm surface. The particle with the grain

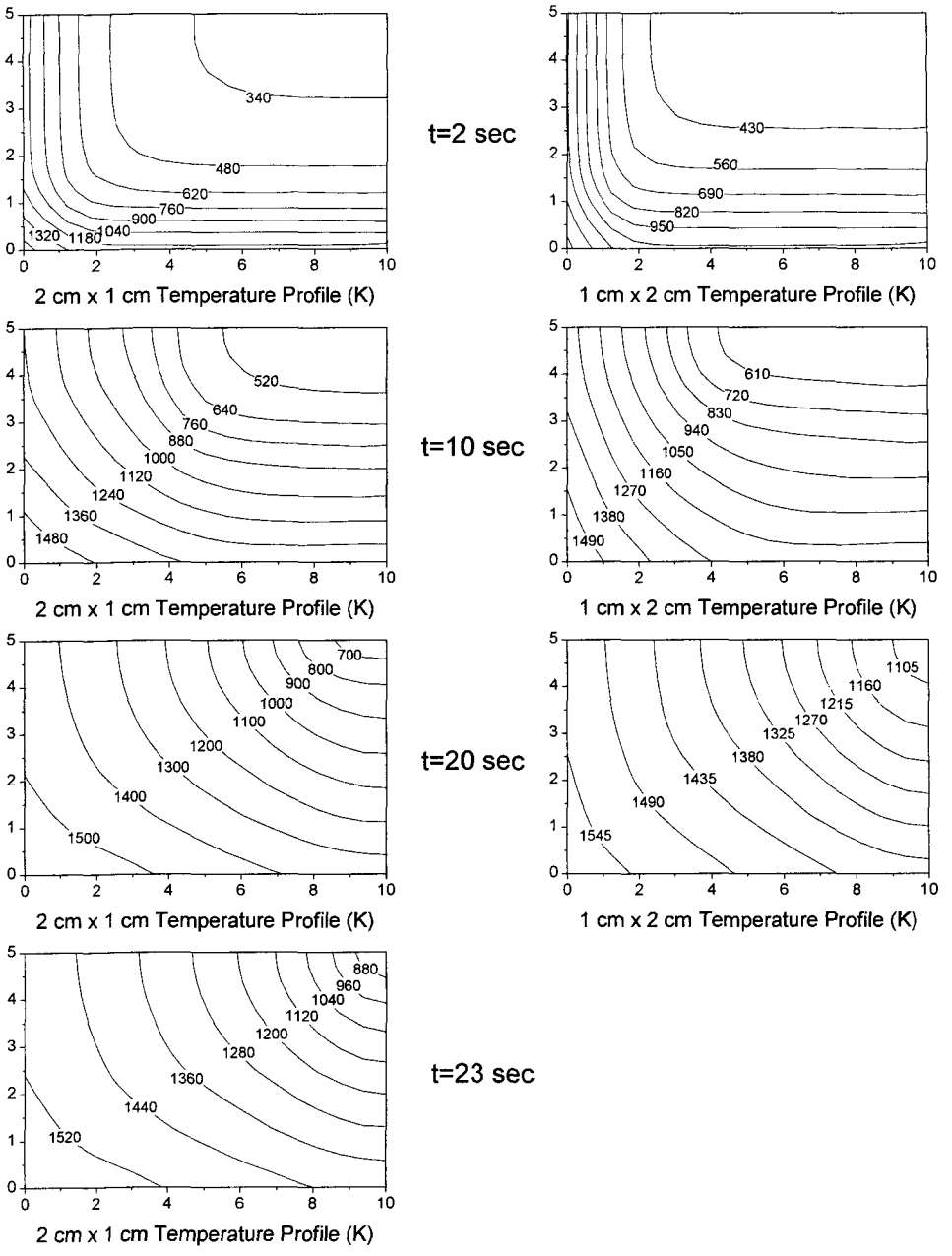

Fig 74. Temperature Profiles for a Grain Direction (2 cm x 1 cm) Particle and for a Cross-Grain Direction (1 cm x 2 cm) Particle at 1600K

direction in the 1 cm direction (1 cm x 2 cm) is about 100K hotter at the center of the particle. As pyrolysis continues, the 1 cm x 2 cm particle remains cooler on the 2 cm surface.The lowered surface temperatures are a result of the higher conductivity in the grain direction. The increased conductivity raises the temperatures in the center of the particle, and the lowered surface temperature allows more external radiation to reach the particle. In this way, large particles at high temperatures are significantly influenced by grain direction.

6.4 Model Results

Fig 75 summarizes the amount of time it takes to devolatilize 90% of the original mass of wood for the range of particles studied in this work. Several observations can be made from these selected set of runs from the two-dimensional computational model. For wood powders at low pyrolysis temperatures, the particle size, shape, thermal conductivity, and directional properties have little influence on the pyrolysis process. The time required to heat the particle is insignificant to the pyrolysis process. For wood powders at elevated temperatures the particle shape, size, and thermal conductivity do not matter. The time required to heat the particle is important, and can account for over 1/3 of the total pyrolysis time. At high temperatures, the shrinkage of the particle increases the pyrolysis times of powders by a few percent by reducing the surface area of the particle.

Pyrolysis reaction rates are determined experimentally. The primary reaction rates are found by heating a large number of very small particles at a specified rate or to a specified temperature. For fine powders at low temperatures, an external temperature can be set and the particles can be assumed to be at the set temperature. For powders at high temperature,

the heat up time of the particles needs to be quantified to accurately determine the rate of pyrolysis reactions.

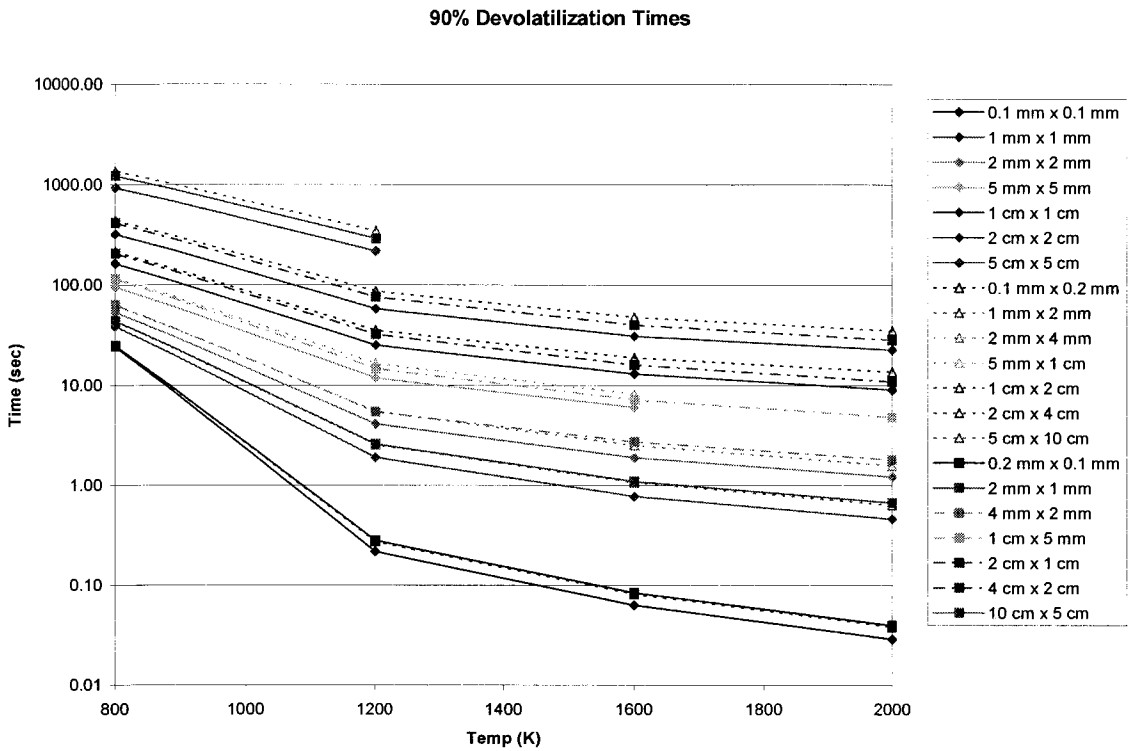

Fig 75. Computational Pyrolysis Times for All Particles

For particles in the 2 mm to 4 mm range, both particle shape and directional properties of shrinkage and conductivity alter the pyrolysis process by a small amount. A rectangular particle with twice the volume has only a 70% increase in peak gas production at 800K, indicating that it takes somewhat longer to pyrolyze a rectangular particle of this size. The increase in pyrolysis time due to a rectangular shape is caused primarily by the reduction in particle surface area relative to the particle volume. Directional conductivity in the grain direction decreases the pyrolysis time, while shrinkage in the cross-grain direction increases the pyrolysis time by reducing the particle surface area. At 800K the directional effects offset

each other. At 1600K, the higher rate of cross-grain shrinkage is more important than the increase in grain direction conductivity and actually slow the pyrolysis times of the particles.

For wood chunks the orientation and shape of the particle is more important than for smaller particles. At low temperatures, a particle with a 2:1 aspect ratio takes 50% longer to pyrolyze than a square particle. The grain direction is relatively unimportant. Rectangular particles with the grain direction in the smaller dimension pyrolyze a few percent faster than particles with the grain direction in the larger dimension. At high temperatures, a rectangular particle takes 50% longer to pyrolyze than a square particle. Grain direction typically alters pyrolysis times by a few percent, but for large particles at high temperature grain direction can alter the pyrolysis times by up to 30%.

The computational model has been used to indicate where particle size, shape, and directional properties are important. Because most pyrolysis models that exist today are one-dimensional, it is useful to compare the two-dimensional model with one-dimensional results to determine what the limitations of existing one-dimensional models are and to determine where and how one-dimensional models can be used. One-dimensional models have been used almost exclusively because of the difficulty and time needed to solve for detailed pyrolysis.

6.5 2D vs 1D Results

Computational modelers have generally been unsuccessful at creating models which can be applied to many different combustion situations without recalibrating the combustion parameters for each situation. This may be due to inaccuracies inherent in using a one-

dimensional model for situations which are not truly one-dimensional. To determine the limitations of one-dimensional models, selected runs from the two-dimensional computational model were repeated as one-dimensional particles. The same computational model was used with adiabatic and impermeable boundaries on the sides to predict one-dimensional performance.

The two-dimensional model showed that for powders at low temperature, the grain direction and conductivity did not matter. A comparison of two-dimensional and one-dimensional 0.1 mm particles at 800K shows that one dimensional and two-dimensional particles have similar pyrolysis times, and gas fluxes. The two-dimensional particle is compared with the one dimensional particle in Fig 76 and Fig 77.

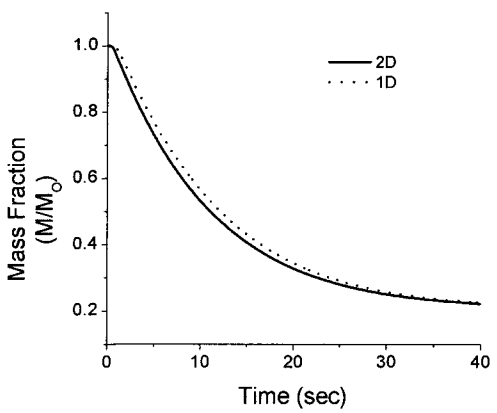

Fig 76. Solid Mass Fraction Remaining for a Two-Dimensional and a One-Dimensional 0.1 mm Particle at 800K

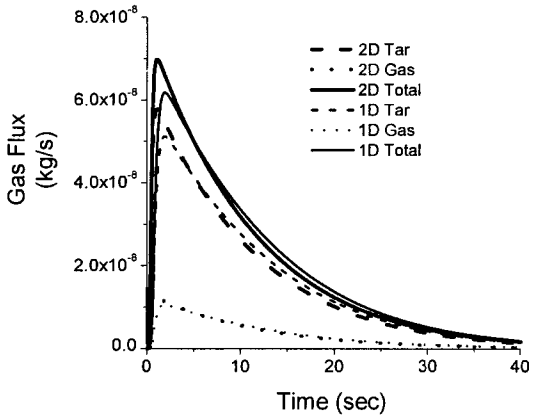

Fig 77. Surface Gas Fluxes for a Two-Dimensional and a One-Dimensional 0.1 mm Particle at 800K

The two-dimensional model predicts a 90% devolatilization time of 24.22 seconds vs. 25.45 seconds for a one-dimensional particle. The two-dimensional particle has a peak gas flux of $6.98*10^{-8}$ at 1.05 seconds vs. $6.175*10^{-8}$ at 1.9 seconds for the one-dimensional case. While both cases produce a similar pyrolysis time, the peak gas fluxes are 14% lower for the one-dimensional case and the initial delay before peak gas flow from the particle is nearly twice as long. These results indicate that a one-dimensional model is adequate to predict the performance of low temperature powders of any shape except for situations where the first few seconds of pyrolysis are critical, such as in ignition studies.

The temperature profiles for a 0.1 mm particle at 800K were also compared with one-dimensional results in Fig 78. The temperature profiles show that one-dimensional particle is 75K cooler at 0.3 seconds, 44K cooler at 0.6 seconds and 2K cooler after 5 seconds. These temperature differences had only a small impact of pyrolysis times and gas fluxes. One-dimensional results were repeated using the properties in the grain direction (dotted lines) and in the cross-grain direction (solid lines). The surface temperature of the one-dimensional particle is similar regardless of the properties used. When the conductivity is increased by a factor of 1.8 in the grain direction, the temperature gradient within the particle is 1.8 times lower. The temperature gradient within the one-dimensional particle appears to be at a quasi-equilibrium state, with the temperature gradient adjusting to the total heat flux at the surface of the particle. There was less than 2K temperature difference in a one-dimensional model with grain direction, indicating that grain direction is unimportant in one-dimensional models, and that any differences between the two-dimensional and the one-dimensional models are not a result of the appropriate selection of material properties.

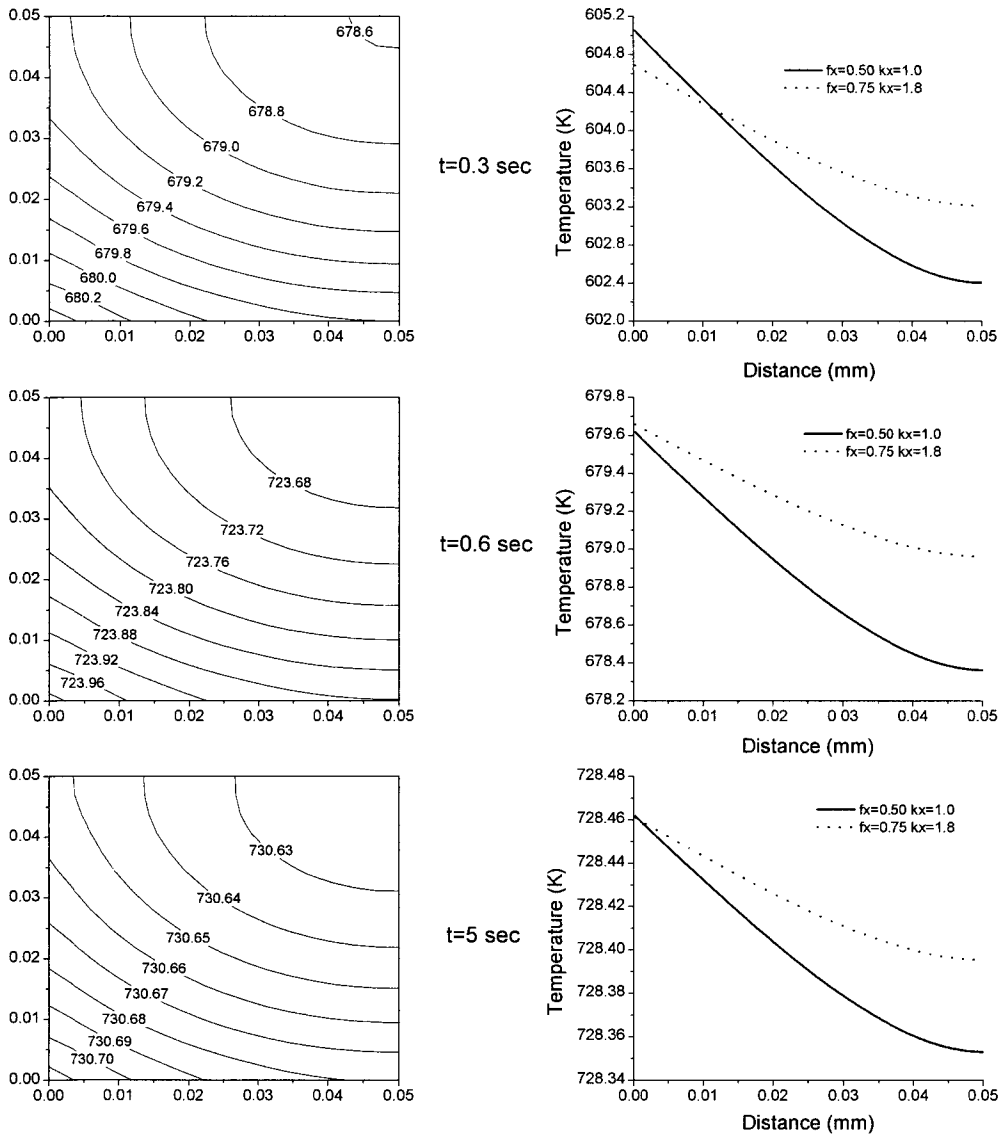

Fig 78. Temperature Profiles for a 0.1 mm Particle at 800K using a Two-Dimensional Model and One-Dimensional Models with Grain and Cross-Grain Properties

The thermal conductivity and shrinkage of a one-dimensional particle have little effect on the pressurization of the particle. A one-dimensional particle showed a peak pressure of 100.025 kPa at 0.88 seconds, regardless of grain direction. The two-dimensional particle had a peak pressure of 100.021 kPa at 0.50 seconds. The pressure profiles for the two-dimensional particle and the one-dimensional particle with cross-grain and grain properties are shown in Fig 79.

For powders at high temperatures, there are important differences between the two-dimensional and one-dimensional results. The two-dimensional mass loss and gas flux curves are compared in Fig 80 and Fig 81 with a one-dimensional particle using cross-grain properties.

The two-dimensional particle has a 90% devolatilization time of 0.063 seconds while the one-dimensional particle takes 0.105 seconds to devolatilize 90% of the wood. The one-dimensional particle takes almost 70% longer to devolatilize. The one-dimensional particle takes 0.027 seconds longer to pyrolyze 10% of the wood, indicating that much of this difference comes from the time required to heat the particle. The remaining 0.015 seconds comes from a lower rate of mass loss for the one- dimensional particle. The two-dimensional particle has a more symmetrical gas flux curve, with peak gas fluxes that are over 50% higher than the one-dimensional case.

The particle was again compared with a one-dimensional particle at 1600K with grain-direction properties. Fig 82 and Fig 83 compare the mass loss and gas flux for a one-dimensional particle with properties in the grain direction.

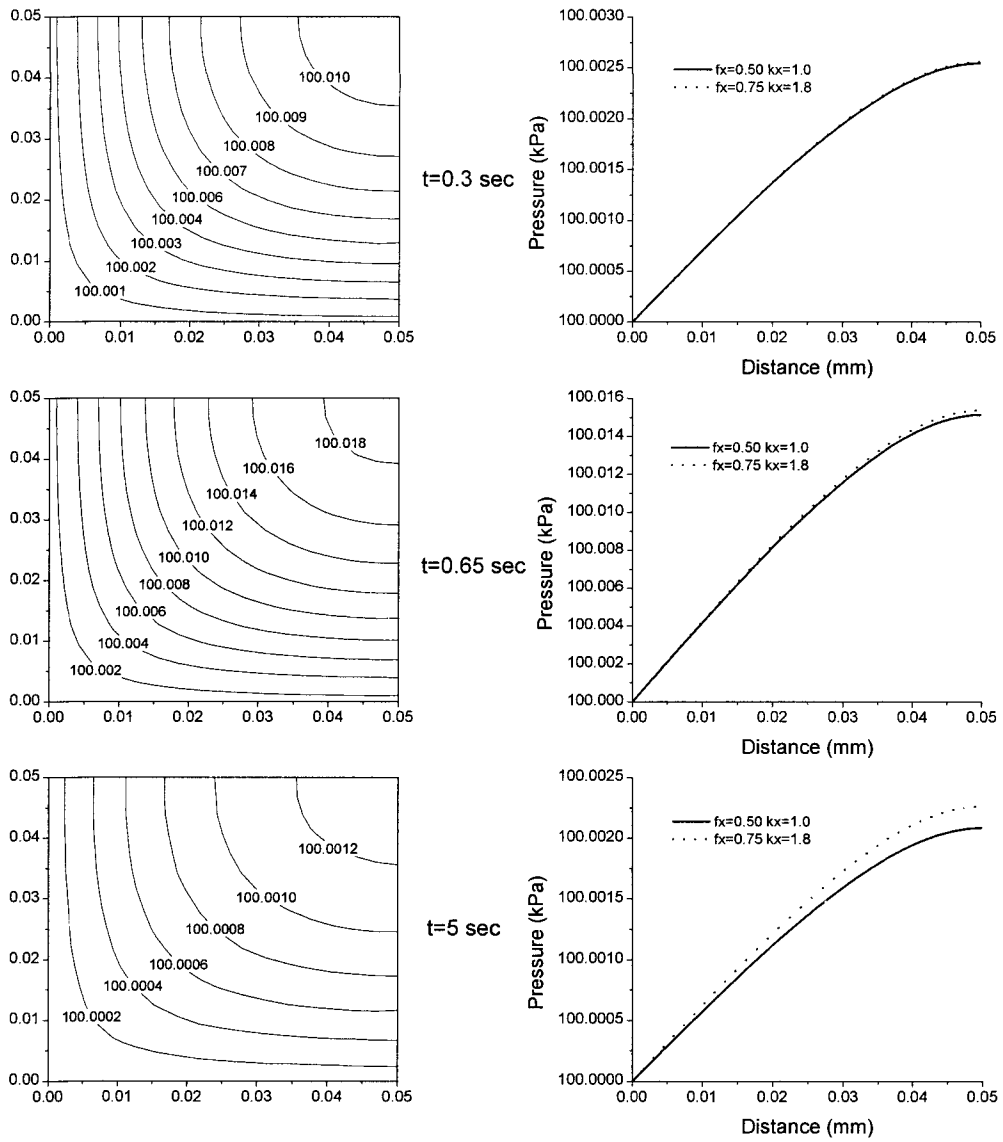

Fig 79. Pressure Profiles for a 0.1 mm Particle at 800K using a Two-Dimensional Model and One-Dimensional Models with Grain and Cross-Grain Properties

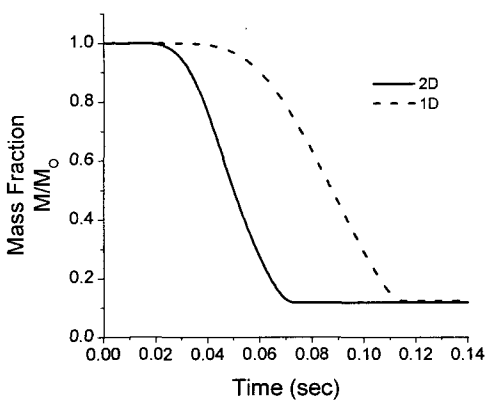

Fig 80. Solid Mass Fraction Remaining for a Two-Dimensional and a One-Dimensional 0.1 mm Cross-Grain Particle at 1600K

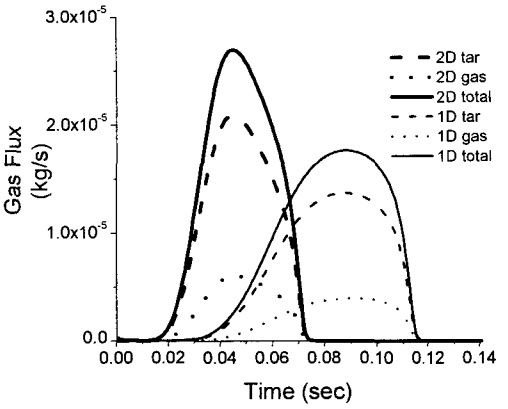

Fig 81. Surface Gas Fluxes for a Two-Dimensional and a One-Dimensional 0.1 mm Cross-Grain Particle at 1600K

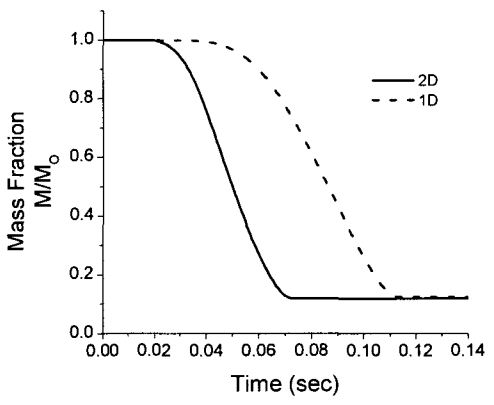

Fig 82. Solid Mass Fraction Remaining for a Two-Dimensional and a One-Dimensional 0.1 mm Cross-Grain Particle at 1600K

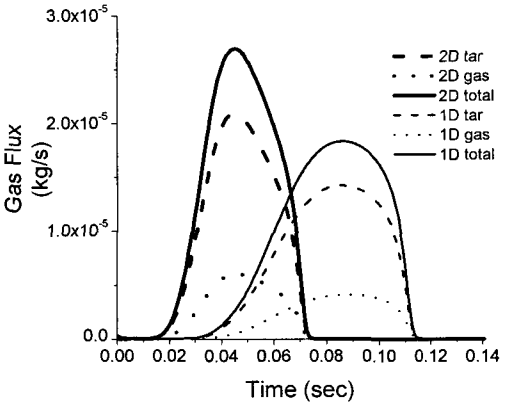

Fig 83. Surface Gas Fluxes for a Two-Dimensional and a One-Dimensional 0.1 mm Cross-Grain Particle at 1600K

The grain-direction properties give the one-dimensional particle slightly higher gas fluxes, and 90% of pyrolysis is done after 0.103 seconds. Once again directional properties have very little influence on the pyrolysis time or the gas fluxes from a one-dimensional particle.

The temperature profiles are shown in Fig 84. At 1600K, the one-dimensional model predicts temperatures that are around 150K cooler than the two-dimensional model, which shows that one-dimensional particles have a longer heat-up time. The directional properties of the one-dimensional particle alter the temperature profile of the particle. The particle with grain-direction properties is 20K cooler at the surface of the particle and 15K hotter at the center of the particle. These relatively small temperature differences allow 1% more radiation from a fixed temperature source to the grain direction particle and decrease pyrolysis times by 2%.

The pressure profiles are compared in Fig 85. The two-dimensional particle has a peak pressure of 101.77 kPa at 0.03 seconds. At this time, the one-dimensional cases are both still pressurizing because of the longer heat-up time. The one-dimensional particle with grain-direction properties has a peak pressure of 101.62 kPa at 0.0525 seconds and the cross-grain particle has a peak pressure of 101.34 kPa at 0.053 seconds.

For powders at high temperature, two-dimensional particles pyrolyze much more quickly than one-dimensional particles. The directional properties of the wood play only a minor role in the pyrolysis of high temperature powders. The difference between the two-dimensional and the one-dimensional model results is a caused by differences in the surface area to volume ratio of the particle. The two-dimensional particle has twice the surface area to volume ratio of the one-dimensional particle. The lesser surface area of the one-

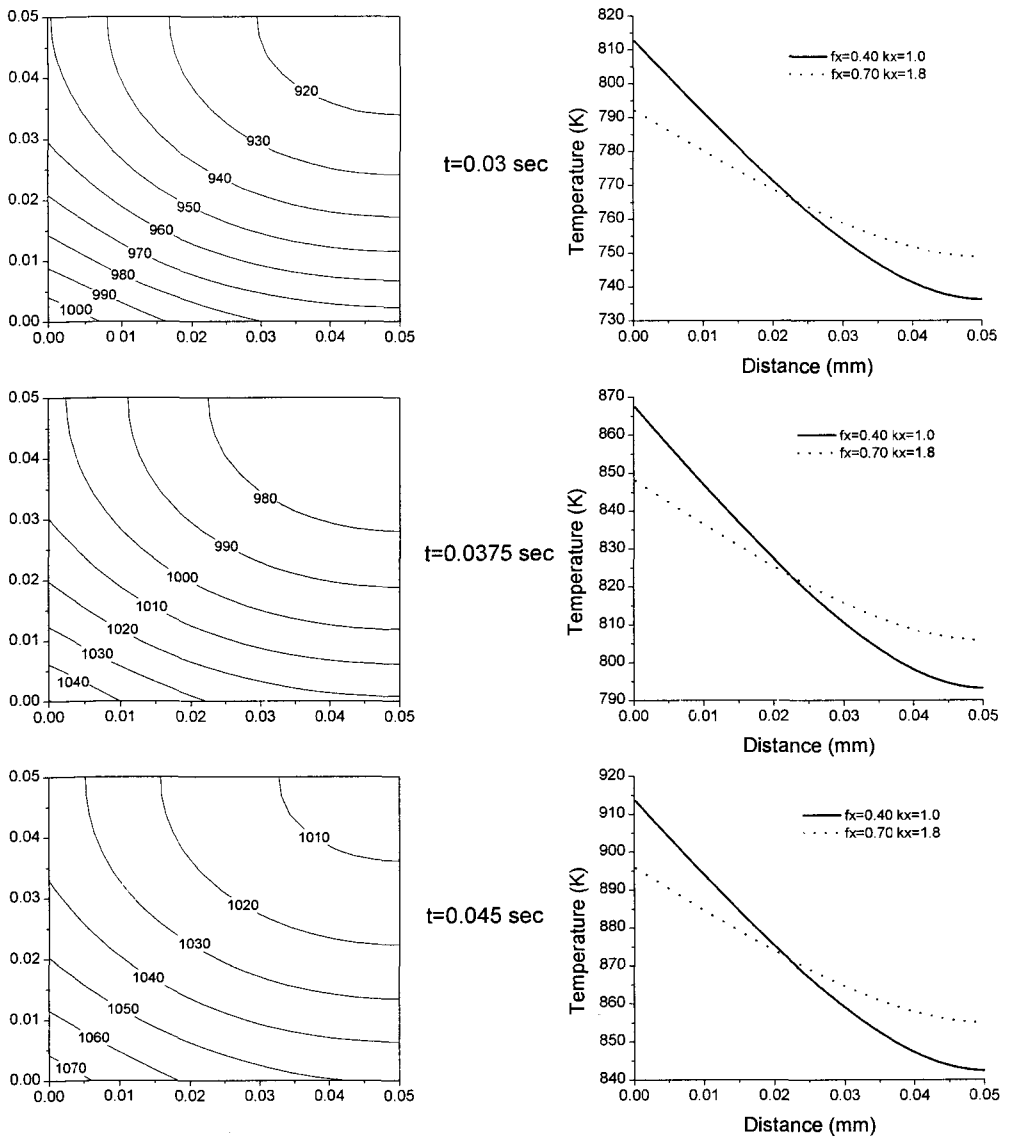

Fig 84. Temperature Profiles for a 0.1 mm Particle at 1600K using a Two-Dimensional Model and One-Dimensional Models with Grain and Cross-Grain Properties

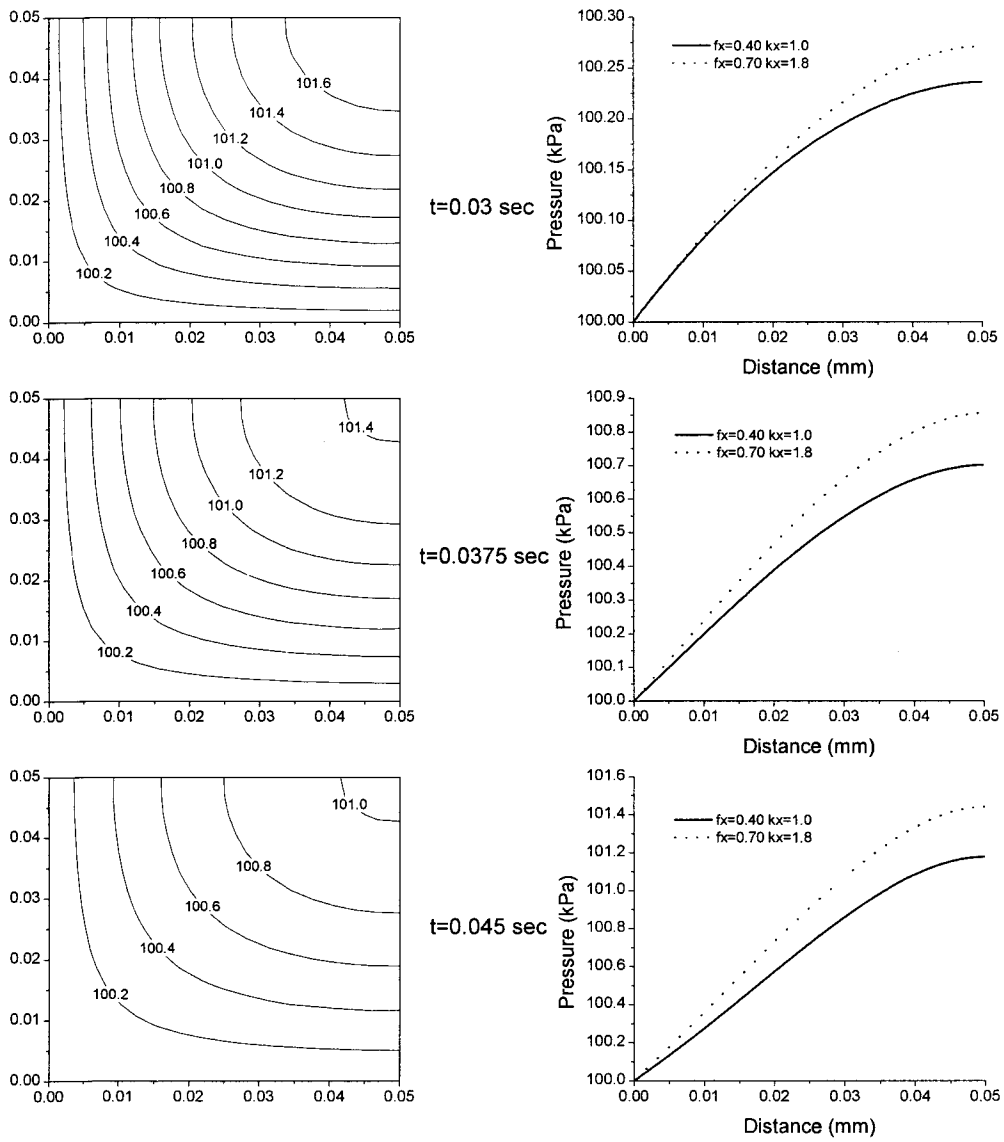

Fig 85. Pressure Profiles for a 0.1 mm Particle at 1600K using a Two-Dimensional Model and One-Dimensional Models with Grain and Cross-Grain Properties

dimensional particle caused 70% longer pyrolysis times and a 35% lower peak gas flux than the two-dimensional particle.

One-dimensional powder models only have a chance to predict the pyrolysis of high temperature powders if they can account for the correct surface area to volume ratio of the particle throughout pyrolysis, which changes as the particle shrinks during pyrolysis. It is unlikely that this is a good solution, because doubling the surface flux of a one-dimensional particle will cause the initial heat flux into a volume near the surface of the particle to be off by a factor of two, even though the heat flux to volume ratio of the whole particle is correct.

The results for a 2mm, 800K, two-dimensional particle and a one-dimensional particle with cross-grain properties are shown in Fig 86 and Fig 87. The one-dimensional particle with cross-grain properties has a slower pyrolysis time of 73.54 seconds vs. 53.68 seconds for the two-dimensional particle. The rate of release of gases from the particles is

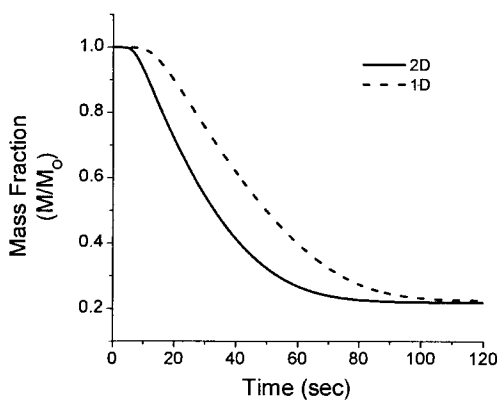

Fig 86. Solid Mass Fraction Remaining for a Two-Dimensional and a One-Dimensional 2 mm Cross-Grain Particle at 800K

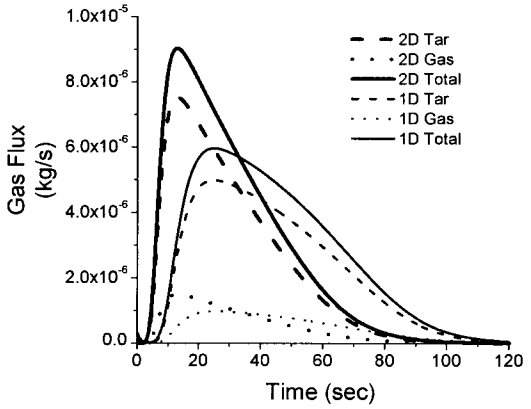

Fig 87. Surface Gas Fluxes for a Two-Dimensional and a One-Dimensional 2 mm Cross-Grain Particle at 800K

different. The two-dimensional particle has 50% higher gas fluxes, and shows a sharper and earlier gas flux peak.

The results for a particle with grain-direction properties are shown in Fig 88 and Fig 89. The one-dimensional particle with grain-direction properties performs similarly to the cross grain particle. The grain direction particle has a 90% devolatilization time of 70.54 seconds, and has only slightly higher peak gas fluxes. The temperature profiles are

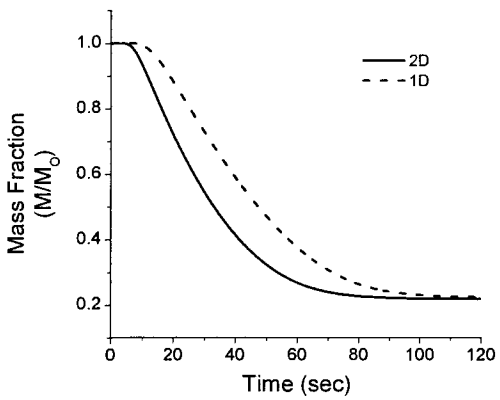

Fig 88. Solid Mass Fraction Remaining for a Two-Dimensional and a One-Dimensional 2 mm Grain Direction Particle at 800K

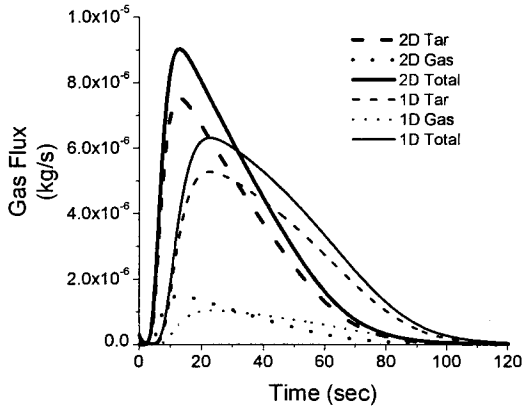

Fig 89. Surface Gas Fluxes for a Two-Dimensional and a One-Dimensional 2 mm Grain Direction Particle at 800K

shown in Fig 90. At 10 seconds, the temperatures within the two-dimensional particle vary from 705K to 680K. The cross-grain particle varies from 660K to 630K and the grain-direction particle varies from 660K to 645K. The two dimensional particle is about 50K hotter, and pyrolysis occurs more quickly. The one-dimensional particles have similar surface temperatures, but the particle with the grain direction properties has a higher center

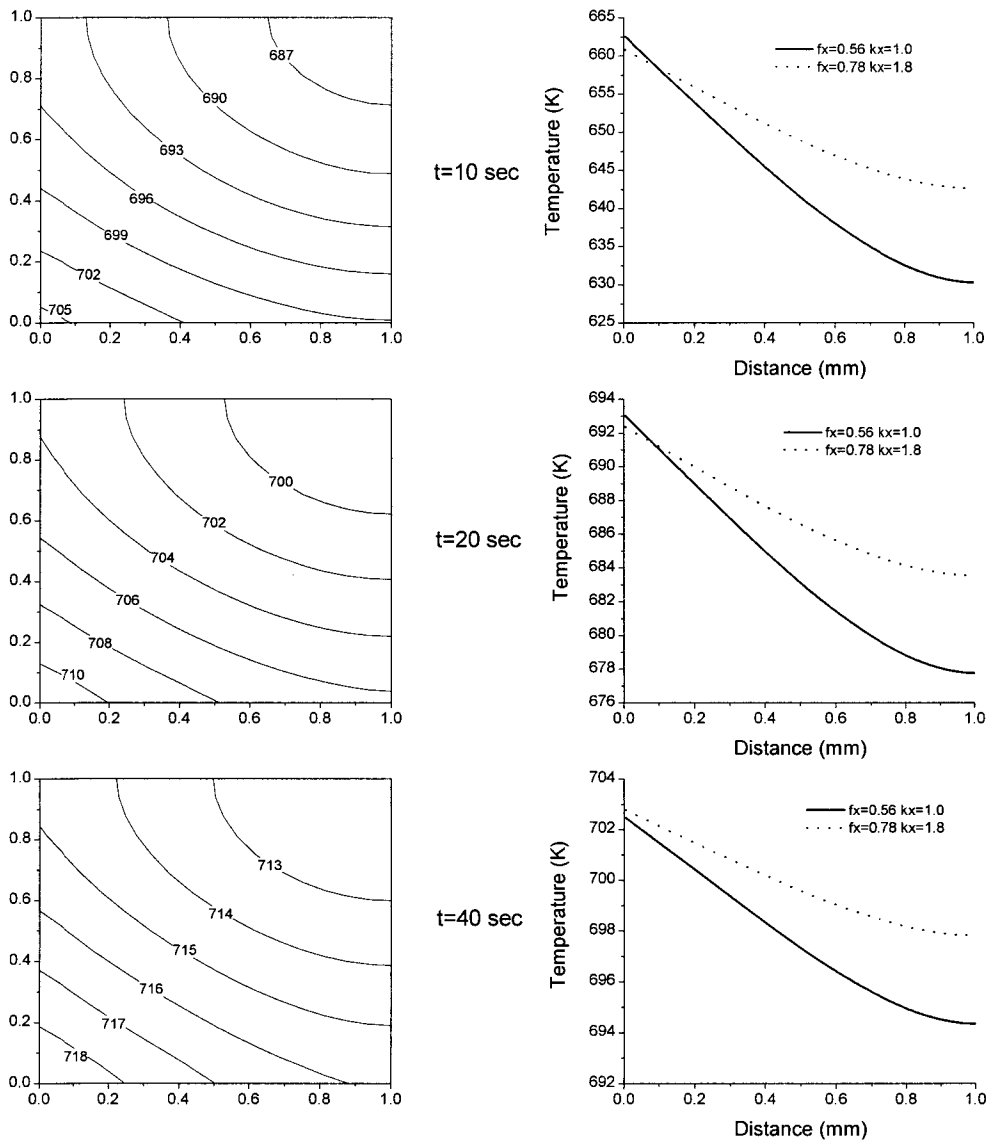

Fig 90. Temperature Profiles for a 2 mm Particle at 800K using a Two-Dimensional Model and One Dimensional Models with Grain and Cross-Grain Properties

temperature because the thermal conductivity is 1.8 times larger. The grain-direction particle differs by a few percent from the cross-grain particle because increased temperatures within the grain-direction particle speed up the pyrolysis process.

The pressure profiles are shown in Fig 91. The two-dimensional particle shows a maximum pressure of 100.85 kPa at 6.8 seconds. The cross-grain particle has a maximum pressure of 100.72 kPa at 12.2 seconds and the grain-direction particle has a maximum pressure of 100.88 kPa at 11.3 seconds. While the pressure of the two-dimensional particle differs from the one-dimensional results at each time step, the overall pressurization of the particle appears to be similar.

The mass fraction and the gas fluxes for the two-dimensional 2mm particle at 1600K and the one-dimensional cross-grain particle are shown in Fig 92 and Fig 93. The one-dimensional particle takes 50% longer to pyrolyze, even though both particles have a 0.2 second heat up time. The shape of the gas flux curves are quite different. Both particles have a peak in gas fluxes around 0.4 seconds, but the one dimensional particle has a secondary peak at 2.5 seconds. For the two-dimensional particle, the amount of gas flux decreases as the amount of virgin wood decreases. A one-dimensional particle acts more like a reacting front, or a thermal wave, where the pyrolysis region moves at a steady rate through the particle and is cooled by the virgin wood at the center of the particle. The one dimensional particle has fairly level gas fluxes, which are followed by a secondary peak when the thermal wave reaches the center of the particle, and there are no longer any cool regions to remove heat from the pyrolysis zone. Pyrolysis temperatures are increased at the center of a one-dimensional particle, producing a secondary peak in pyrolysis gases at the surface of the particle.

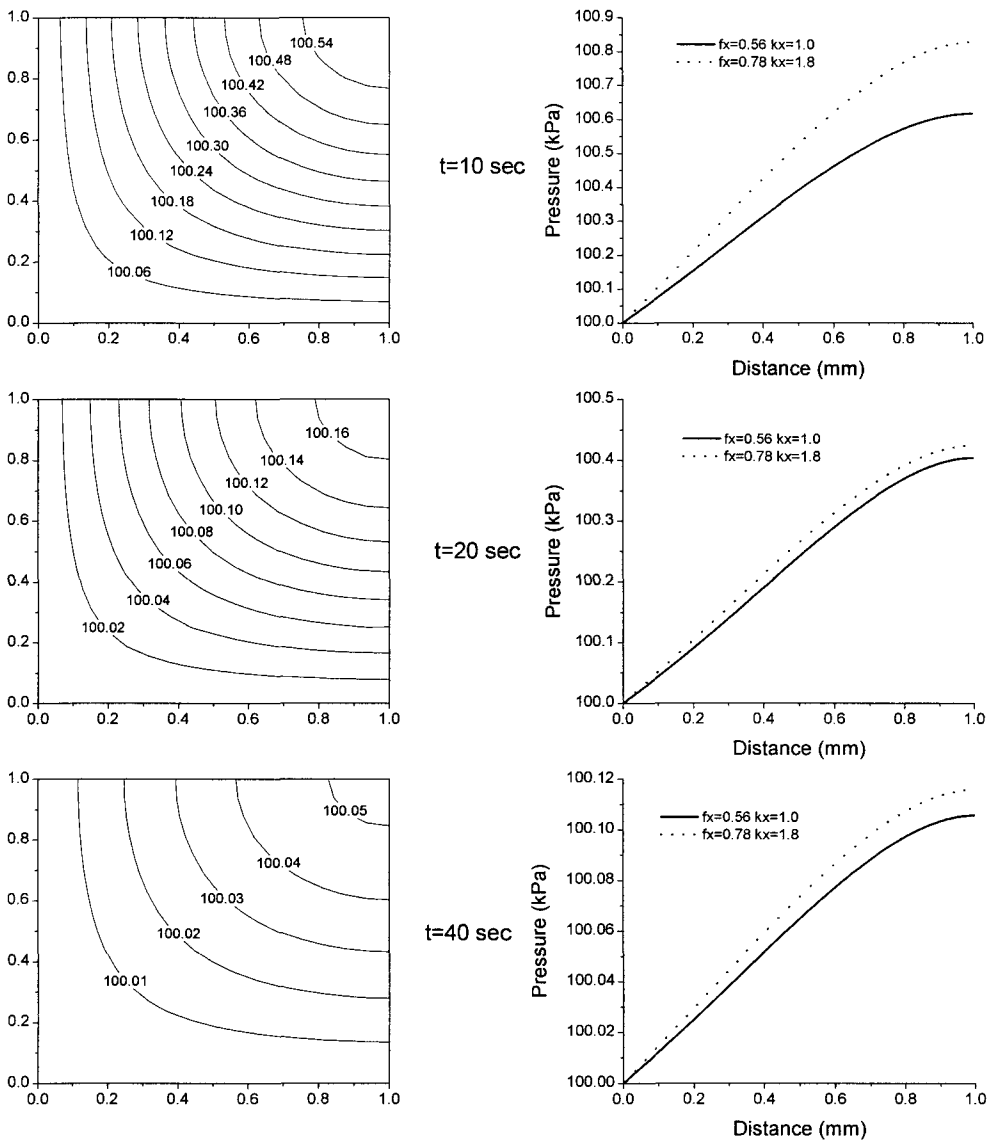

Fig 91. Pressure Profiles for a 2 mm Particle at 800K using a Two-Dimensional Model and One Dimensional Models with Grain and Cross-Grain Properties

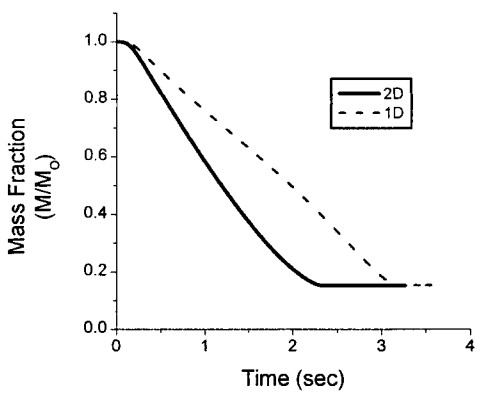

Fig 92. Solid Mass Fraction Remaining for a Two-Dimensional and a One-Dimensional 2 mm Cross-Grain Particle at 1600K

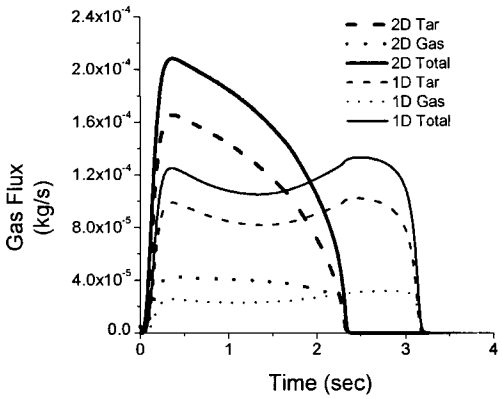

Fig 93. Surface Gas Fluxes for a Two-Dimensional and a One-Dimensional 2 mm Cross-Grain Particle at 1600K

The grain-direction particle is shown in Fig 94 and Fig 95. The increased conductivity in the grain direction increased the pyrolysis time by 0.5 seconds for the one-dimensional particle. The first peak in pyrolysis gas production is similar to the cross-grain case, but the secondary peak is much larger. A higher conductivity increases the secondary peak in a one-dimensional model because energy is transferred to the center of the particle more rapidly.

The 2mm particle at 1600K shows that the conductivity of a one-dimensional particle can be increased to help match two-dimensional pyrolysis times, but the increase conductivity will not significantly alter the primary peak in gas fluxes, but will cause a larger secondary peak. Thus, as conductivity is increased and pyrolysis times become closer, the shape of one-dimensional gas fluxes will differ more dramatically.

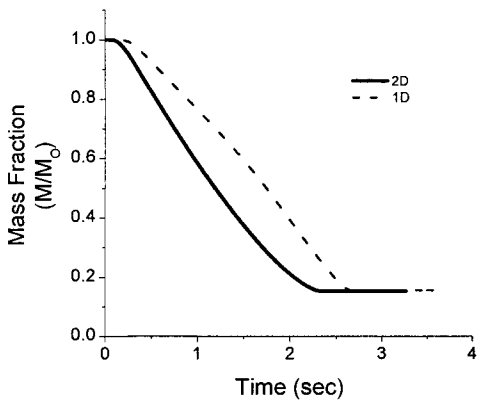

Fig 94. Solid Mass Fraction Remaining for a Two-Dimensional and a One-Dimensional 2 mm Grain Direction Particle at 1600K

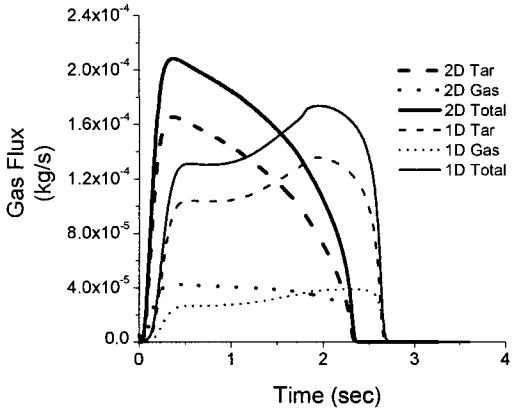

Fig 95. Surface Gas Fluxes for a Two-Dimensional and a One-Dimensional 2 mm Grain Direction Particle at 1600K

The temperature profiles are shown in Fig 96. The two-dimensional particle is about 50K hotter at the center of the particle and 150K hotter at the corners than the one-dimensional particle with grain direction properties. The high corner temperatures account for the larger peak in gas fluxes at the beginning of pyrolysis for the two-dimensional particle. Increased temperatures within the particle cause pyrolysis to happen more quickly. The heat travels from the corner of the particle towards the center. The volume of wood remaining decreases as the pyrolysis front travels towards the center of the particle, causing total gas production to decrease.

The cross-grain direction particle has a 50 to 70K hotter surface and an 80K cooler center than the grain-direction particle. The cross-grain direction particle acts more like a thermal wave because of its lowered thermal conductivity and produces a sharper

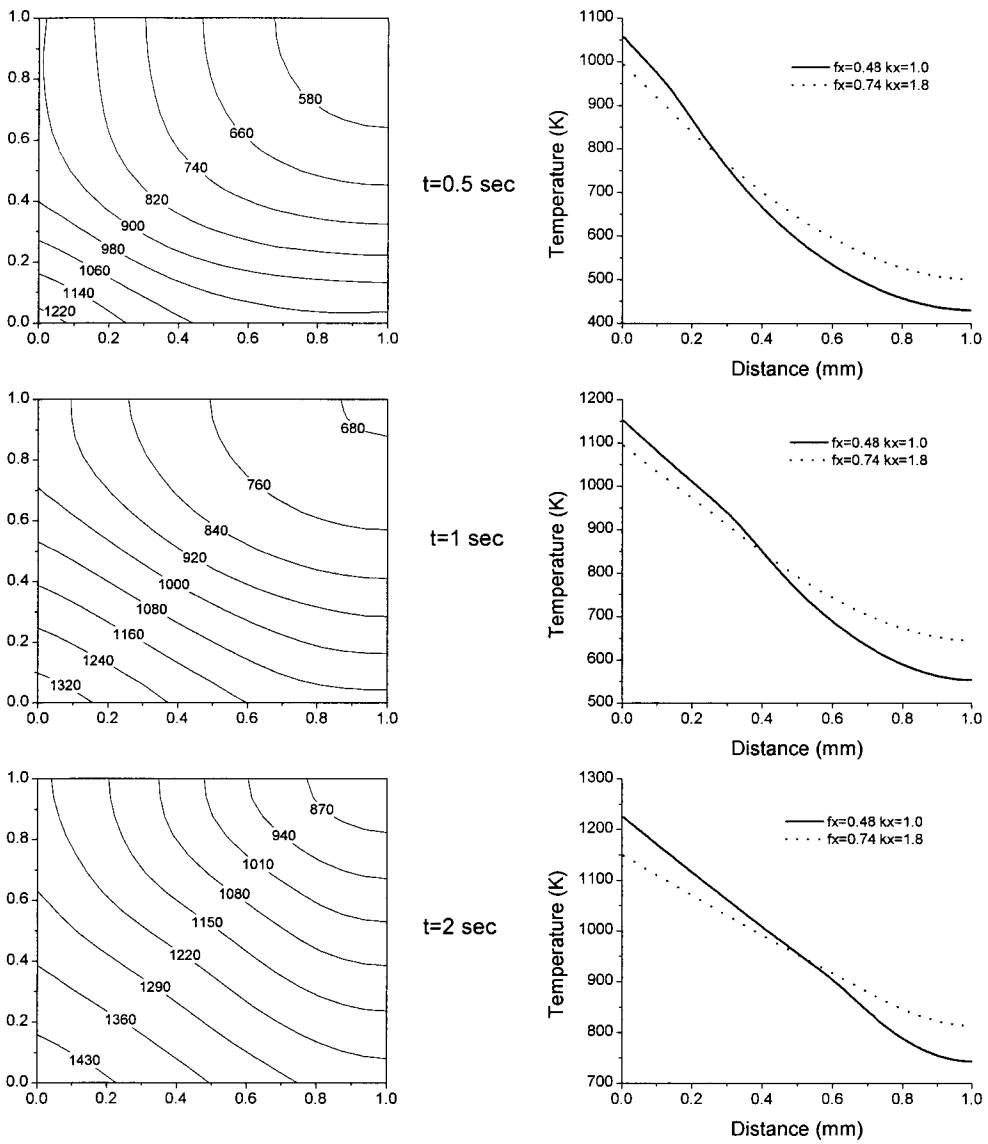

Fig 96. Temperature Profiles for a 2 mm Particle at 1600K using a Two-Dimensional Model and One Dimensional Models with Grain and Cross-Grain Properties

temperature gradient across the pyrolysis region. These differences look small on the temperature profiles, but these differences result in a 20% difference in pyrolysis times and illustrate how difficult it is to predict pyrolysis performance.

The pressures are shown in Fig 97. The two-dimensional particle has a maximum pressure of 105.1 kPa at 1.44 seconds. The one-dimensional cross-grain particle has a peak pressure of 103.7kPa at 2.07 seconds and the grain-direction particle has a peak pressure of 106.1 kPa at 1.84 seconds.

All of these particles have a maximum pressure after the first peak in gas fluxes which indicates that gas production and the temperature rise are high enough to increase the pressure within the particle. The one-dimensional models are unable to replicate a maximum pressure anywhere other than at the center of the particle. Pressurization of the one-dimensional particle can vary by a factor of two depending on the choice of directional properties, even though there is only a 20% difference in pyrolysis times.

For large particles, the one dimensional particles also give different results. The mass fraction and gas fluxes for a two-dimensional particle are compared with a one-dimensional particle with cross-grain properties for a 1 cm particle at 800K in Fig 98 and Fig 99.

The rate of mass loss is slower for the one-dimensional particle, resulting in an increase of over 50% in pyrolysis time. The gas fluxes from the one-dimensional particle peak much later, and have only 60% of the peak gas fluxes of the two-dimensional particle. The one-dimensional grain-direction particle is shown in Fig 100 and Fig 101.

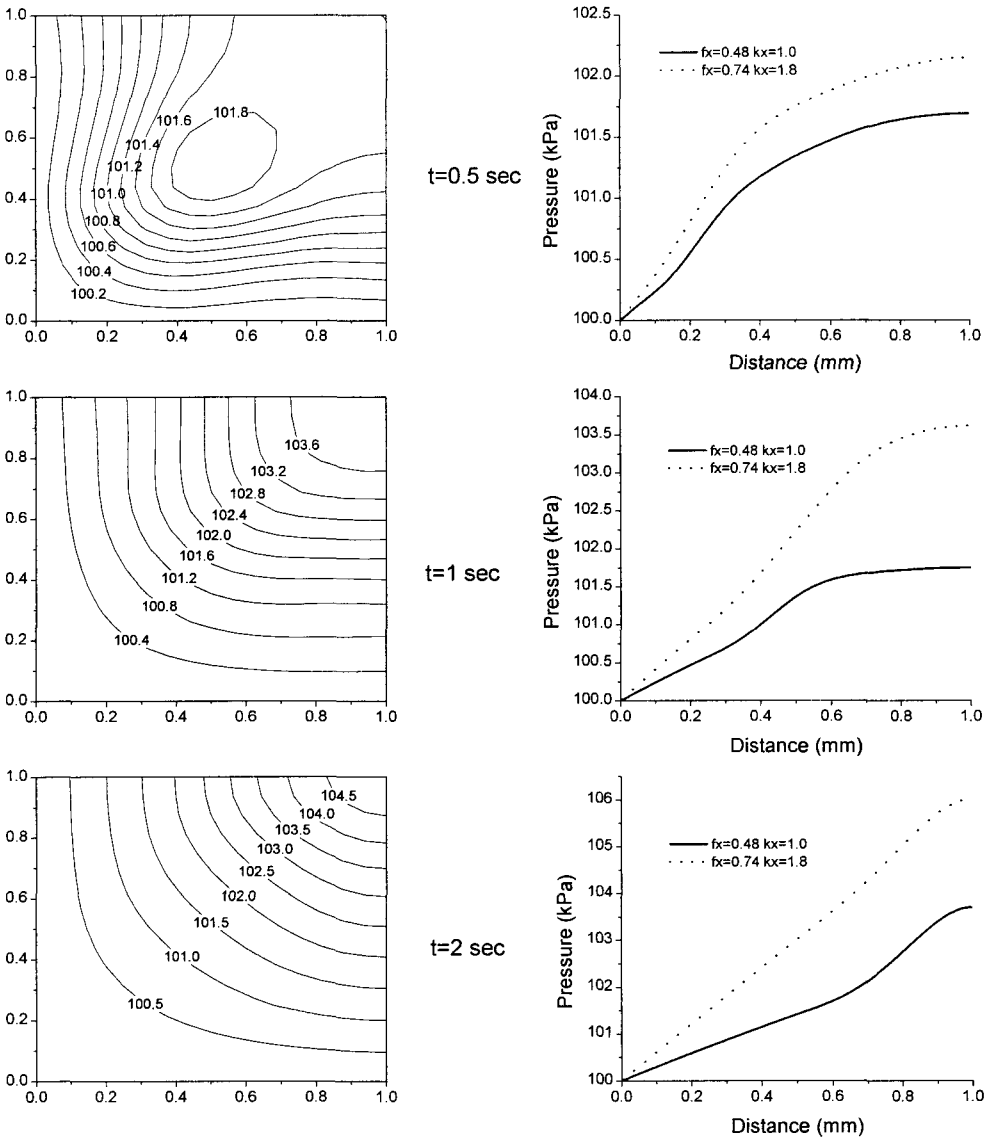

Fig 97. Pressure Profiles for a 2 mm Particle at 1600K using a Two-Dimensional Model and One Dimensional Models with Grain and Cross-Grain Properties

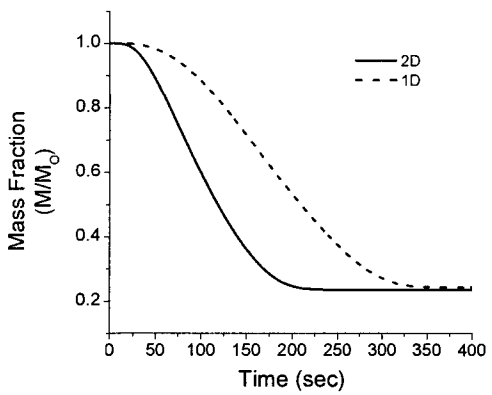

Fig 98. Solid Mass Fraction Remaining for a Two-Dimensional and a One-Dimensional 1 cm Cross-Grain Particle at 800K

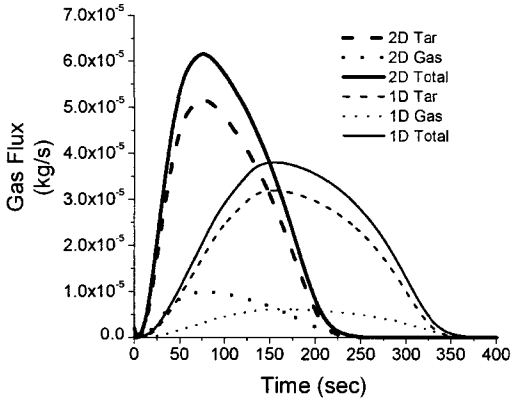

Fig 99. Surface Gas Fluxes for a Two-Dimensional and a One-Dimensional 1 cm Cross-Grain Particle at 800K

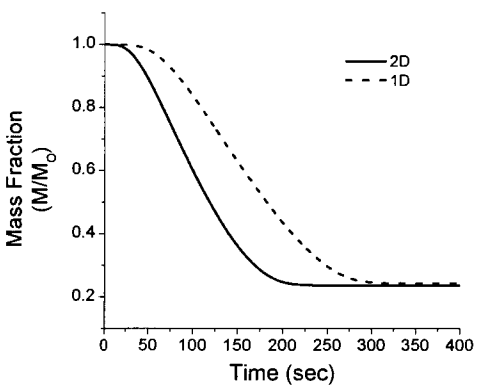

Fig 100. Solid Mass Fraction Remaining for a Two-Dimensional and a One-Dimensional 1 cm Grain Direction Particle at 800K

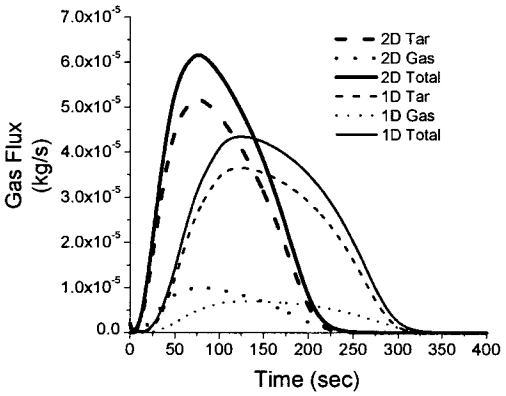

Fig 101. Surface Gas Fluxes for a Two-Dimensional and a One-Dimensional 1 cm Grain Direction Particle at 800K

The increased conductivity of the grain-direction properties helps to speed up pyrolysis times, and produces a gas flux curve more similar to the two-dimensional particle. The 1 cm particle is the first low temperature (800K) particle in which directional properties altered pyrolysis times by more than a few percent. At this size of particle, internal properties become important, even with a low external heat flux.

The temperature profiles are shown in Fig 102. The two-dimensional particle is 20 to 30K hotter than the grain-direction particle. The two-dimensional particle has a surface temperature of 670 to 680K at the center of the surface, 700K at the corners, and 620 K at the center of the particle. The grain-direction particle has a surface temperature of 660K and a center temperature of 590K. A 20 to 30K temperature difference can alter pyrolysis times by 50% for low temperature pyrolysis. Both one-dimensional cases have a similar surface temperature, bit the grain-direction particle is almost 30K hotter at the center of the particle, which speeds up pyrolysis by over 10%.

The pressure profiles are shown in Fig 103. The two-dimensional and one-dimensional particles have a similar maximum pressurization, with the two-diemnsional particle pressurizing and depressurizing in less time. The two-dimensional particle pressurizes to a maximum value of 102.02 kPa after 46 seconds, the grain-direction particle pressurizes to 102.16 kPa after 65 seconds, and the cross-grain direction particle pressurizes to 101.36 kPa after 90 seconds. The pressurization of the one-dimensional particles differs during the first 100 seconds of pyrolysis, but is similar during the latter half of pyrolysis.

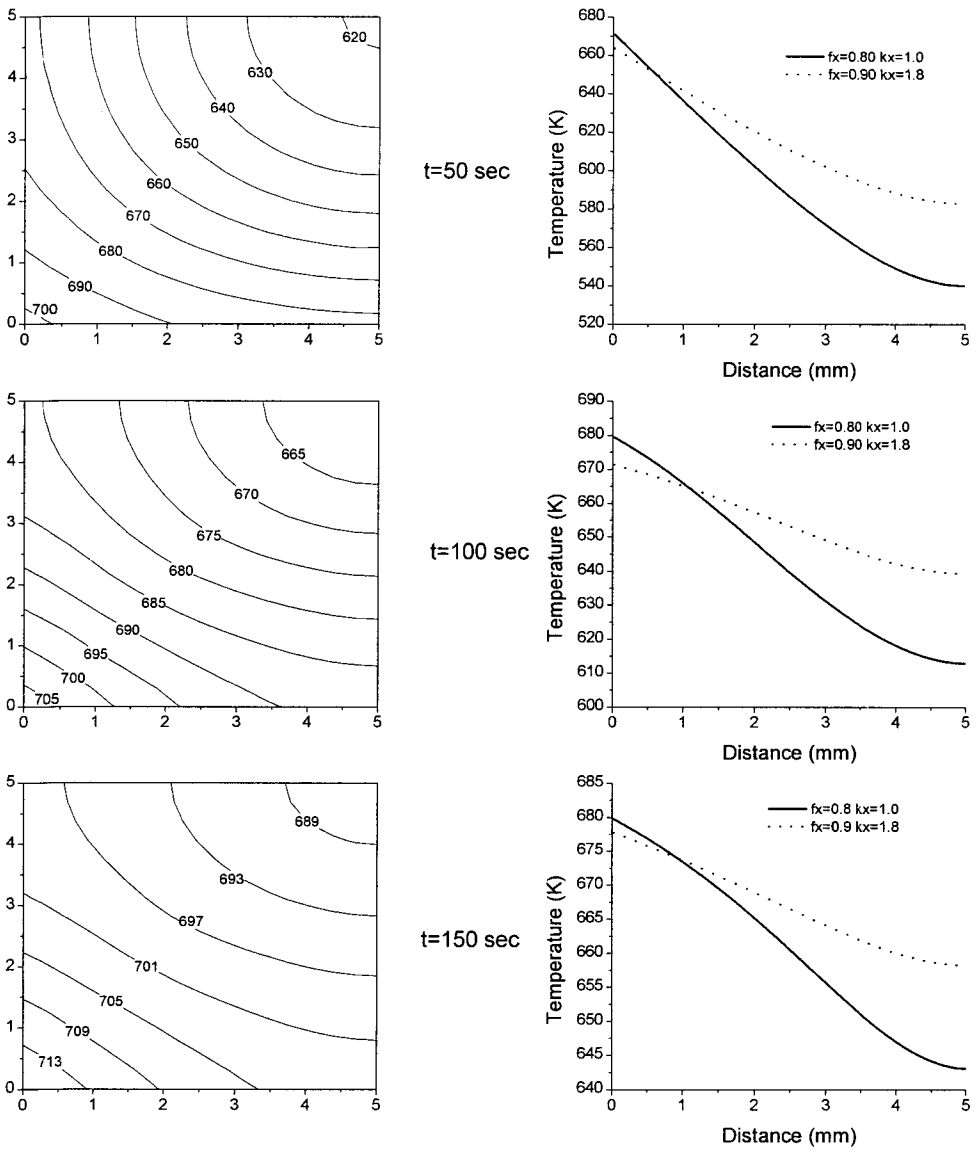

Fig 102. Temperature Profiles for a 1 cm Particle at 800K using a Two-Dimensional Model and One Dimensional Models with Grain and Cross-Grain Properties

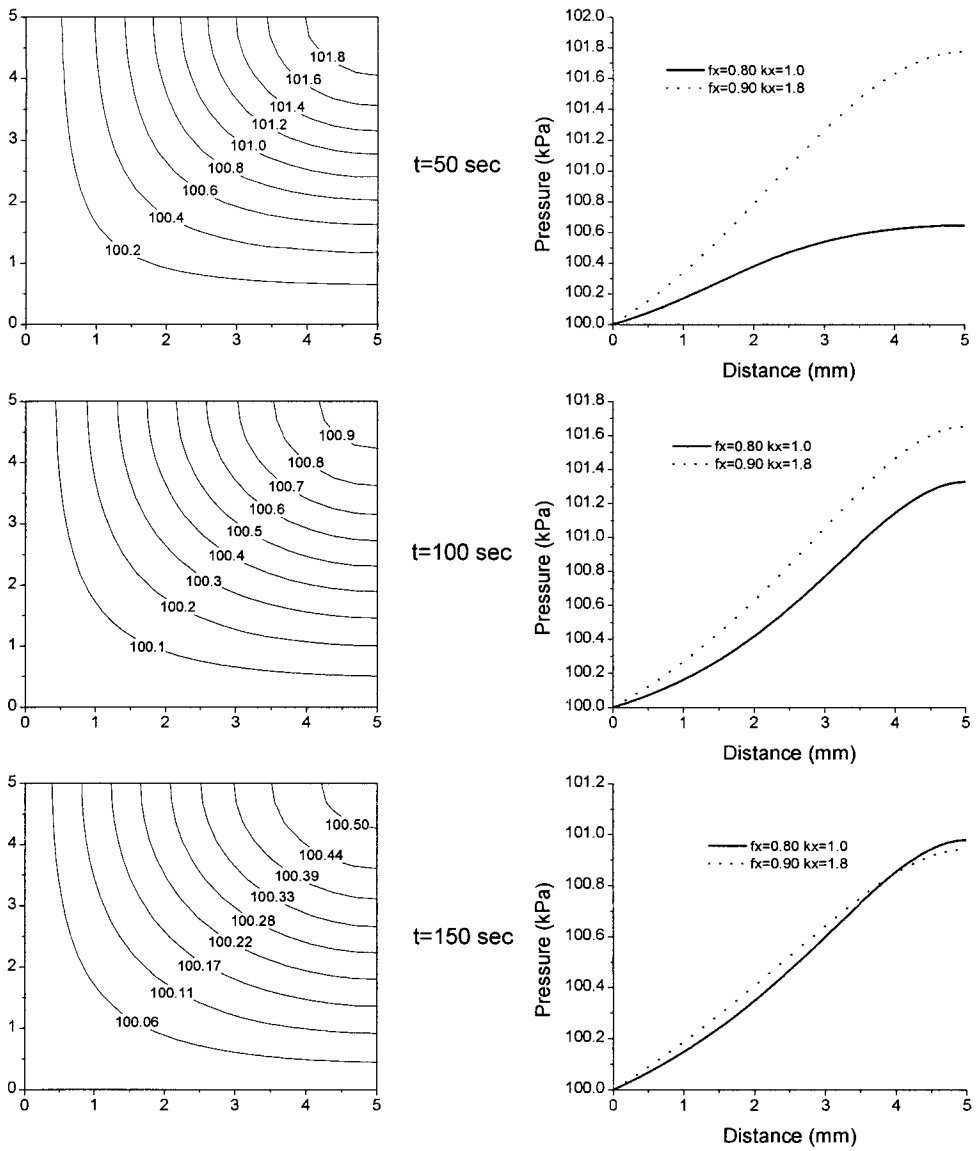

Fig 103. Pressure Profiles for a 1 cm Particle at 800K using a Two-Dimensional Model and One Dimensional Models with Grain and Cross-Grain Properties

At 1600K, a 1 cm particle takes almost twice as long to pyrolyze when a one-dimensional cross-grain particle is used. Fig 104 and Fig 105 show the mass fraction and the gas fluxes, respectively. Both the two-dimensional and the one-dimensional particle show a large peak in gas fluxes during the first second of pyrolysis. This initial peak is in response to a large heat flux to the surface of the particle. This peak is nearly twice as high for a two-dimensional particle because the two-dimensional particle has twice the surface area of the one dimensional particle. The gas fluxes for the two-dimensional particle drop rapidly from the initial peak, drop more gradually from 4-12 seconds, and then drop rapidly at the end of pyrolysis. The one-dimensional particle has an initial peak, a rapid drop in gas production, a steady period of gas production, and a gradual secondary peak.

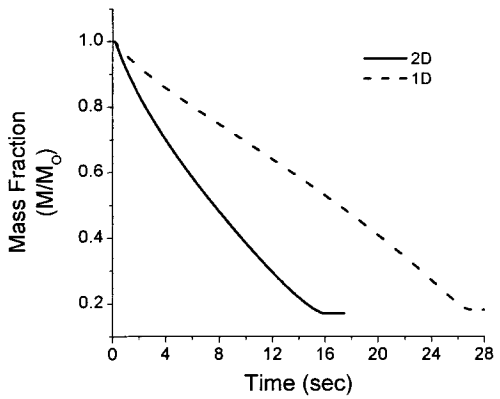

Fig 104. Solid Mass Fraction Remaining for a Two-Dimensional and a One-Dimensional 1 cm Cross-Grain Particle at 1600K

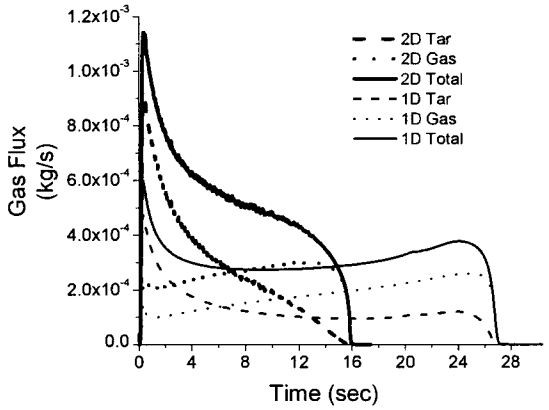

Fig 105. Surface Gas Fluxes for a Two-Dimensional and a One-Dimensional 1 cm Cross-Grain Particle at 1600K

The grain-direction particle is compared in Fig 106 and Fig 107. Thermal conductivity is important for 1 cm particles. The grain-direction particle has a much closer pyrolysis time to the two-dimensional particle, but still has a different shape for the gas flux curve. The increased conductivity does not alter the primary gas flux peak for the one-dimensional particle from the cross-grain case. The secondary gas flux peak increases by almost 50% because the grain-direction conductivity is increased by a factor of 1.8.

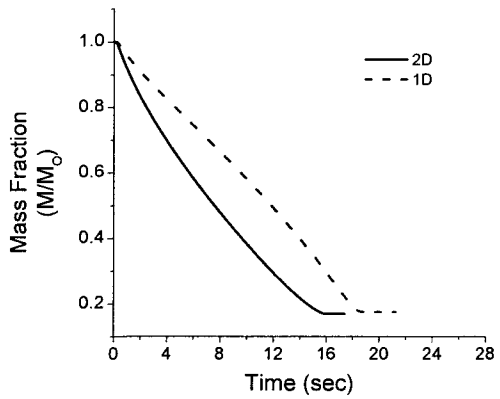

Fig 106. Solid Mass Fraction Remaining for a Two-Dimensional and a One-Dimensional 1 cm Grain Direction Particle at 1600K

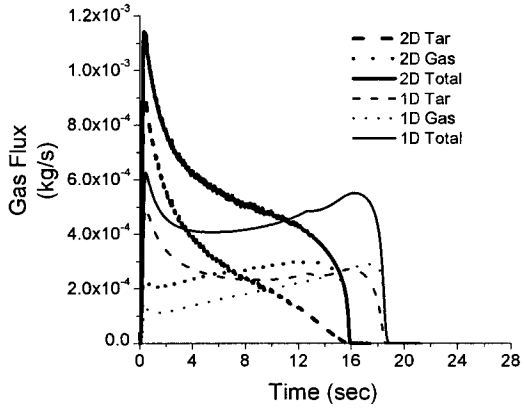

Fig 107. Surface Gas Fluxes for a Two-Dimensional and a One-Dimensional 1 cm Grain Direction Particle at 1600K

The temperature profiles are shown in Fig 108. The two-dimensional particle is about 50K hotter than the one-dimensional grain-direction particle, which results in faster pyrolysis times. At 1 second, the temperature profiles of the one-dimensional cases are similar. The temperature rise during the first second of pyrolysis is a simple response of the surface wood

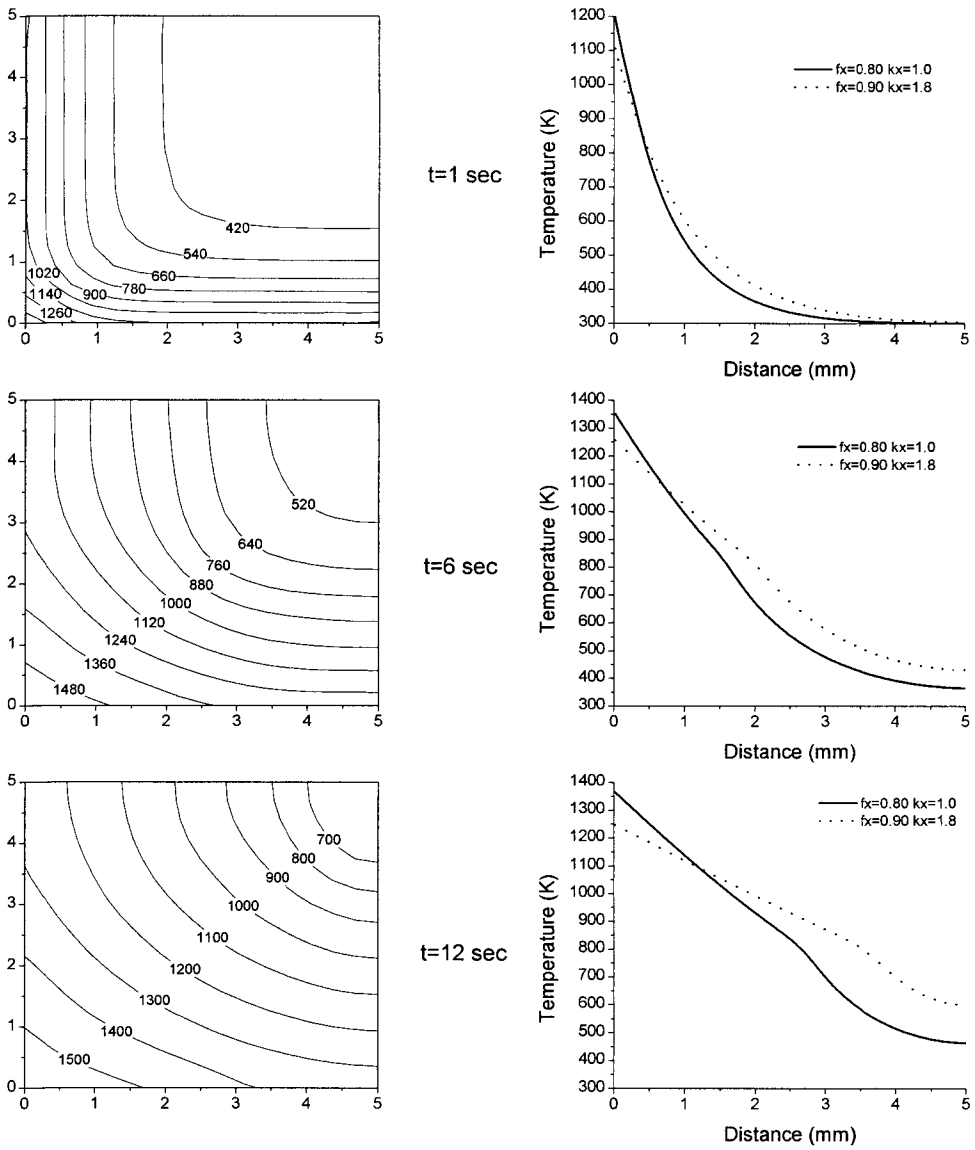

Fig 108. Temperature Profiles for a 1 cm Particle at 1600K using a Two-Dimensional Model and One Dimensional Models with Grain and Cross-Grain Properties

to radiant heat flux, and direction properties do not influence this response. At 6 seconds, the cross-grain particle is 70K cooler at the center and at 12 seconds, the cross-grain particle is 150K cooler. This 150K temperature difference causes the 50% difference in the secondary gas flux peak.

The pressure profiles are shown in Fig 109. The two-dimensional particle has a similar maximum pressure to the one-dimensional grain-direction particle at each time. The two-dimensional particle shows a maximum pressure that is not at the center of the particle during much of pyrolysis. The cross-grain particle has a pressure that is up to 50% lower at the center of the particle throughout pyrolysis. Even though the cross grain particle has a lower central pressure, the pressure gradient at the surface is similar after 1 second to the grain-direction particle, and produces the same total gas fluxes from the surface during the primary peak.

These sample cases show that one-dimensional models are appropriate for modeling powders at low temperatures. For any other case the one-dimensional results have a different pyrolysis time and/or a different rate of gas release form the surface of the particle. The one-dimensional results differ because they do not have the correct surface area to volume ratio of a multi-dimensional particle. The thermal conductivity of a one-dimensional particle can be increased above the actual value to obtain similar pyrolysis times, but the shape of the gas flux peaks will differ dramatically. Real particles do not show the secondary peak that is predicted by a one-dimensional model, unless heat transfer really occurs under a one-dimensional situation. Corrections to surface area to volume ratios for a one-dimensional model will cause too much heat flux at the surface of the particle, and will only enhance the secondary gas flux peak in the one-dimensional model.

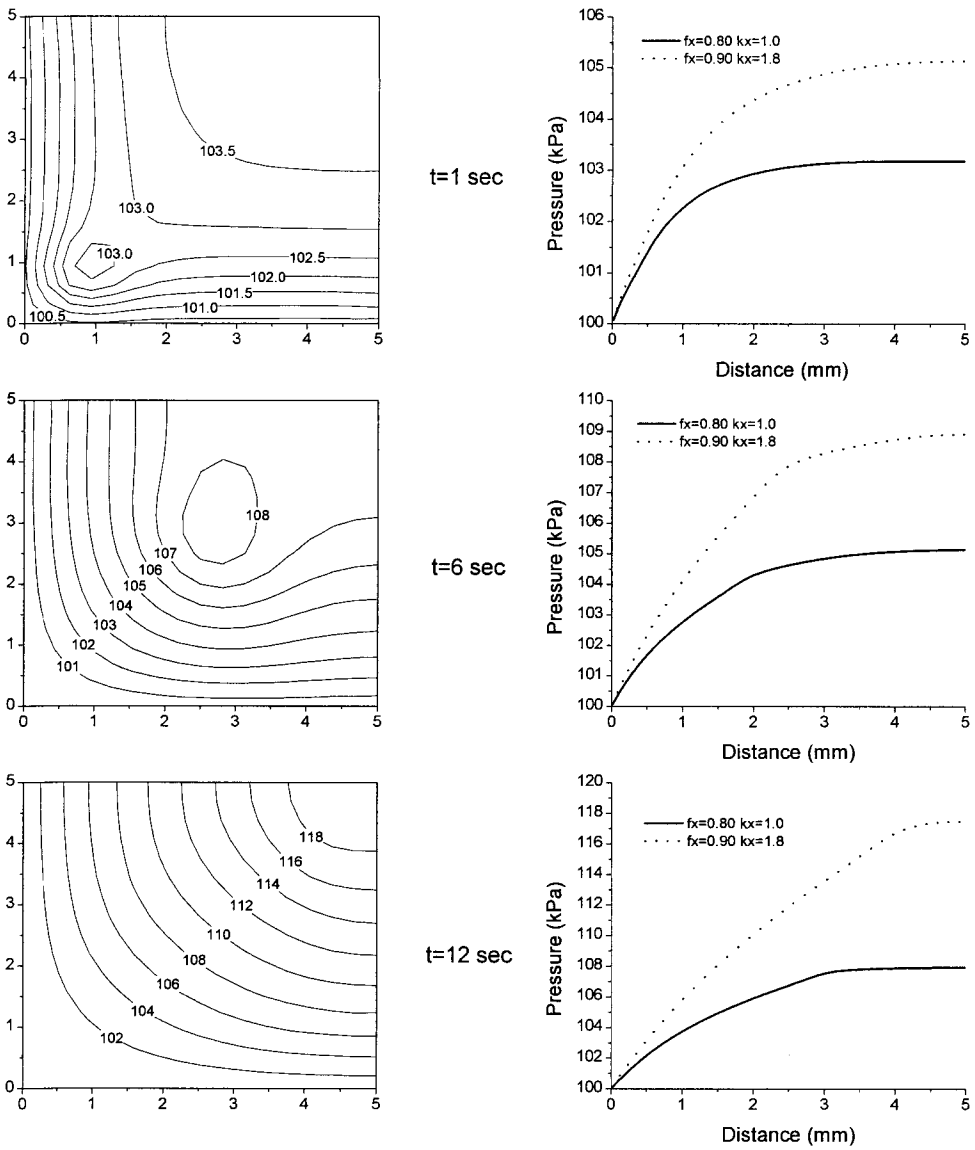

Fig 109. Pressure Profiles for a 1 cm Particle at 1600K using a Two-Dimensional Model and One Dimensional Models with Grain and Cross-Grain Properties

Chapter 7

Conclusions

The detailed computational model is a useful tool for many reasons. It can be used to determine quantities which are costly, difficult, or impossible to measure experimentally. The computational model can be used to find which physical properties influence the pyrolysis process. A detailed model can be used to determine where shrinkage, moisture, cracking, and multi-dimensional effects are important. These results can be used to determine where simplifications can be made in the computational model without a loss of accuracy.

Several things were learned in the validation of the two-dimensional model. Many physical properties played only a minor role in the pyrolysis process. The rate of pyrolysis reaction and the specific heat of the wood, char and pyrolysis gases had only a small impact on the total pyrolysis time for most pyrolysis conditions. The porosity of a particle helps to determine the pressurization of the particle and the release of gases from the particle, but gas flows have only a minor affect on pyrolysis times because gases have a smaller thermal capacity than the solid portion of the particle.

For most pyrolysis conditions, the rate of internal heat transfer is the dominant factor in determining pyrolysis times. For these particles, the conductivity within the particle is the most important physical parameter for determining pyrolysis times. Computational modelers have previously used values for conductivity that vary by a factor of 10. As the composition of the particle changes, the conductivity of the particle changes. Detailed models may include a wood, char, and radiation contribution to conductivity. The wood and char conductivity may or may not be temperature dependent. The radiation contribution to conductivity has

previously been modeled as a temperature dependent function that depends on the pore size, the void fraction, and the temperature raised to the third power (Panton and Rittman, 1971). The mechanisms by which the conductivity of the particle changes are not well-understood. As a result, most computational modelers input reasonable property data and use a conductivity that matches an experimental result. The problem with this procedure is that the computational model conductivity needed to match experimental results changes as the size, shape, and rate of heating of the solid particle are changed.

During the validation process, the rate of internal heat transfer was studied for a range of particle sizes and temperatures. Several different formulations for conductivity were tried in the validation process. The simplest procedure is to assume that that the conductivity of both wood and char are constant, and that radiation does not contribute to the conductivity of the particle. Experimental measurements put the conductivity of wood and char at around 0.1 $\frac{W}{m \cdot K}$. The 1/8 x 1 x 1 inch particle, the ¼ x 1 x 1 inch particle, and the ½ x 1 x 1 inch particle from Hoerning's work were each run at 800°C, 1100°C, and 1400°C using a two-dimensional computational model. Using a constant thermal conductivity, the two-dimensional computational model predicts that small particles (1/8 x 1 x 1) at high temperatures (1400°C) are about 25% faster than experimental results and that large particles (1/2 x 1 x 1) at low temperatures (800°C) take about 30% longer than the measured pyrolysis time when using constant char conductivity. These results indicate a problem with using a radiation term for conductivity, because the radiation term is temperature dependent and will increase the error between the computational model and the experimental results. Two important conclusions can be made by comparing the computational model with the

experimental results. The first conclusion is that conductivity can not be nearly as temperature dependent as previous modelers have assumed. The second conclusion is that the conductivity of the particle must increase as the thickness of the char layer increases. The second conclusion indicates that char cracking is the dominant process by which the char conductivity increases with the size of the char layer.

Cracks develop at the surface of a particle and relieve stresses formed near the surface of the particle from pressurization or shrinkage and deformation of the particle. Cracks typically grow with the char layer and extend into the active pyrolysis layer. As the crack grows into the particle, the crack separates near the surface of the particle, creating a gap between the two crack surfaces. For a crack that is perpendicular to the surface of the particle, an equal amount of external radiation will reach both crack surfaces. As a result, both surfaces of the crack will have similar temperatures and very little energy will be exchanged by radiation from one crack surface to another. The crack allows external radiation to travel directly from some external source to regions along the crack surfaces within the particle. Cracking will speed up the rate of internal heat transfer by radiating energy into the interior of the particle, and more radiant energy will reach the particle because the external source radiates to a cooler temperature within the particle. In a computational model that does not compute cracking, the effect of cracking can be included by assuming that the conductivity of the char layer increases as the size of the char layer grows.

The effects of char cracking were included in this work by assuming that the char conductivity increases as the char layer grows according to the following equation.

$$k_{char} = 0.105 + 1400(L_{char})^{1.4} \text{ W/m K} \quad k_{char,\max} = 0.605 \text{ W/m K} \qquad [78]$$

The length of the char layer was defined as the shortest distance to the surface of the particle from a region containing 90% wood. The exact nature of the increase in char conductivity is unknown and the correlation was used to best fit the pyrolysis times for the nine cases from Hoerning. The two-dimensional model showed less than 5% error for the 1/8 x 1 x 1 inch particle, less than 16% error for a ¼ x 1 x 1 inch particle, and less than 13% error for a ½ x 1 x 1 inch particle for all temperatures. Given that experimental pyrolysis times will often vary by around 10%, the computational model does a good job of predicting pyrolysis times for a range of particle sizes and temperatures.

The two-dimensional model under predicts pyrolysis times using correct property data because a two-dimensional particle has a lower surface area to volume ratio than does the real particle. This effect can be counteracted by using a value for char conductivity that is higher than the true conductivity within the particle. In the validation of the computational model, the formulation for char conductivity increasing with the size of the char layer overestimates the value of char conductivity. This explains why the maximum error in the validation process occurs for the middle sized particle (1/4 x 1 x 1) as compared with the data of Hoerning. The real conductivity of the particle likely only increases by a factor of two or three because of char cracking, indicating that char conductivity may vary from 0.1 W/m K to 0.3 W/m K as measured in the laboratory.

The validation process highlights an important concept. Some physical parameters have to be altered from their true values to overcome the limitations of a two-dimensional

model. Because two-dimensional models can not accurately recreate a real (3D) particle, the computational value for conductivity has to be increased above experimental values to compensate for the error associated with assuming a two-dimensional particle.

Once the numerical model had been validated, the numerical model was used to study how particle size, shape and grain direction altered the pyrolysis performance with various external temperatures. The influence of particle shape, size, and grain direction can be related to the relative importance of the rate of internal heat transfer, the amount of time needed to heat the particle, and the rate of pyrolysis reactions. For fine powders at low temperatures only the rate of pyrolysis reaction matters. Particle shape, size, and grain direction do not need to be known for low temperature powders. Only the initial mass of the particle is needed to predict pyrolysis performance. At high temperatures, the amount of time required to heat a powder is also important and grain direction has an influence on pyrolysis.

For sawdust sized particles (~1mm), both the rate of external and internal heat transfer are important. When the rate of internal heat transfer matters, particle shape and size will influence the amount of time it takes to pyrolyze the particle. The pyrolysis time increases with particle size. The particle shape changes the total surface area of the particle and will alter the rate of external heat transfer as well as the importance of directional properties. The grain direction has little influence on the pyrolysis process because the reduction in particle surface area from shrinkage is countered by the increased conductivity in the grain direction.

For finely cut wood chunks (~5mm) at 800K, the particle reacts similarly to the sawdust particle. At temperatures above 1000K, the rate of internal heat transfer becomes more important than the rate of external heat transfer. In these particles, the rate of pyrolysis

is limited by the ability to get energy into the particle. The particle size and shape are important because they change the amount of energy the particle receives. Grain direction is also important because increased conductivity and shrinkage will improve the rate of heat transfer within the particle.

For wood chunks (~2cm), the rate of internal heat transfer controls the pyrolysis process. The particle shape, size, grain direction and the amount of shrinkage in each direction are needed to accurately predict the performance of a wood chunk. Pyrolysis times can vary by 30% depending on the orientation of a rectangular particle. This work indicates that researchers need to do a better job of recording property data during experimental investigations.

Computational modelers have had a difficult time predicting the performance of biomass particles. Most researchers have attributed the difficulty to uncertainties in obtaining property values within a particle during pyrolysis. A comparison of two-dimensional and one-dimensional results using the same model shows that much of this confusion comes from applying a one-dimensional model to a process which can not be adequately described by a one-dimensional model. The two-dimensional model agreed with the one-dimensional runs only for fine powders at low temperature. For all of the other cases, the one dimensional-model was not able to predict the total pyrolysis times because of errors in the surface area to volume ratio or because the internal heat transfer could not be adequately represented using a one-dimensional model.

An important finding in the comparison of two-dimensional and one-dimensional models is that a one-dimensional model will have to use different property data than a two-dimensional model to obtain the same pyrolysis time. For sawdust and larger particles, a one-

dimensional model will need a higher thermal conductivity to obtain the same pyrolysis time and may need to correct the surface area to volume ratio for all particle sizes. The amount of correction would depend on the particle size, shape, external temperature, and the directional properties, making this a difficult process. Even if these corrections could properly be made to a one-dimensional model, the rate of release of gases from the particle would differ dramatically from the performance of the actual particle. A one-dimensional model often exhibits a primary gas peak at the beginning of pyrolysis and a secondary peak as heat transfer reaches the center of the particle. A two-dimensional model shows that a particle heated on all sides will have a peak at the beginning of pyrolysis and the gas fluxes will gradually drop form this maximum.

There are additional complications in using a one-dimensional model. Shrinkage has been shown to reduce pyrolysis times by over 40% for one-dimensional particles. In a real particle, shrinkage acts in a more complicated fashion. Shrinkage reduces the surface area of the particle, limiting external heat transfer to the particle, while increasing the temperature gradient within the particle. Shrinkage can cause large scale deformation of the particle when regions within the particle shrink at different rates and shrinkage is probably the primary cause of the cracking process. One-dimensional models have only been able to account for the increased temperature gradient within the particle and have predicted that shrinkage always decreases pyrolysis times. Two-dimensional results seem to indicate that the loss of particle surface area is countered by the increased temperature gradient within the particle for most situations, and that the net influence of shrinkage is likely through the cracking process.

The available property and pyrolysis data do a very good job of describing a wood particle during pyrolysis and this work demonstrates that the difficulties in computational

modeling have come from the inability to adequately describe the physical system rather than from insufficient property data. The existing detailed one-dimensional models can be used to predict performance for situations that are truly one-dimensional, such as the heat flux to the surface of a board. One-dimensional models should be used with caution, and with an understanding of the limitations of the model, when describing the performance of biomass particles or combustion situations that are not truly one-dimensional.

The two-dimensional model created for this work is also limited its ability to adequately describe the physical situation of a particle surrounded by a fixed temperature radiant heat source. A comparison of the computational model with the (validation) mass loss data of Hoerning shows that the experimental data shows a somewhat larger rate of mass loss at the beginning of pyrolysis and a more gradual drop in mass near the end of pyrolysis. A three-dimensional computational model would be expected to have a larger initial rate of mass loss because of additional radiation from the third dimension, and would be expected to drop off more gradually at the end of pyrolysis because there is less virgin wood available in the cool core of a three-dimensional volume. The differences between the model and the real performance of the particle are inherent in the two-dimensional assumption and would be expected. The goal of this work was to create a model for wood pyrolysis that describes the physical process accurately enough that the model can be applied to many different situations. The key to using this model is in understanding the limitations of the model.

Chapter 8

Future Work

The existing computational model can be used to examine a number of things beyond the scope of this thesis. While the existing model contains shrinkage, a detailed study of shrinkage values for a variety of particle sizes would give insight into where and how shrinkage is important in the pyrolysis process. A detailed study of moisture content would also give insight into how moisture movement, vaporization, and recondensation will alter the performance of biomass.

Another avenue of research would be to reduce the limitations of the current model. The two-dimensional model could be expanded to include gas phase combustion reactions. This would allow the study of combustion systems with a model that can describe the interaction between the gas phase reactions and the solid particle. Current research in this area is limited by the understanding of the performance of the solid particle. The two-dimensional model could be improved by including cracking and deformation of the particle. Cracking is known to be an important process, but the detailed influence of cracking is not well-understood. The unstructured solution procedures used in this model would make the implementation of cracking routine a relatively straight-forward process. The current model can already be used to study the three-dimensional performance of a solid particle. Current research in this area is limited by the time required for a solution and practical implementation of the three-dimensional model would require streamlining the solution procedures, relaxing the tolerances, and the use of parallel computing resources.

References

Alves, S. S., Figueiredo, J. L., 1989. A model for pyrolysis of wet wood. *Chemical Engineering Science,* 44, 2861-2869.

Antal, M. J., 1995. Cellulose pyrolysis kinetics: The current state of knowledge. *Industrial and Engineering Chemistry Research*, 34, 703-717.

Bamford, C. H., Crank, J., Malan, D. H., 1946. The combustion of wood. Part I. *Proceedings of the Cambridge Philosophical Society*, 42, 166-182.

Berger, J., 1997. *Charging Ahead: The business of renewable energy and what it means for America.* Henry Holt and Company, New York, NewYork.

Bilbao, R., Millera, A., Murillo, M.B., 1993. Temperature profile and weight loss in the thermal decomposition of large spherical wood particles. *Industrial Engineering Chemistry Research*, 32, 1811-1817.

Biomass Energy: Data Analysis and Trends, Conference Proceedings, 1998. Paris, France.

Bonnefoy, F., Gilot, P., Prado, G., 1993. A three-dimensional model for determination of kinetic data from the pyrolysis of beech wood. *Journal of Applied Pyrolysis*, 25, 387.

Bryden, K. M., Ragland, K. W., 1997. Combustion of a single log under furnace conditions. In *Developments in Thermochemical Biomass Conversion*, Blackie Academic and Professional, London, 1331-1345.

Bryden, K. M. 1998. *Computational Modeling of Wood Combustion.* Ph.D. Thesis, University of Wisconsin-Madison.

Bryden, K. M., Ragland, K. W., Rutland, C. J., 2002. Modeling thermally thick pyrolysis of wood. *Biomass and Energy*, 22, 41-53.

Chan, W. R., Kelbon, M., Krieger, B. B., 1985. Modeling and experimental verification of physical and chemical processes during pyrolysis of a large biomass particle. *Fuel*, 64, 1505-1513.

Di Blasi, C.,1993a. Analysis of convection and secondary reaction effects within porous solid fuels undergoing pyrolysis. *Combustion Science and Technology*, 90, 315-340.

Di Blasi, C., 1993b. Modeling and simulation of combustion processes of charring and non-charring fuels. *Progress in Energy and Combustion Science*, 19, 71-104.

Di Blasi, C., 1994. Processes of flames spreading over the surface of charring fuels: Effects of the solid thickness. *Combustion and Flame*, 97, 225-239.

Di Blasi, C., 1996. Heat, momentum, and mass transport through a shrinking biomass particle exposed to thermal radiation. *Chemical Engineering Science*, 51,1121-1132.

Di Blasi, C.,1998. Physico-chemical processes occurring inside a degrading two-dimensional anisotropic porous medium. *International Journal of Heat and Mass Transfer*, 41, 4139-4150.

Diebold, J. P., 1985. *The cracking kinetics of depolymerized biomass vapors in a continuous, tubular reactor.* Master Thesis, Colorado School of Mines, Golden Colorado.

Font, T., Marcilla, A., Verdu, E., Devesa, J., 1990. Kinetics of the pyrolysis of almond shells and almond shells impregnated with $CoCl_2$ in a fluidized bed reactor and in a Pyroprobe 100. *Industrial and Engineering Chemistry Research*, 29, 1846-1855.

Forest Products Laboratory 1987. *Wood Handbook: Wood as an Engineering Material*

Agricultural Handbook 72. U.S. Department of Agriculture, Washington, DC.

Hadiwinata, D., 2004. *Numerical model of equivalent wood conductivity due to cracking*. Masters Thesis, Iowa State University.

Hagge, M. J., Bryden, K. M., 2002. Modeling the impact of shrinkage on the pyrolysis of dry biomass. *Chemical Engineering Science*, v 57, n 14, Jul 29, 2002, p 2811-2823.

Hajaligol, M. R., Howard, J. B., Longwelll, J.P., Peters, W. A., 1982. Product compositions and kinetics for rapid pyrolysis of cellulose. *Industrial and Engineering Chemistry Research*, 21, 457-465.

Hoerning, J. M., 1999. *Wood pyrolysis in a high temperature environment*. Ph.D. Thesis, University of Wisconsin-Madison.

Kansa, E. J., Perlee, H. E., Chaiken, R. F., 1977. Mathematical model of wood pyrolysis including internal forced convection. *Combustion and Flame*, 29, 311-324.

Kosstrin, H. M., 1980. Direct formulation of pyrolysis oil from biomass. In *Proceedings of the specialists workshop on fast pyrolysis of biomass*, Copper Mountain, Colorado., 105-121.

Koufopanos, C. A., Papayannakos, N., Mashio, G., Lucchesi, A. 1991. Modeling the pyrolysis of biomass particles. Studies on kinetics, thermal and heat transfer effects. *The Canadian Journal of Chemical Engineering*, 69, 907-915.

Kung, H. C., 1972. The burning of vertical wooden slabs. In *Fifteenth Symposium (International) on Combustion*, The Combustion Institute, Pittsburgh, PA, 243-253.

Laurendeau, N., 1978. Heterogeneous kinetics of coal char gassification and combustion. *Progress of Energy Combustion Science*, 4, 221-269.

Lee, C. K., Chaiken, R. F., Singer, J. M. 1976. Charring pyrolysis of wood in fires by laser simulation. *Sixteenth Symposium (International) on Combustion*. pp. 1459-1470. The Combustion Institute, Pittsburgh.

Liden, A. G., Berruti F., Scott D. S. 1988. A kinetic model for the production of liquids from the flash pyrolysis of biomass. *Chemical Engineering Communications*, 65, 207-221.

Makino, A., Araki, N., Mihara, Y., 1994. Combustion of artificial graphite in stagnation flow: Estimation of global kinetic parameters from experimental results. *Combustion and Flame*, 96, 261-274.

Matsumoto, T., Fujiwara, T., Kondo, J., 1969. Nonsteady thermal decomposition of plastics. In *Twelfth Symposium (International) on Combustion*, The Combustion Institute, Pittsburgh, PA, 515-524.

Melaaen, M. C., Grønli, M. G. 1997. Modeling and simulation of moist wood drying and pyrolysis. *Developments in Thermochemical Biomass Conversion* edited by A. V. Bridgwater and D. B. G. Boocock. pp. 132-146. Blackie, London.

Nunn, T. R., Howard, M. R., Longwell, J. B., Peters, W. A. 1985. Product compositions and kinetics in the rapid pyrolysis of sweet gum hardwood. *Industrial and Engineering Chemical Process Design and Development*, 24, 836-844.

Oulhazi, N., Arnaud, G., Fohr, 1992. A two dimensional study of wood plank drying. The effect of gaseous pressure below the boiling point. *Transport In Porous Media*, 7, 39-61.

Panton, R. L., Rittman, J. G. 1971. Pyrolysis of a slab of porous material. In *Thirteenth*

Symposium (International) on Combustion, The Combustion Institute, Pittsburgh, PA, 881-891.

Parker, W.J. 1988. Prediction of heat release rate in wood. Ph.D. Thesis, George Washington University.

Ragland, K.W., Boerger, J.C., Baker, A.J. 1988. A model of chunkwood combustion. *The Forest Products Journal*, 38(2), 27-32.

Renewable Energy Annual, 2003, Energy Information Administration.

Roberts, A. F., 1971. Problems associated with the theoretical analysis of the burning of wood. In *Thirteenth Symposium (International) on Combustion*, The Combustion Institute, Pittsburgh, PA, 893.

Saastamoinen, J.J. 1993. Model for drying and pyrolysis in an updraft gasifier. *Advances in Thermochemical Biomass Conversion* edited by A. V. Bridgwater. pp. 186-200. Blackie, London.

Samolada, M.C., Vasalos, I. A., 1991. A kinetic approach to the flash pyrolysis of biomass in a fluidized bed reactor. *Fuel*, 70, 883-889.

Shafizadeh, F., Chin, P., 1977. Thermal deterioration of wood. In *Wood Technology*, ACS Press, Washington, DC.

Simmons, W. W. 1983. Analysis of Single Particle Wood Combustion in Convective Flow. Ph.D. Thesis, University of Wisconsin-Madison.

Tannehill, J. C., Anderson, D. A., Pletcher, R. H.,1997. *Computational Fluid Mechanics and Heat Transfer*, Second Edition. Taylor and Francis, Washington DC.

Thurner, F., Mann, U. 1981. Kinetic investigation of wood pyrolysis. *Industrial and Engineering Chemical Process Design and Development*, 20, 482-488.

Tinney, E. R., 1965. The combustion of wooden dowels in heated air. In *Tenth Symposium (International) on Combustion*, The Combustion Institute, Pittsburgh, PA, 925-930.

Tran, H. C., White R. H. 1992. Burning rate of solid wood measured in a heat release rate calorimeter. *Fire and Materials*, 16, 197-206.

Villermaux, J., Antoine, B., Lede, J., Soulignac, F. 1986. A new model for thermal volatilization of solid particles undergoing fast pyrolysis. *Chemical Engineering Science*, 41, 151-157.

White, R.H. 1988. *Charring Rates of Different Wood Species*. Ph.D. Thesis, University of Wisconsin-Madison.